4

David Taylor Research Center

Bethesda, Maryland 20084-5000

AD-A210 121

DTRC-SME-89/05 January 1989

Ship Materials Engineering Department
Research and Development Report

A HYBRID COLLOCATION TECHNIQUE FOR SOLUTION OF THE FINITE BODY SINGLE ENDED CRACK PROBLEM

by
M. T. Kirk

DTRC-SME-89/05 A Hybrid Collocation Technique for Solution of the Finite Body Single Ended Crack Problem

Approved for public release; distribution unlimited

MAJOR DTRC TECHNICAL COMPONENTS

CODE 011 DIRECTOR OF TECHNOLOGY, PLANS AND ASSESSMENT

12 SHIP SYSTEMS INTEGRATION DEPARTMENT

14 SHIP ELECTROMAGNETIC SIGNATURES DEPARTMENT

15 SHIP HYDROMECHANICS DEPARTMENT

16 AVIATION DEPARTMENT

17 SHIP STRUCTURES AND PROTECTION DEPARTMENT

18 COMPUTATION, MATHEMATICS & LOGISTICS DEPARTMENT

19 SHIP ACOUSTICS DEPARTMENT

27 PROPULSION AND AUXILIARY SYSTEMS DEPARTMENT

28 SHIP MATERIALS ENGINEERING DEPARTMENT

DTRC ISSUES THREE TYPES OF REPORTS:

1. **DTRC reports, a formal series,** contain information of permanent technical value. They carry a consecutive numerical identification regardless of their classification or the originating department.

2. **Departmental reports, a semiformal series,** contain information of a preliminary, temporary, or proprietary nature or of limited interest or significance. They carry a departmental alphanumerical identification.

3. **Technical memoranda, an informal series,** contain technical documentation of limited use and interest. They are primarily working papers intended for internal use. They carry an identifying number which indicates their type and the numerical code of the originating department. Any distribution outside DTRC must be approved by the head of the originating department on a case-by-case basis.

UNCLASSIFIED
SECURITY CLASSIFICATION OF THIS PAGE

REPORT DOCUMENTATION PAGE

1a REPORT SECURITY CLASSIFICATION UNCLASSIFIED	1b RESTRICTIVE MARKINGS
2a SECURITY CLASSIFICATION AUTHORITY	3 DISTRIBUTION / AVAILABILITY OF REPORT APPROVED FOR PUBLIC RELEASE, DISTRIBUTION UNLIMITED
2b DECLASSIFICATION / DOWNGRADING SCHEDULE	
4 PERFORMING ORGANIZATION REPORT NUMBER(S) DTRC/SME-89-5	5 MONITORING ORGANIZATION REPORT NUMBER(S)
6a NAME OF PERFORMING ORGANIZATION DTRC — 6b OFFICE SYMBOL (If applicable) Code 2814	7a NAME OF MONITORING ORGANIZATION
6c ADDRESS (City, State, and ZIP Code) Bethesda, MD 20084-5000	7b ADDRESS (City, State, and ZIP Code)
8a NAME OF FUNDING / SPONSORING ORGANIZATION DTRC — 8b OFFICE SYMBOL (If applicable) 011	9 PROCUREMENT INSTRUMENT IDENTIFICATION NUMBER
8c ADDRESS (City, State, and ZIP Code) Bethesda, MD 20084-5000	10 SOURCE OF FUNDING NUMBERS PROGRAM ELEMENT NO: 62234N — PROJECT NO: RS34S91 — TASK NO: — WORK UNIT ACCESSION NO: DN 507603

11 TITLE (Include Security Classification) (U) A HYBRID COLLOCATION TECHNIQUE FOR SOLUTION OF THE FINITE BODY SINGLE ENDED CRACK PROBLEM

12 PERSONAL AUTHOR(S) MARK T. KIRK

13a TYPE OF REPORT	13b TIME COVERED	14 DATE OF REPORT (Year, Month, Day)	15 PAGE COUNT
R&D	FROM 870901 TO 890101	January 1989	100

16 SUPPLEMENTARY NOTATION

1-2814-198-20

17 COSATI CODES			18 SUBJECT TERMS (Continue on reverse if necessary and identify by block number)
FIELD	GROUP	SUB-GROUP	Crack Arrest, Stress Intensity Fractor, Collocation, Photoelasticity.

19 ABSTRACT (Continue on reverse if necessary and identify by block number)

A hybrid experimental / numerical collocation technique was developed for analysis of two dimensional, finite body, single-ended crack problems. Both boundary stress conditions, known a priori, and interior stress conditions, determined from photoelastic model, were used to specify the loading imposed on the specimen. It was determined that including the interior stress conditions in the analysis increases the rate of solution convergence. Additionally, the interior stress conditions allowed both the stress intensity factor (K_I) and the crack mouth opening displacement to be determined over a wider range of crack lengths than was possible with boundary collocation alone. Using the hybrid collocation technique, a single edge notched tension, SE(T), specimen, modified by introduction of a semi-circular cutout in front of the crack, was developed and characterized. This specimen was found to produce fixed grip K_I values two times greater than is possible with a conventional SE(T) specimen of the same size. This new specimen could be used to investigate upper transition crack arrest phenomena with smaller specimens and testing machine capacities than have been possible previously.

20 DISTRIBUTION / AVAILABILITY OF ABSTRACT	21 ABSTRACT SECURITY CLASSIFICATION
☐ UNCLASSIFIED/UNLIMITED ☒ SAME AS RPT ☐ DTIC USERS	UNCLASSFIED

22a NAME OF RESPONSIBLE INDIVIDUAL	22b TELEPHONE (Include Area Code)	22c OFFICE SYMBOL
M.T. Kirk	(301) 267-3755	DTRC 2814

DD FORM 1473, 84 MAR — 83 APR edition may be used until exhausted. All other editions are obsolete.

SECURITY CLASSIFICATION OF THIS PAGE

TABLE OF CONTENTS

		Page
LIST OF TABLES		v
LIST OF FIGURES		vi
ABSTRACT		x
ADMINISTRATIVE INFORMATION		x
ACKNOWLEDGEMENTS		x
CHAPTER 1 -- INTRODUCTION		
1.1	Techniques for Determination of K_I and CMOD for Fracture Specimens	1
1.2	Specimen Geometry Investigated	9
CHAPTER 2 -- MATHEMATICAL DETAILS		
2.1	Generalized Westergaard Equations	15
2.2	Hybrid Collocation	16
	2.2.1 Solution Procedure	19
	2.2.2 Numerical Validation and Comparison to Boundary Collocation	24
	2.2.3 Effect of Random and Systematic Errors in the Photoelastic Data	26
	2.2.4 Effect of the Ratio of Internal to Boundary Collocation Stations	32
2.3	Fixed Grip Stress Intensity Factor Calibrations	34
CHAPTER 3 -- EXPERIMENTAL TECHNIQUES		39
CHAPTER 4 -- RESULTS AND DISCUSSION		
4.1	Conventional SE(T) Specimen	45
4.2	Modified SE(T) Specimen	52
CHAPTER 5 -- SUMMARY AND CONCLUSIONS		69

Page

APPENDIX A -- SERIES EXPANSIONS OF STRESS AND DISPLACEMENT EQUATIONS 71

APPENDIX B -- PARTIAL DERIVATIVES FOR THE [H] MATRIX 75

APPENDIX C -- FORMULAS RELATING K_I AND CMOD TO SERIES COEFFICIENTS 81

APPENDIX D -- SERIES SOLUTIONS FOR THE CONVENTIONAL SE(T) SPECIMEN 84

APPENDIX E -- SERIES SOLUTIONS FOR THE MODIFIED SE(T) SPECIMEN 88

REFERENCES 97

LIST OF TABLES

		Page
Table 1:	Effective length for the modified SE(T) specimen having a cutout of radius 20.2% of the maximum specimen width.	38
Table 2:	Comparison of hybrid and boundary collocation K_I^* and CMOD* results for a conventional SE(T) specimen with literature values.	51
Table 3:	Comparison of hybrid and boundary collocation K_I^* results for a modified SE(T) specimen.	61

LIST OF FIGURES

		Page
Figure 1:	Comparison of various literature stress intensity factor calibrations for a conventional SE(T) specimen with values calculated using boundary collocation.	7
Figure 2:	Dark field isochromatic fringe patterns for a conventional SE(T) specimen at (a) a/W = 0.10 and (b) a/W = 0.85. Regions of the specimen beyond those shown by the continuous tone photographs exhibited no significant fringe features.	8
Figure 3:	Variation of crack arrest toughness with temperature for various reactor grade pressure vessel steels, after ref. [21].	10
Figure 4:	Fixed grip stress intensity factor calibration for a conventional SE(T) specimen having a length between fixed ends of twice the specimen width.	12
Figure 5:	Prototype modified SE(T) specimen.	14
Figure 6:	Comparison of hybrid and global collocation solutions for dimensionless (a) K and (b) CMOD for a conventional SE(T) specimen having the crack tip at 0.51·W.	25
Figure 7:	Effect of systematic crack tip position error on dimensionless K and CMOD for a conventional SE(T) specimen having the crack tip at 0.51·W.	28
Figure 8:	Effect of systematic crack tip position error on root mean square error measures for a conventional SE(T) specimen having the crack tip at 0.51·W.	29

Page

Figure 9: Effect of random error on dimensionless K and CMOD values for a conventional SE(T) specimen having the crack tip at 0.51·W. 31

Figure 10: Effect of the ratio of internal to boundary stations on the convergence rate of dimensionless K for a conventional SE(T) specimen having the crack tip at 0.51·W. 33

Figure 11: Multiple pin linkage used to impose a constant stress boundary condition on the photoelastic models. 40

Figure 12: Fringe order error from a two term local collocation solution based on photoelastic data from a conventional SE(T) specimen having the crack tip at 0.40·W. Data points having high residuals relative to the data set were deleted prior to use in the hybrid collocation analysis. 43

Figure 13: Literature (a) K and (b) CMOD calibrations for a conventional SE(T) specimen loaded with a constant remote stress. 46

Figure 14: Dimensions and optical properties of the conventional SE(T) specimen tested. 48

Figure 15: Convergence of dimensionless K calculated using hybrid collocation with increasing model order for a conventional SE(T) specimen having the crack tip at (a) 0.10·W, (b) 0.40·W, and (c) 0.80·W. 49

Figure 16: Comparison of hybrid collocation and boundary collocation estimates of dimensionless (a) K and (b) CMOD with the empirical formulas due to Tada [9]. 50

Page

Figure 17: Comparison of experimental isochromatic fringe patterns with those calculated using hybrid collocation and boundary collocation for a conventional SE(T) specimen. Comparison is shown at (a-b) 0.10·W, (c-d) 0.60·W, and (e-f) 0.80·W. 53-55

Figure 18: Fixed grip stress intensity factor calibration for conventional SE(T) specimens having various length to width ratios. 56

Figure 19: Dimensions and optical properties of the modified SE(T) specimen tested. 57

Figure 20: Convergence of dimensionless K, calculated using hybrid and boundary collocation, with increasing model order for a modified SE(T) specimen having the crack tip at 0.506·W. 58

Figure 21: Comparison of hybrid collocation and boundary collocation estimates of dimensionless K for the modified SE(T) specimen. (a) all a/W, (b) a/W < 0.6 only. 60

Figure 22: Comparison of experimental isochromatic fringe patterns (lower) with those calculated (upper) using hybrid collocation and boundary collocation for a modified SE(T) specimen at (a-b) 0.1·W, and (c-d) 0.4·W. 62-63

Figure 23: Comparison of experimental isochromatic fringe patterns (lower) with those calculated (upper) using hybrid collocation and boundary collocation for a modified SE(T) specimen at 0.506·W. Both collocation techniques give comparable results at this crack depth. 64

Page

Figure 24: Comparison of experimental isochromatic fringe patterns with those calculated using boundary collocation for the modified SE(T) specimen at 0.9·W. 65

Figure 25: Comparison of fixed grip stress intensity factor calibrations for conventional and modified SE(T) specimens having length to width ratios of (a) 2:1, and (b) 4:1. 68

ABSTRACT

A hybrid experimental / numerical collocation technique was developed for analysis of two dimensional, finite body, single-ended crack problems. Both boundary stress conditions, known a priori, and interior stress conditions, determined from a photoelastic model, were used to specify the loading imposed on the specimen. It was determined that including the interior stress conditions in the analysis increases the rate of solution convergence. Additionally, the interior stress conditions allowed both the stress intensity factor (K_I) and the crack mouth opening displacement to be determined over a wider range of crack lengths than was possible with boundary collocation alone. Using the hybrid collocation technique, a single edge notched tension, SE(T), specimen, modified by introduction of a semi-circular cutout in front of the crack, was developed and characterized. This specimen was found to produce fixed grip K_I values two times greater than is possible with a conventional SE(T) specimen of the same size. This new specimen could be used to investigate upper transition crack arrest phenomena with smaller specimens and testing machine capacities than have been possible previously.

ADMINISTRATIVE INFORMATION

This report was prepared as part of the Surface Ship and Craft Materials Block under the sponsorship of Mr. I Caplan (DTRC 011.5). This effort was performed at this Center under Program Element 62234N, Task Area RS34S91, Work Unit 1-2814-198-20. This effort was supervised by T.W. Montemarano.

ACKNOWLEDGEMENTS

The author wishes to thank Dr. R.J. Sanford of the University of Maryland for his guidance and many helpful suggestions made during the course of this research.

CHAPTER 1

INTRODUCTION

1.1 Techniques for Determination of K_I and CMOD for Fracture Specimens

A ubiquitous problem in fracture mechanics is the determination of how the opening mode stress intensity factor (K_I) and the crack mouth opening displacement (CMOD) vary with crack length for a particular geometric configuration. One traditional approach to solving this problem is to perform an experimental compliance calibration [1]. While this technique provides the needed information at any crack length, it is not without its drawbacks. A primary disadvantage is the need to use very sensitive displacement transducers to accurately measure the small elastic displacements imposed on the specimen. Further, no general information regarding stresses or displacements is obtained at other than the instrumented locations. Thus, while a fair degree of effort is required to conduct the experiment, only very limited information can be obtained.

Of the other experimental techniques available, many make use of data obtained from photoelastic experiments. Ostervig [2] reviewed these methods, which may be broadly categorized as either deterministic, requiring only as

many experimental datum as unknown parameters, or over deterministic, requiring more data than unknown parameters. Of these two classes, over-deterministic techniques are generally less sensitive to experimental errors [3]. One over-deterministic technique, referred to as local collocation, was first developed by Sanford and Dally [3]; with further refinements due to Sanford and Chona [4], as well as Barker, Sanford, and Chona [5]. This method uses experimental data from a region bounded by a minimum radius of one-half of the model thickness and a maximum radius on the order of 15% of the specimen width to determine the coefficients of a modified Westergaard series expansion. While quite efficient for determination of K_I at any crack length, this method cannot determine displacements at locations remote from the data acquisition region, and thus is not useful for determining CMOD.

A different general approach to solving these problems is the use of numerical techniques requiring either discretization of the entire body (e.g. finite element, finite difference) or of only the external boundary (e.g. boundary collocation). To use a boundary collocation technique, the stress function for the body must be known, and be representable as an infinite series having each term defined to within an arbitrary constant. As a result

of this requirement, collation techniques are computationally more efficient than finite element or finite difference approaches due to the lower level of approximation involved. Because this series expansion is, in the limit, the exact solution to the problem under consideration, the series coefficients at different crack lengths can be interpolated to estimate the solution at any intermediate crack length values. Further, boundary collocation results can be used to calculate the stress or strain at any location in the body from a simple, continuous, algebraic function. Finite element and finite difference solutions have neither of these characteristics.

The stress function used in a boundary collocation solution must explicitly satisfy the boundary conditions on the crack faces, as well as account for all internally applied loads. Having satisfied these conditions, the problem is solved by determining the constants which approximately satisfy the desired external boundary conditions. For the single ended crack problem, stress functions for various internal boundary/internal loading configurations are well established. Newman [6] applied the complex potentials due to Kolosov and Muskhelishvili [7] to the problem of cracks emanating from holes, exploiting the applicability of these functions to

multiply connected regions. Sanford and Berger [8] presented a method for converting the wide variety of published infinite body Westergaard solutions [9] into series forms amenable to use in boundary collocation analysis. In so doing, these authors made available for computational studies a large class of functions describing cracks subjected to internal point and pressure loading. For simpler problems not involving internal loading or multiply connected domains, either the Williams stress function [10] (in polar coordinates) or the modified Westergaard function [11] (in Cartesian coordinates) is most appropriate.

Boundary collocation methods may be either deterministic or over-deterministic. Early investigators [12-14] employed deterministic techniques. This allowed the stress intensity factor to be determined by simple matrix inversion, with the reported value being the stabilized K_I reached as the number of series coefficients, and boundary conditions, was increased. While an efficient technique, Kobayashi, Cherepy, and Kinsel [12] noted that the accuracy of K_I thus determined depended upon the location of the collocation stations.

In a book concerning numerical solutions to two-dimensional elasticity problems, Hulbert [15] indicated

that the phenomenon observed by Kobayashi, et al. can be explained by considering the position of the collocation stations relative to the maxima and minima of the terms in the stress function along the external boundary. Unless collocation stations and extrema coincide, residuals between stations tend to be quite large. To alleviate this difficulty, Hulbert developed an over-determined boundary collocation procedure based on a least squares minimization of the external boundary residuals over all of the collocation stations. The first application of Hulbert's procedure to a fracture problem (known to this author) was by Newman [6], who compared over-determined and deterministic collocation for the problem of two cracks emanating from a circular hole in an infinite plate stressed normal to the crack line at infinity. In that study, the over-determined solution converged with less than half the number of series coefficients needed by the deterministic solution. Subsequent studies using the over-determined approach [16,17] have not reported any difficulties associated with collocation station placement.

An over-determined boundary collocation approach can be used to determine the variation of K_I and displacements remote from the crack tip (e.g. CMOD) with crack length. However, when the crack tip is near an external boundary,

these estimates become quite inaccurate. This shortfall is illustrated in Figure 1, which compares boundary collocation results for a single edge notched tension, SE(T), specimen with other numerical solutions published in the literature [13, 18-20]. At crack length to specimen width (a/W) ratios greater than 0.6 and less than 0.3, the normalized stress intensity factor calculated using boundary collocation deviates from that determined using a wide variety of other computational techniques. The cause of this disagreement becomes apparent upon examination of isochromatic fringe patterns for either shallow or deep cracks, as shown in Figure 2. For these extreme cases, the majority of the fringes are confined to a small region about the crack tip, indicating that the stress gradients at the boundary are virtually zero. As these are the data from which a boundary collocation solution determines the strength of the crack tip singularity, inaccurate results would be expected in either case.

Clearly, neither experimental or numerical methods employed independently can determine the variation of both K_I and CMOD over a wide range of crack lengths. The objective of this research is to develop a hybrid numerical/experimental technique which can. This technique combines local collocation, previously presented

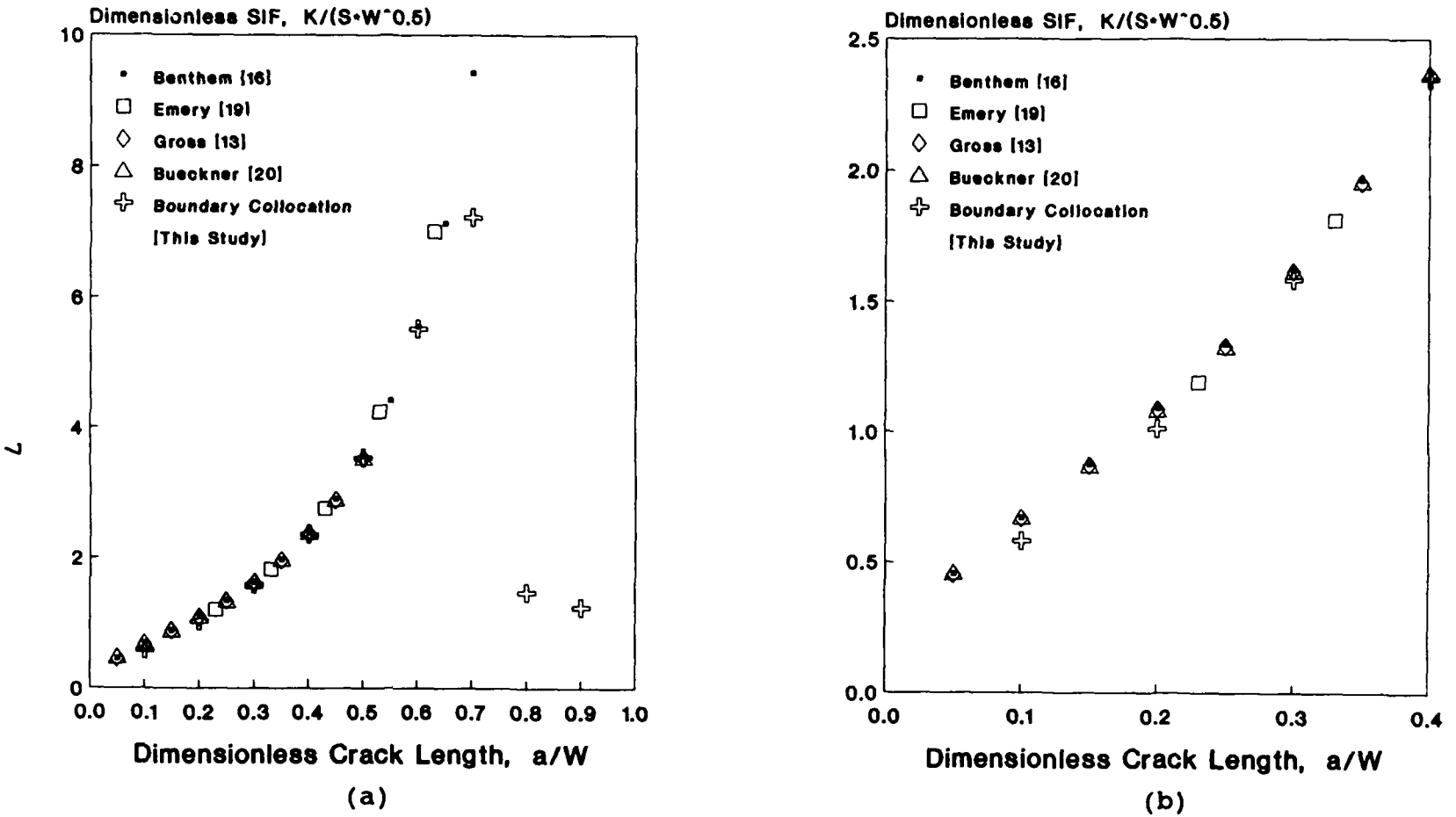

Figure 1: Comparison of various literature stress intensity factor calibrations for a conventional SE(T) specimen with values calculated using boundary collocation (*S = Applied remote tensile stress*). (a) For a/W < 0.9, (b) For a/W < 0.4

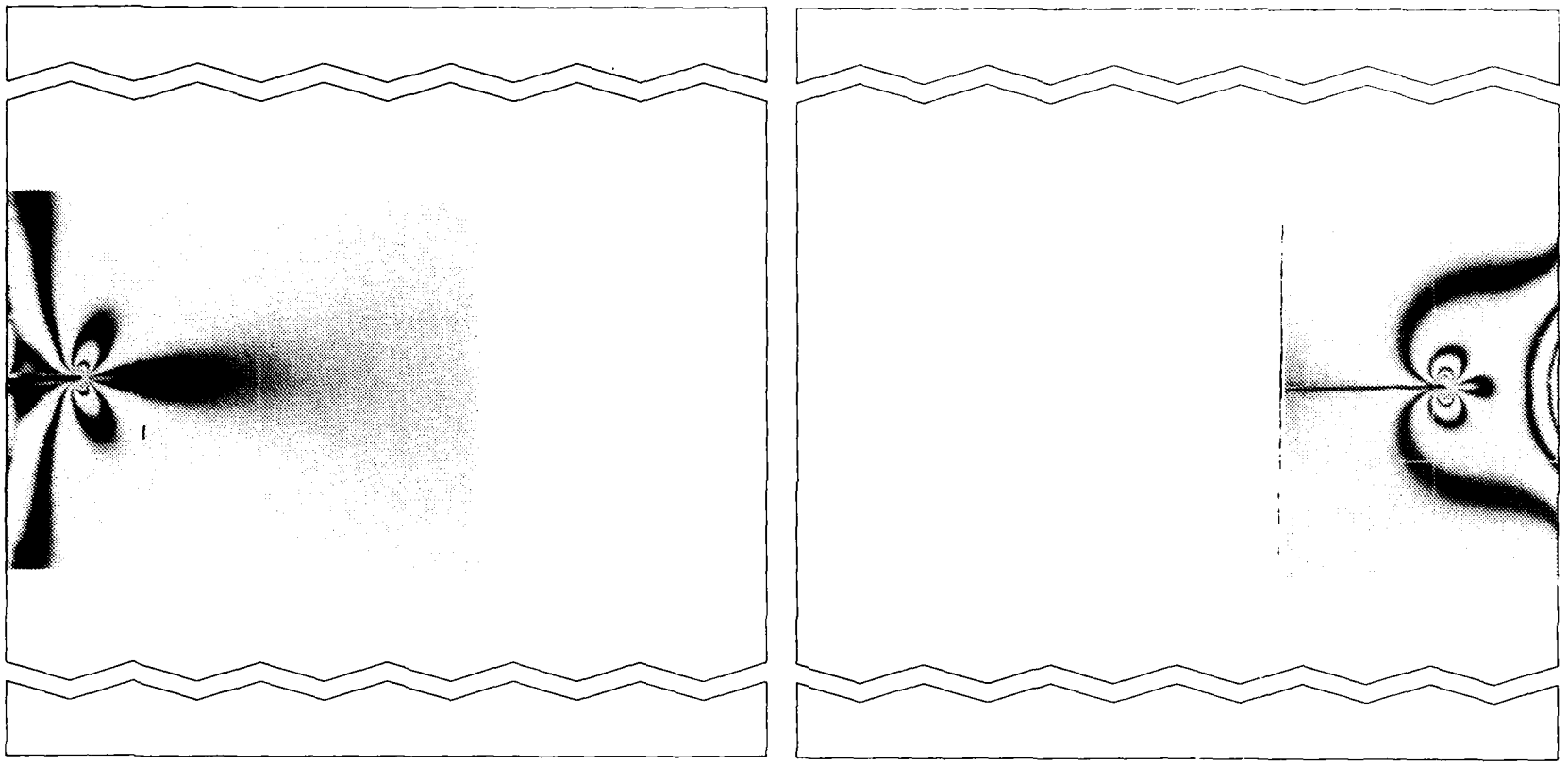

(a) (b)

Figure 2: Dark field isochromatic fringe patterns for a conventional SE(T) specimen at (a) a/W = 0.10 and (b) a/W = 0.85. Regions of the specimen beyond those shown by the continuous tone photographs exhibited no significant fringe features.

by Sanford and Dally [3], with boundary collocation using the generalized Westergaard functions, as recently demonstrated by Sanford and Berger [8]. Results will be presented for a conventional SE(T) specimen and for a SE(T) specimen modified by placing a stress concentrating cutout in front of the crack. Rationale for development and practical use of this new specimen is presented in the following section.

1.2 Specimen Geometry Investigated

In materials testing, it is frequently of interest to measure the crack arrest toughness of a material and, in materials which experience a ductile - to - brittle toughness transition, determine the variation of this property with test temperature. Crack arrest toughness is most frequently quantified in terms of the value of K_I occurring at crack arrest (K_{Ia}); Figure 3 shows the variation of K_{Ia} with temperature for a reactor grade pressure vessel steel [21]. The rapid increase at high temperatures is typical of steels tested in this fashion and denotes the onset, above the temperature of the vertical asymptote, of fully ductile fracture behavior. Crack propagation in these experiments is quite rapid; crack speeds on the order of 1,000 m/s (39,370 in/s) in high strength steel and 150 to 300 m/s (5,905 to 11,811

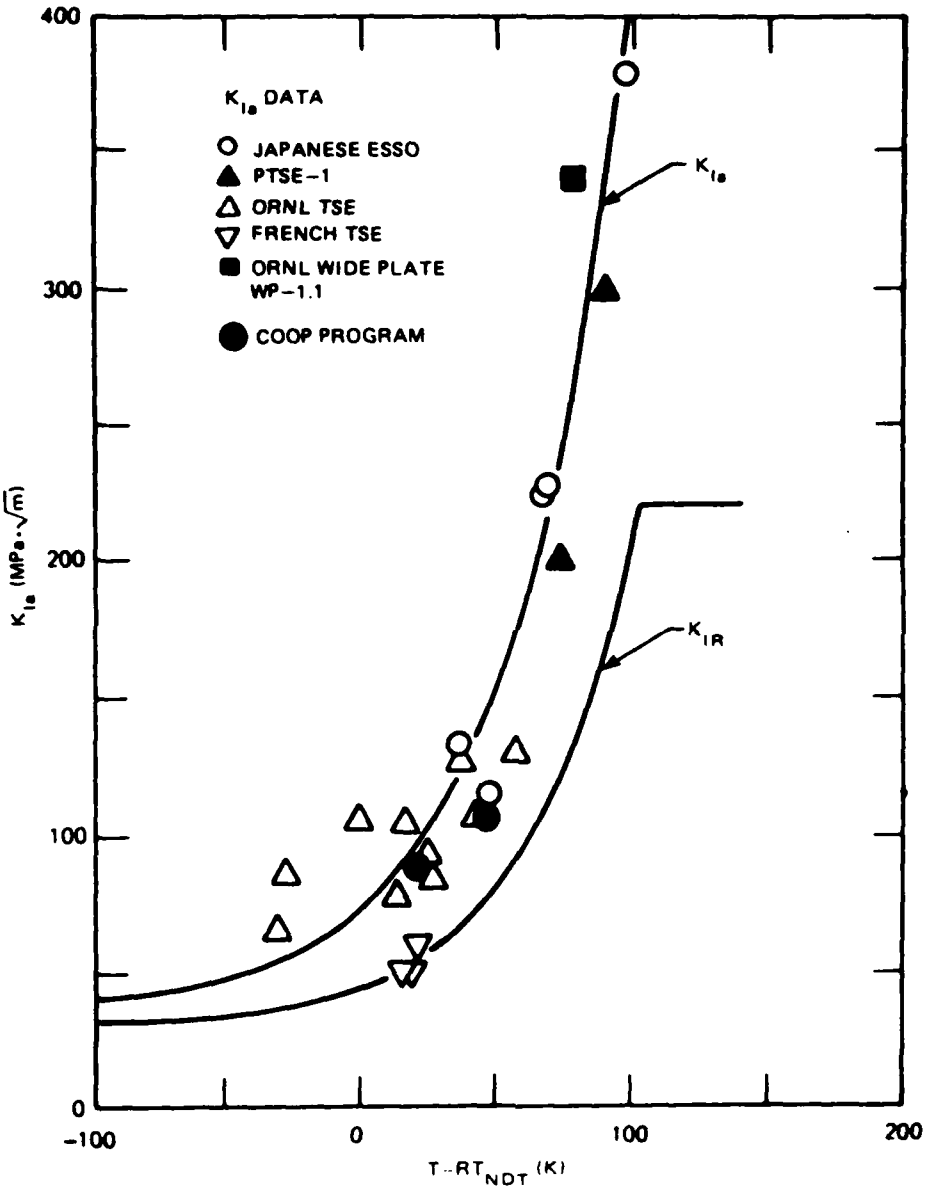

Figure 3: Variation of crack arrest toughness with temperature for various reactor grade pressure vessel steels, after ref. [21].

in/s) in ARALDITE B have been measured [22]. Provided that the specimen is sufficiently large to limit interaction of boundary reflected stress waves with the moving crack tip, a simple engineering approximation to K_{Ia} may be obtained using static K_I formulas which assume fixed load point displacement (fixed grips) during the crack run - arrest event [23].

The American Society for Testing and Materials Standard Test Procedure for Measurement of K_{Ia}, E1221 [24], recommends use of a crack-line wedge-loaded compact tension specimen. The reduction of K_I with increasing crack length for fixed grip boundary conditions in this specimen, combined with an upward shift of the ductile - to - brittle transition temperature caused by elevated crack tip loading rate during the crack arrest experiment, make this specimen useful only for determining crack arrest data at low temperature/toughness combinations. To determine higher K_{Ia} values, SE(T) specimens are frequently employed [23]. These specimens are subjected to a linear thermal gradient, cold at small a/W and hot at large a/W, to create a toughness gradient across the specimen width. This feature allows the specimen to arrest cracks at the higher than initiation K values that are generated under fixed grip loading conditions in this specimen geometry, as illustrated in Figure 4. Better

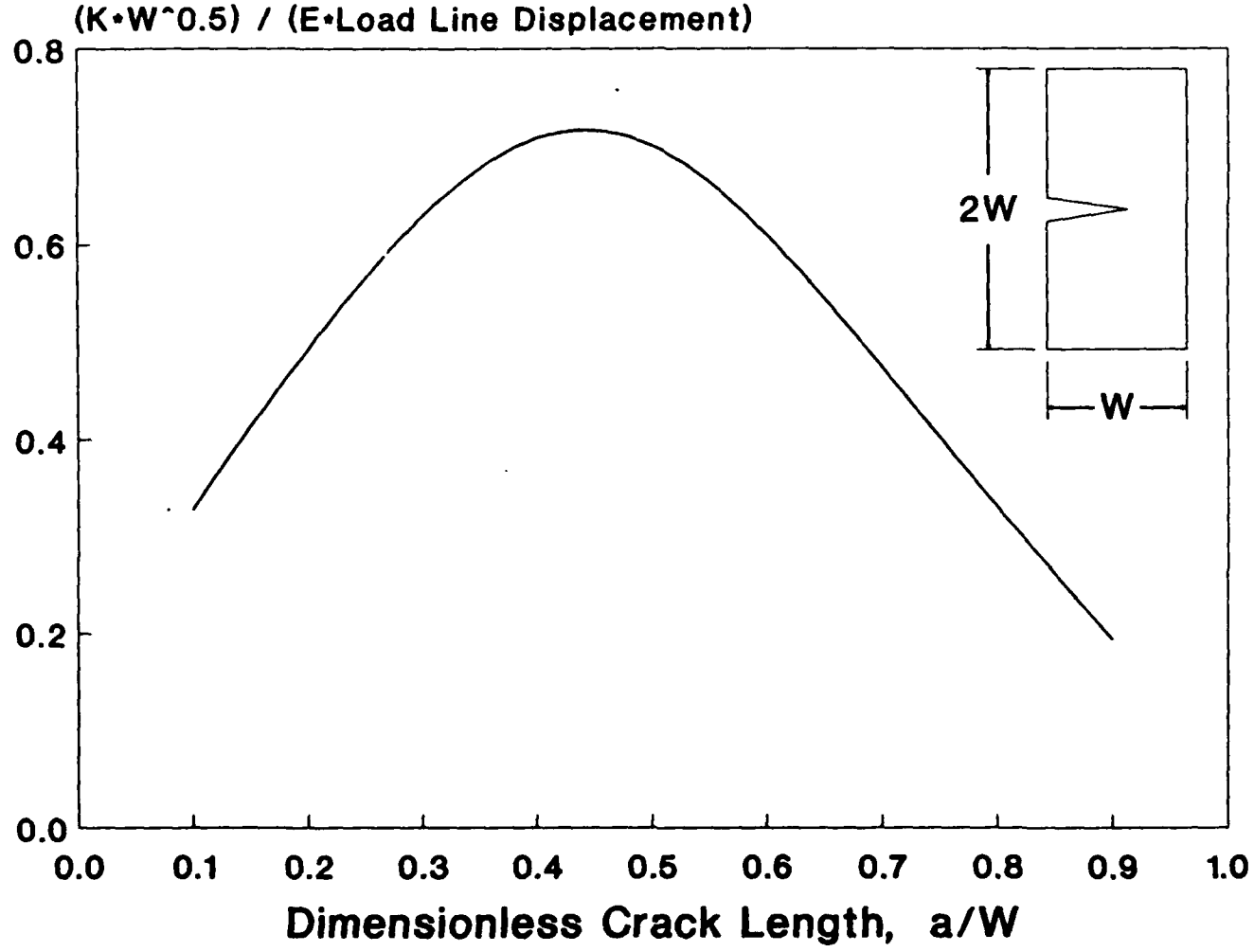

Figure 4: Fixed grip stress intensity factor calibration for a conventional SE(T) specimen having a length between fixed ends of twice the specimen width.

definition of the upper asymptote of the K_{Ia} - temperature transition curve could be obtained by increasing the maximum K_I achievable, and by maximizing the portion of the specimen over which K_I increases with increasing crack length. To this end, a modified SE(T) specimen of the type illustrated in Figure 5 will be developed in this investigation.

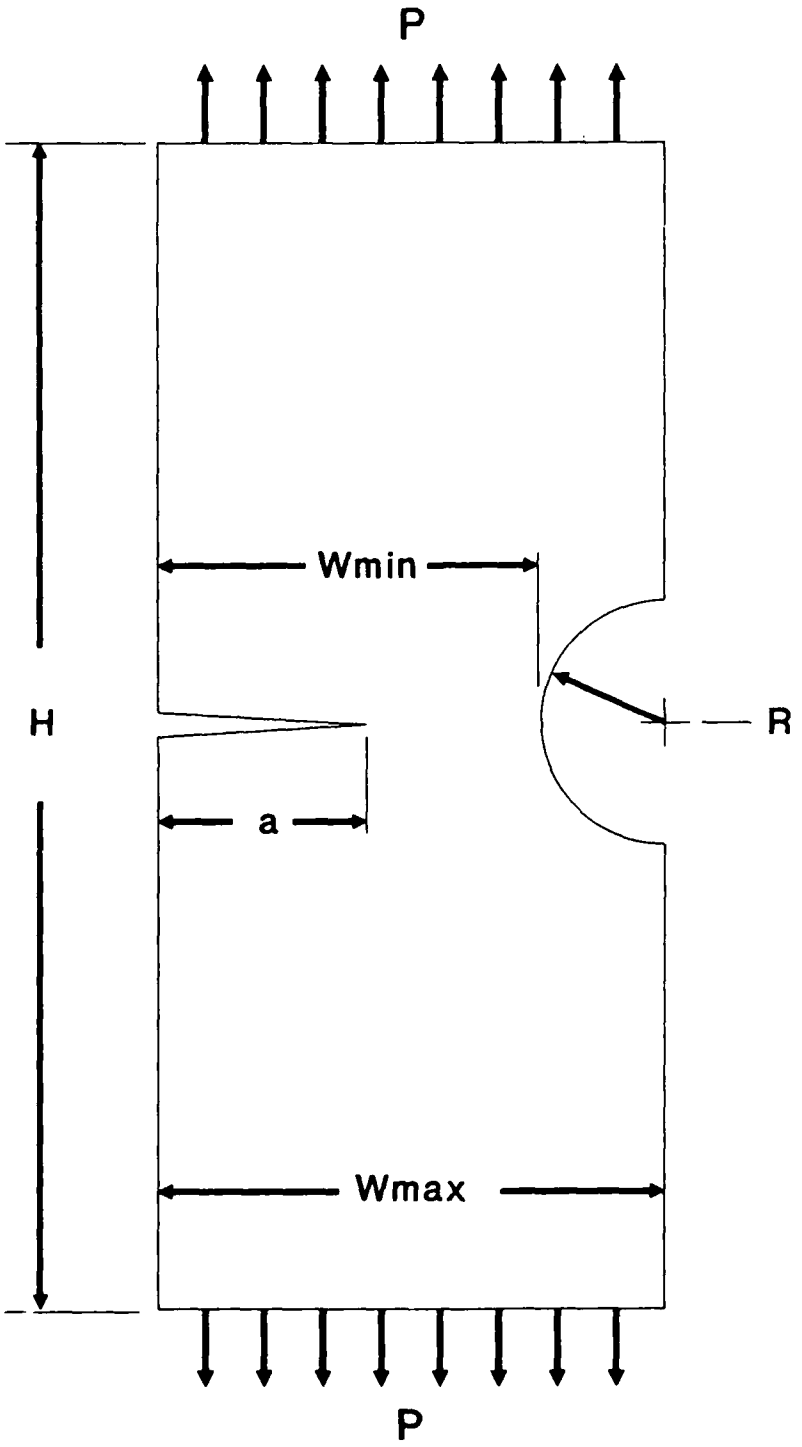

Figure 5: Prototype modified SE(T) specimen.

CHAPTER 2

MATHEMATICAL DETAILS

2.1 Generalized Westergaard Equations

Sanford [11] demonstrated that the generalized form of the Westergaard equation [25] is an Airy stress function given by:

$$\Phi = \mathrm{Re}[\bar{\bar{Z}}(z)] + y\,\mathrm{Im}[\bar{Z}(z)] + y\,\mathrm{Im}[\bar{Y}(z)] \qquad (1)$$

where

$$Z(z) = \frac{d\bar{Z}(z)}{dz} \; ; \quad \bar{Z}(z) = \frac{d\bar{\bar{Z}}(z)}{dz}$$

$$Y(z) = \frac{d\bar{Y}(z)}{dz}$$

$$z = x + iy$$

Functions of this kind are useful for solution of finite body crack problems, provided that functions $Z(z)$ and $Y(z)$ can be found, such that $\mathrm{Re}[Z(z)] = 0$ on the traction free surfaces of the crack (i.e. $\sigma_{yy} = \sigma_{xy} = 0$ on the crack faces) and $\mathrm{Im}[Y(z)] = 0$ along the crack line (i.e. $\tau_{xy} = 0$ on $y = 0$ for all x). For these problems, the in-plane stresses may be expressed as follows:

$$\sigma_{xx} = \partial^2\Phi/\partial y^2 = \mathrm{Re}\ Z - y\,\mathrm{Im}\ Z' - y\,\mathrm{Im}\ Y' + 2\mathrm{Re}\ Y \qquad (2a)$$

$$\sigma_{yy} = \partial^2\Phi/\partial x^2 = \mathrm{Re}\ Z + y\,\mathrm{Im}\ Z' + y\,\mathrm{Im}\ Y' \qquad (2b)$$

$$\tau_{xy} = \partial^2\Phi/\partial x\partial y = -y\mathrm{Re}\ Z' - y\mathrm{Re}\ Y' - \mathrm{Im}\ Y \qquad (2c)$$

where

$Y = Y(z)$
$Z = Z(z)$

2.2 Hybrid Collocation

To use eqn. (2) in a collocation solution, Z(z) and Y(z) must be expressed in series form. For the conventional SE(T), a single series expansion having its origin at the crack tip was used [4]. For this specimen, Z(z) and Y(z) are as follows:

$$Z(z) = \sum_{j=0}^{J} A_j \cdot z^{j-1/2} \qquad (3a)$$

$$Y(z) = \sum_{m=0}^{M} B_m \cdot z^m \qquad (3b)$$

where

z = a complex coordinate having its origin at the crack tip

These series exactly satisfy the stress free crack face and crack line symmetry conditions; the negative powers of z below $z^{-1/2}$ having been eliminated to prevent displacements from becoming unbounded at the crack tip. For the modified SE(T), an additional series expansion was needed because the series given in eqn. (3) do not allow stresses or displacements to increase around any point other than the crack tip. Clearly, this was not the case

for the modified SE(T), where stresses also increase quite rapidly around the base of the cutout. By using a series expansion that includes negative powers of z, a pole (location of infinite displacement) was placed in the solution at the center of the cutout. This pole allowed the rapid increase of stress around the base of the cutout to be explicitly accounted for in the mathematical formulation of the problem. Because there was no material at the location of the pole, the negative powers could be included while maintaining single valued displacements for all points within the specimen. The form suggested by Newman [6] for this negative power series was used to satisfy the stress-free crack face and crack line symmetry conditions. Thus, the series expansions for the modified SE(T) specimen were as follows:

$$Z(z) = \sum_{j=0}^{J} A_j \cdot z^{j-1/2} + \sum_{u=1}^{U} C_u \cdot \frac{1}{\sqrt{z} \cdot (z-z_o)^u} \qquad (4a)$$

$$Y(z) = \sum_{m=0}^{M} B_m \cdot z^m + \sum_{v=1}^{V} D_v \cdot \frac{1}{(z-z_o)^v} \qquad (4b)$$

where

z_o = the center of the circular cutout

To impose the applied boundary conditions, series representations of eqn. (2) in real coordinates, constructed using (3) and (4), are needed. These equations are presented in Appendix A.

In addition to boundary information, the hybrid collocation technique requires information regarding stress or displacement conditions that can be imposed on the specimen interior. While any experimental method of sufficient accuracy could be used to determine these conditions (e.g. photoelasticity, moire interferometry, speckle interferometry, resistance strain gages), photoelastic data was used in this investigation. In this way, experimental details were simplified while fringe patterns were obtained which are sensitive to the non-singular terms in the series expansion for stress [26].

To use photoelastic data, an equation relating the maximum shear stress to the measured fringe order (N) is required. This relationship may be written as follows:

$$\tau_{max} = \left[[(\sigma_{xx} - \sigma_{yy})/2]^2 + \tau_{xy}^2 \right]^{1/2} \qquad (5)$$

$$= N \cdot f_\sigma/(2 \cdot t) = N \cdot Q$$

where

f_σ = photoelastic fringe constant
t = photoelastic model thickness
Q = $f_\sigma/(2 \cdot t)$

In terms of the Westergaard Z(z) and Y(z) functions, eqn. (5) becomes

$$\tau_{max} = \left[(-y\mathrm{Im}\ Z' - y\mathrm{Im}\ Y' + \mathrm{Re}\ Y)^2 + (-y\mathrm{Re}\ Z' - y\mathrm{Re}\ Y' - \mathrm{Im}\ Y)^2\right]^{1/2} \quad (6)$$

A series representation of eqn. (6) in real coordinates, constructed using (3) and (4), is presented in Appendix A.

2.2.1 Solution Procedure

The nonlinear character of eqn. (6) necessitates use of an iterative solution technique, such as that proposed by Sanford [26], to determine the unknown series coefficients. In this technique, the stress equations (A1-A4) are expressed in a homogeneous form

$$g_k\,(A'_0, A'_1, \ldots, A'_J, B'_0, B'_1, \ldots, B'_M, C'_0, C'_1, \ldots, C'_U, D'_0, D'_1, \ldots, D'_V, Q) = 0 \quad (7)$$

and expanded as a first order Taylor's series

$$g_k|_{i+1} = g_k|_i + \left[\frac{\partial g_k}{\partial A_0}\right]_i \Delta A'_0 + \left[\frac{\partial g_k}{\partial A_1}\right]_i \Delta A'_1 + \ldots + \left[\frac{\partial g_k}{\partial A_J}\right]_i \Delta A'_J + \left[\frac{\partial g_k}{\partial B_0}\right]_i \Delta B'_0 + \left[\frac{\partial g_k}{\partial B_1}\right]_i \Delta B'_1 + \ldots + \left[\frac{\partial g_k}{\partial B_M}\right]_i \Delta B'_M +$$

$$\left[\frac{\partial g_k}{\partial C_0}\right]_i \Delta C'_0 + \left[\frac{\partial g_k}{\partial C_1}\right]_i \Delta C'_1 + \ldots + \left[\frac{\partial g_k}{\partial C_U}\right]_i \Delta C'_U +$$

$$\left[\frac{\partial g_k}{\partial D_0}\right]_i \Delta D'_0 + \left[\frac{\partial g_k}{\partial D_1}\right]_i \Delta D'_1 + \ldots + \left[\frac{\partial g_k}{\partial D_V}\right]_i \Delta D'_V +$$

$$\left[\frac{\partial g_k}{\partial Q}\right]_i \Delta Q \qquad (8)$$

where

i = Iteration counter
Δ = Correction to previous estimate A_j, B_m, C_u, or D_v
k = Indicator of location in specimen, $0 > k > L$
L = Total number of imposed boundary and interior conditions

By including the photoelastic material parameter, Q, as a variable in the least squares solution, slight measurement inaccuracies associated with the model thickness, the material fringe constant, and the applied load are automatically accounted for by using a value for Q which best fits the input data. The validity of this auto-calibration approach can be checked by comparing the best fit value of Q with the expected value.

To satisfy eqn. (7) in the $(i+1)^{st}$ iteration step, eqn. (8) must be equal to zero. From this observation, eqn. (8) may be expressed in matrix form as

$$\left[-\{g\} = [H]\cdot\{\Delta\} \right]_i \qquad (9)$$

where

[H] L x (J+M+U+V+3) matrix (L > J+M+U+V+3). Matrix values depend on boundary condition type and station location.

{Δ} (J+M+U+V+3) x 1 column vector of corrections to the current estimates of the unknown series coefficients.

{g} L x 1 column vector having values described by eqn. (8).

For the problems under consideration, eqn. (7) may take on any of the following forms depending upon the position of the collocation station, k:

$$\begin{aligned} g = 0 &= \sigma_{xx} \\ &= \sigma_{yy} - \sigma_{APPLIED} \\ &= \tau_{xy} \\ &= \sigma_{rr} \\ &= \tau_{r\theta} \\ &= \tau_{max} - N\cdot f_\sigma/(2\cdot t) \end{aligned} \qquad (10)$$

where

$\sigma_{APPLIED}$ = applied value of remote stress

For each of these cases, the partial derivatives necessary to define the entries in [H] are presented in Appendix B.

Because eqn. (9) represents an over-determined system, {Δ} must be determined using the method of least squares. For large matrices, Berger [17] found that a least squares solution of the normal equations exhibits numerical instabilities. To avoid this problem, a least squares solution based on a QR decomposition of the [H] matrix was

employed [27]. Briefly, this involves decomposing [H] as follows:

$$[H] = [Q] \cdot [R] \tag{11}$$

where

[R] is upper triangular with a non-zero main diagonal
[Q] has orthonormal columns

Substituting eqn. (11) into eqn. (9) gives

$$\{\Delta\} \cdot [R] = -[Q] \cdot \{g\} \tag{12}$$

which can be solved for $\{\Delta\}$ by simple back substitution. In this study, LINPACK [28] subroutines were used to implement the QR decomposition.

To obtain stable values for the series coefficients, eqn. (9) was solved iteratively using the following procedure:

1. Select the number of photoelastic data and boundary stations to be used.
2. Provide initial guesses for the A_0' and B_0' coefficients.
3. Compute {g} and [H] using eqs. (A1-A4) and (B1-B18), respectively.
4. Compute $\{\Delta\}$ using eqn. (12).
5. Revise the coefficient estimates using the $\{\Delta\}$ values.
6. Repeat steps 3 to 5 until the values of K_I, the root mean square boundary stress residual (σ_r), and the root mean square fringe order residual (N_r) do not change by less than some

acceptably small value. The error measures $\overline{\sigma_r}$ and $\overline{N_r}$ are defined as follows:

$$\overline{\sigma_r} = \left[\frac{1}{n_1} \sum_{k=1}^{n_1} (\hat{\sigma}_k - \sigma_k)^2 \right]^{1/2} \tag{13a}$$

$$\overline{N_r} = \left[\frac{1}{n_2} \sum_{k=1}^{n_2} (\hat{N}_k - N_k)^2 \right]^{1/2} \tag{13b}$$

where

$n = n_1 + n_2$
n_1 = number of boundary collocation stations
n_2 = number of internal collocation stations
$\hat{\sigma}_k$ = specified stress boundary condition at point k
$\hat{N}_k$ = measured photoelastic fringe order at point k
σ_k = computed stress boundary condition at point k
N_k = computed photoelastic fringe order at point k

7. Repeat steps 2 to 6, each time including one or more additional terms in the series expansion. Use the most recent coefficient estimates as guesses at step 2 when the new coefficients are added. Continue to add terms to the series expansions until both

   a. The value of K_I becomes a constant independent of increasing model order.

   b. The values of $\overline{\sigma_r}$ and $\overline{N_r} \cdot f_\sigma/(2 \cdot t)$ become small compared to $\sigma_{APPLIED}$.

FORTRAN 77 software was used to implement this procedure. All computations were performed on a MICRO VAX-II in single precision.

2.2.2 Numerical Validation and Comparison to Boundary Collocation

Before using the hybrid collocation procedure to analyze experimental data, it is necessary to demonstrate that the technique produces correct results. This was accomplished by numerical simulation of the hybrid solution scheme. The photoelastic data used in this analysis was numerically generated from a 100 coefficient boundary collocation solution. The SE(T) specimen considered had a length to width ratio of 2/1 and a crack tip at $0.51 \cdot W$, where W is the specimen width. The specimen was loaded with a uniform stress perpendicular to the crack line on the boundary parallel to the crack. To minimize errors resulting from boundary discretization, 320 boundary stations were placed on each side of the specimen creating a total of 1920 applied boundary conditions. A data set consisting of 132 points taken from integer order fringes was numerically generated from this solution. These data, as well as the boundary data, were used as input to the hybrid collocation program. To insure comparability to the boundary collocation result, the total number of constraints imposed on the model was held constant at 1920.

In Figure 6, the variation of the normalized stress intensity factor ($K_I^* = K_I/(\sigma \cdot \sqrt{W})$) and the normalized CMOD

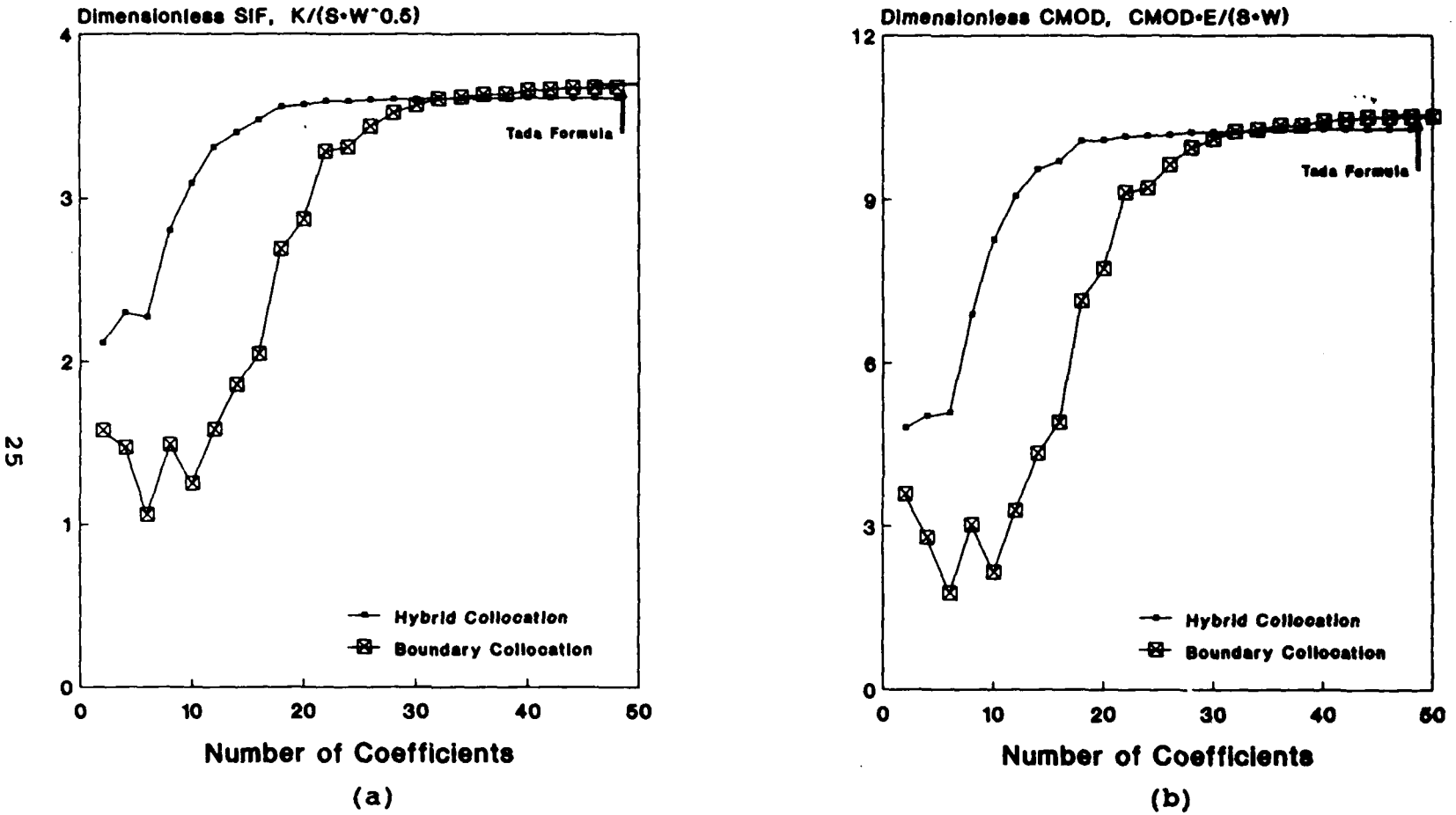

Figure 6: Comparison of hybrid and global collocation solutions for dimensionless (a) K_I and (b) CMOD for a conventional SE(T) specimen having the crack tip at 0.51·W.

($CMOD^* = CMOD \cdot E/(\sigma \cdot W)$) with model order for both the boundary and hybrid collocation techniques are compared with the result of Tada [9], who gives an empirical equation fit to the published data available for this specimen geometry; previously shown in Figure 1. (Appendix C presents relationships between K_I, CMOD, and the series coefficients from the collocation solution.) These data indicate that both techniques have equivalent accuracy for determination of these parameters at a/W ratios where both techniques converge; the slight difference between the converged K_I^* and $CMOD^*$ values calculated using the two collocation techniques having occurred due to the limited accuracy of single precision arithmetic. Further, the hybrid collocation approach appears to offer an advantage over boundary collocation in terms of convergence rate; determining stable estimates of these parameters in models of at most two-thirds the order required for a stable boundary collocation solution. This accelerated convergence results directly from inclusion of the photoelastic data, which are influenced by the crack tip singularity more than the boundary data.

2.2.3 Effect of Random and Systematic Errors in the Photoelastic Data

As pointed out by Barker, et al. [5], errors inherent to

full field optical stress analysis data may either be systematic or random. Systematic errors result from inaccuracies in location of the crack tip, while random errors result from being unable to locate the exact fringe maxima in a photograph without resorting to sophisticated image analysis techniques. The degree of resolution required of experimental measurements can be determined by imposing both types of errors on the numerically generated photoelastic data, and observing the effect on the calculated values of K_I^* and $CMOD^*$.

Figure 7 illustrates the effect of a systematic mis-location of the crack tip along the crack line on estimates of K_I^* and $CMOD^*$. These data show that small errors in crack tip position do not greatly alter either value. This is because K_I^* is proportional to the magnitude of the stress singularity at the crack tip, and thus depends on the relative spacing between isochromatic fringes, which is not dramatically altered by small crack tip position errors. $CMOD^*$, being a measure of displacement remote from the crack tip, is also not strongly influenced. These small inaccuracies can be eliminated altogether if, during the analysis, the crack tip is varied slightly from its expected location to minimize the root mean square error terms, $\overline{\sigma_r}$ and $\overline{N_r}$. The data in Figure 8 shows that if $\overline{\sigma_r}$ and $\overline{N_r}$ are used to

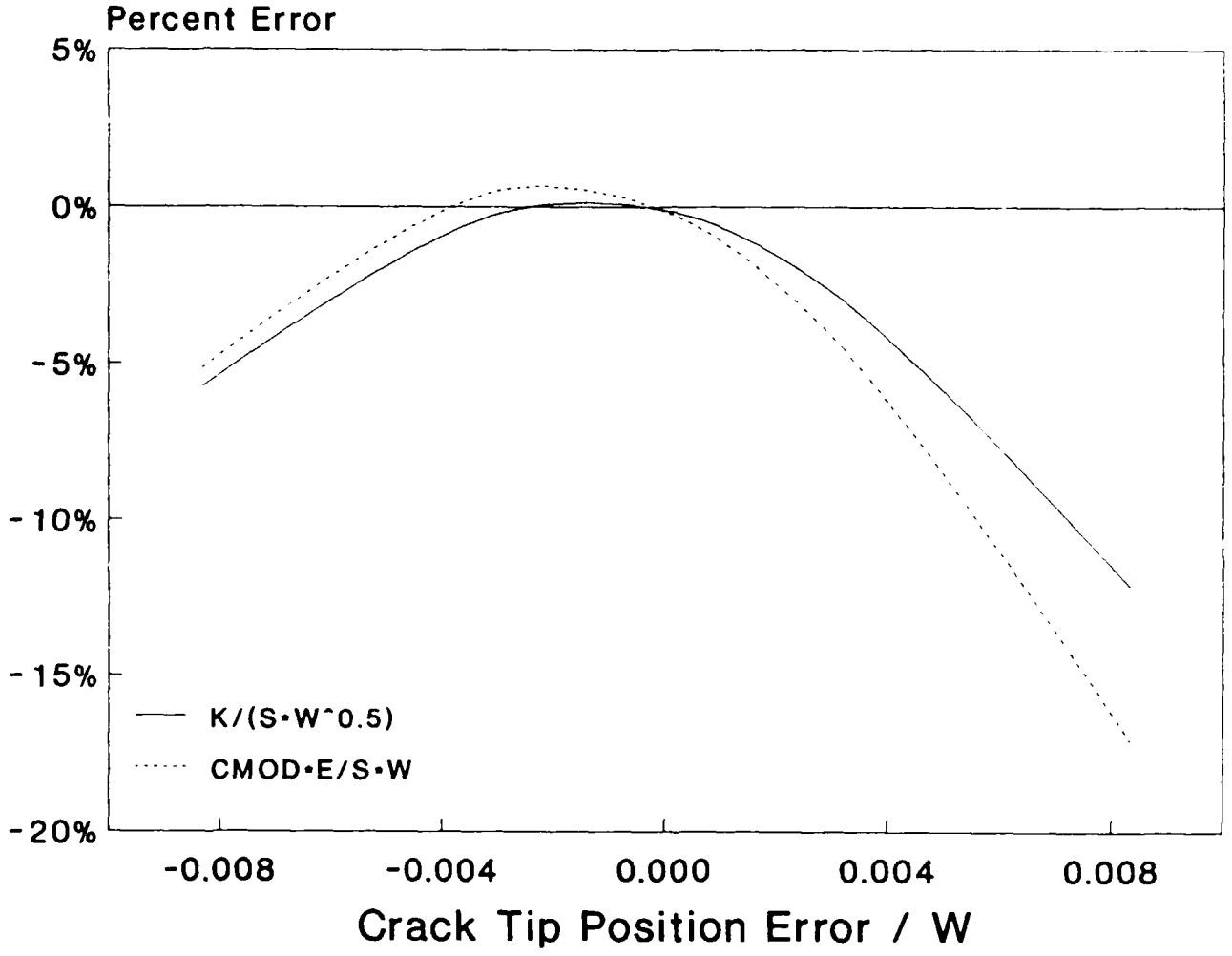

Figure 7: Effect of systematic crack tip position errors on dimensionless K and CMOD for a conventional SE(T) specimen having the crack tip at 0.51·W.

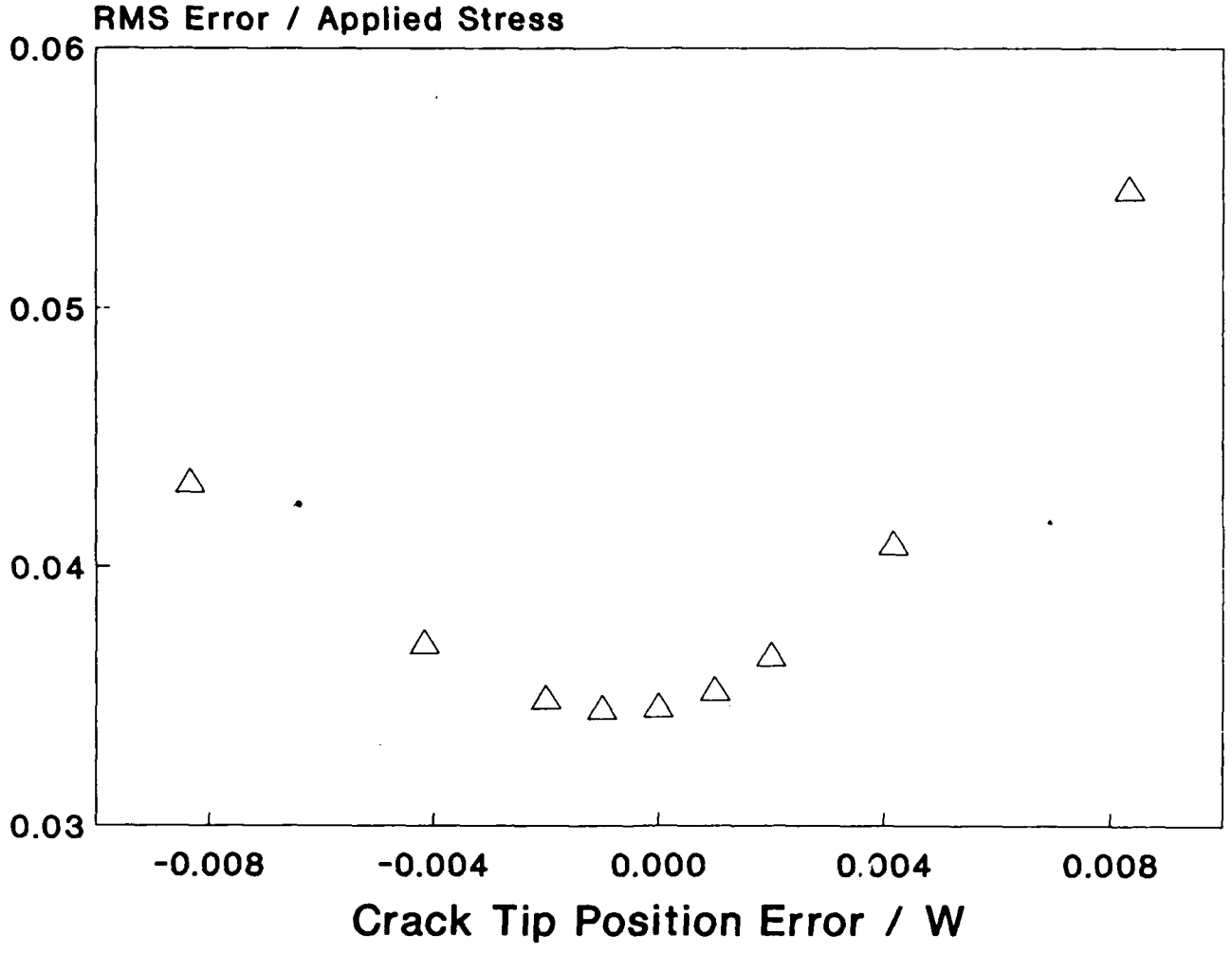

Figure 8: Effect of systematic crack tip position error on root mean square error, $\bar{C}$, for a conventional SE(T) specimen having the crack tip at 0.51·W.

calculate a single residual, weighted to reflect the ratio of internal to boundary collocation stations, this residual approaches a minimum value as the crack tip position used in the analysis approaches the correct location. The formula used to calculate the weighted residual is as follows:

$$\bar{C} = \left[\frac{\overline{\sigma_r}^2 \cdot n_1 + (\overline{N_r} \cdot f_\sigma / 2 \cdot t)^2 \cdot n_2}{n_1 + n_2} \right]^{1/2} \qquad (14)$$

To assess the effects of random error on K_I^* and $CMOD^*$, maximum random errors of $0.0021 \cdot W$, $0.0042 \cdot W$, and $0.0084 \cdot W$ inches were imposed on the numerically generated photoelastic data. The new position of each data point was calculated using the following equations:

$$X' = X + RAND \cdot ERROR_{MAX} \qquad (15a)$$

$$Y' = Y + RAND \cdot ERROR_{MAX} \qquad (15b)$$

where

X and Y = Original coordinates of the datum
RAND = A random number ranging from -1 to +1
$ERROR_{MAX}$ = Maximum random error

The results of these analyses are presented in Figure 9. These data indicate that maximum random position errors up to $0.004 \cdot W$, e.g. 0.6 mm in a 152 mm wide specimen, do not appreciably effect the calculated values of these coefficients.

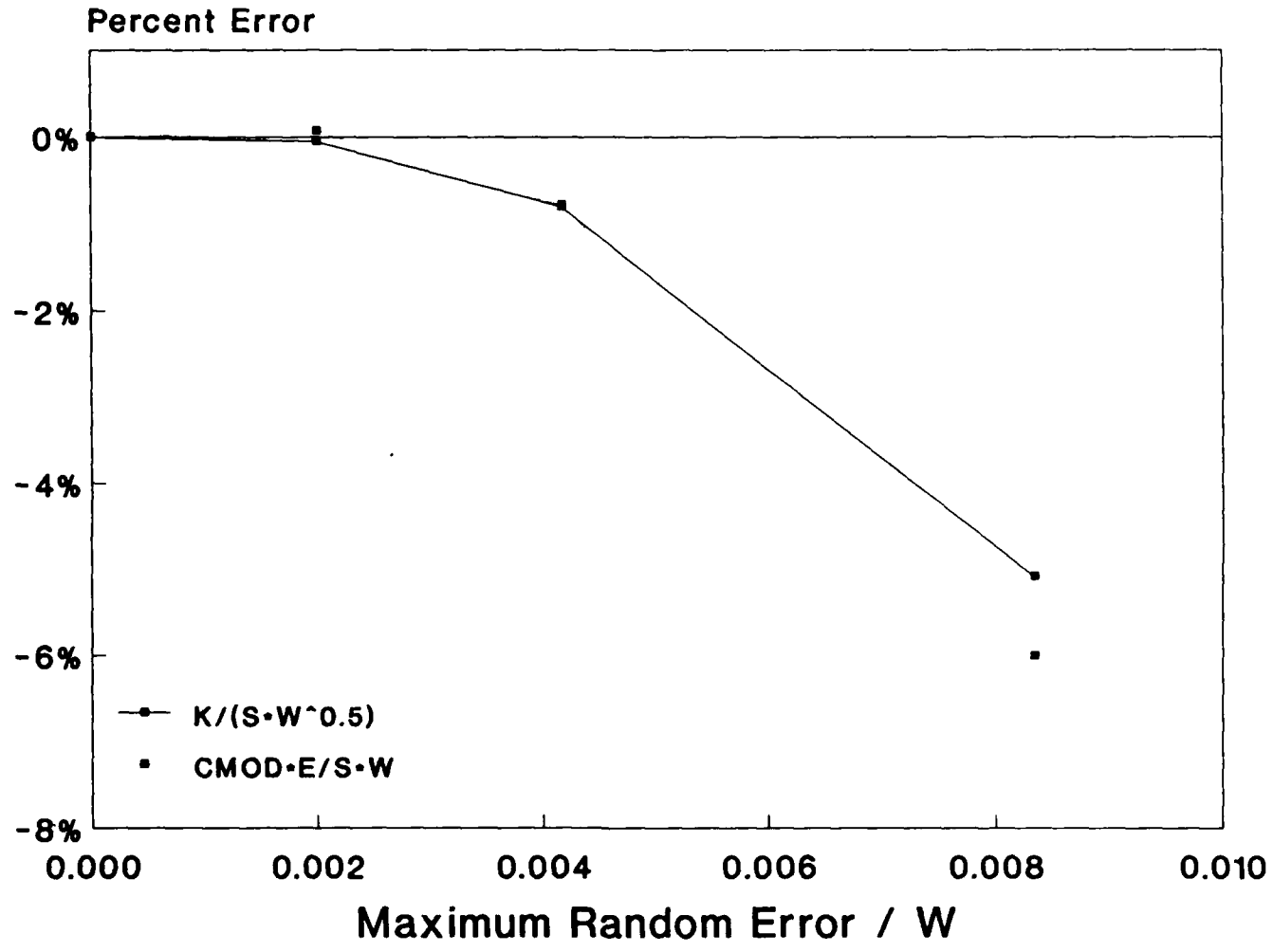

Figure 9: Effect of random error on dimensionless K and CMOD values for a conventional SE(T) specimen having the crack tip at 0.51·W.

2.2.4 Effect of the Ratio of Internal to Boundary Collocation Stations

When performing a hybrid collocation analysis, an arbitrary decision must be made regarding the relative numbers of collocation stations to be placed in the interior and on the boundary of the specimen. To investigate the influence this partitioning might have on values derived from the analysis, calculations were performed for various proportions of interior stations to boundary stations over the range of 1/7.3 to 3/1. The convergence of K_I^* with model order for these various ratios, as well as for boundary collocation, is shown in Figure 10. These data indicate that as the percentage of internal collocation stations are increased, K_I^* estimates at low model orders become progressively better approximations to the converged solution. This occurs because the interior stations possess considerable information regarding the near tip stress gradients. Inclusion of these data allow the leading series coefficients to home in on the correct values rapidly without first reducing the boundary errors to small values by including a large number of coefficients in the expansion, as is required for boundary collocation.

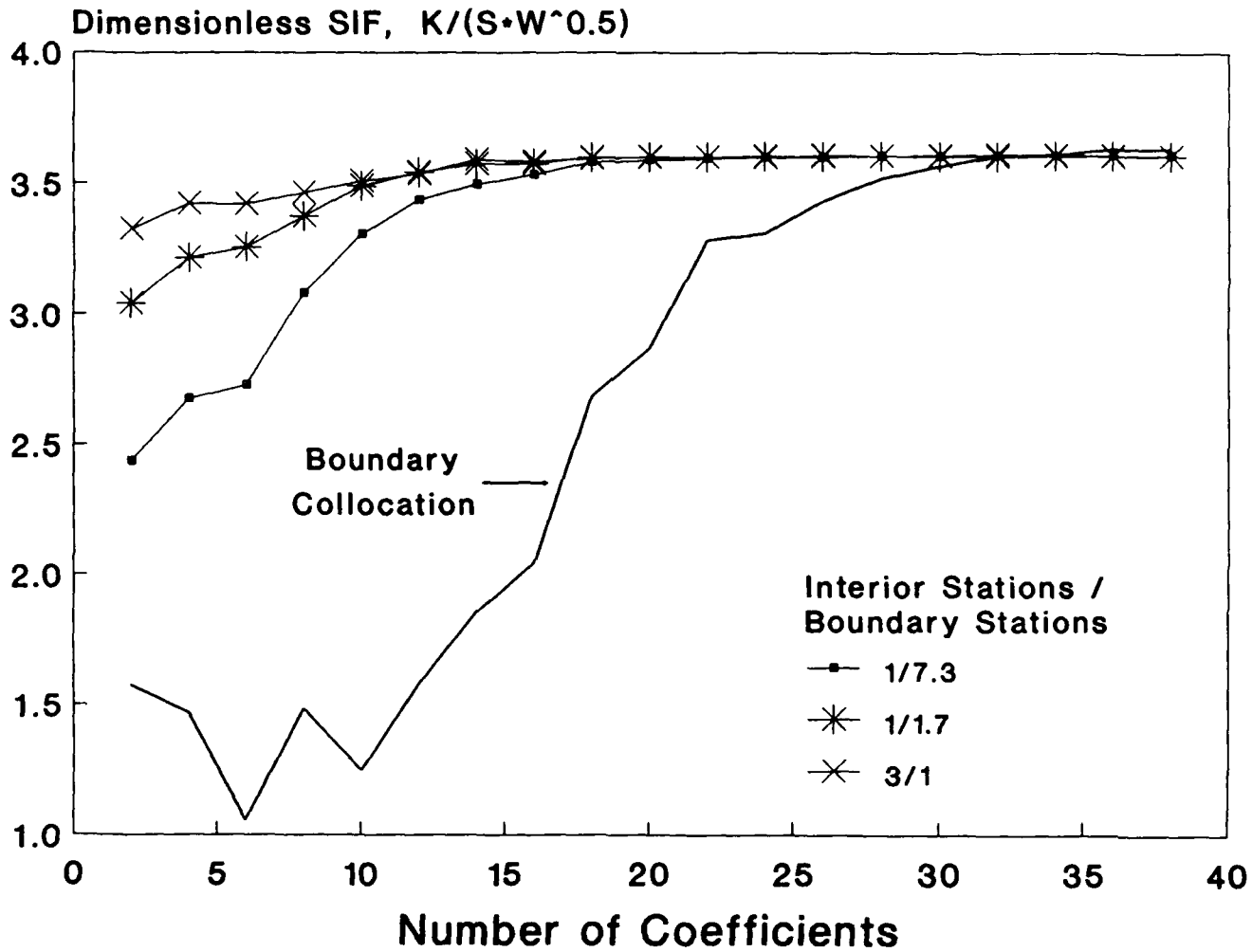

Figure 10: Effect of the ratio of internal to boundary stations on the convergence rate of dimensionless K for a conventional SE(T) specimen having the crack tip at 0.51·W.

2.3 Fixed Grip Stress Intensity Factor Calibrations

While the intent of this investigation was to determine the variation of K_I with a/W for two SE(T) geometries under fixed grip conditions, it was experimentally more convenient to apply a constant remote stress to the photoelastic models. However, Paris [29] demonstrated that a fixed grip K_I calibration can be derived from a constant stress K_I calibration by determining the relation between load (P) and load point displacement (D_P) using Castigliano's theorem. Castigliano's theorem states that the displacement of a load in its own direction is given by

$$D_P = \frac{\partial U_T}{\partial P} \tag{16}$$

where

U_T = Total strain energy

The total strain energy is the sum of that resulting from the applied load acting on an uncracked body, as well as the additional strain energy that results from introduction of a crack with the load held constant. Thus,

$$U_T = U_{NO\ CRACK} + \int_0^A \frac{\partial U_T}{\partial A}\, dA \tag{17}$$

where

A = crack area

Noting that the integrand in eqn. (17) is the strain energy release rate (G), eqn. (17) may be substituted into eqn. (16) to give

$$D_P = \frac{\partial U_{NO\ CRACK}}{\partial P} + \int_0^A \frac{\partial G}{\partial P}\, dA \qquad (18)$$

The first term in eqn. (18) is simply the load point displacement of the uncracked body. Recalling that, for an opening mode problem in plane stress,

$$G_I = \frac{K_I^2}{E} \qquad (19)$$

eqn. (18) becomes

$$D_P = D_P^{NO\ CRACK} + \frac{2}{E} \cdot \int_0^A K_I \frac{\partial K_I}{\partial P}\, dA \qquad (20)$$

For a tension loaded specimen of constant thickness, where the constant load K_I calibration is given by

$$K_I = \sigma \cdot \sqrt{\pi a} \cdot F(a/W) \qquad (21)$$

eqn. (20) may be expressed as

$$\frac{D_P \cdot E}{\sigma} = L_{eff} + \frac{2 \cdot \pi}{W} \cdot \int_0^a a \cdot F^2(a/W)\, da = H(a) \qquad (22)$$

L_{eff} represents the contribution of the uncracked specimen

to $D_p \cdot E/\sigma$. For the conventional SE(T) specimen, this is simply the distance between the loading points. However, due to the complex geometry of the uncracked modified SE(T), L_{eff} could not be determined explicitly. Instead it was calculated by first using a boundary collocation approach to generate a series solution for the stresses in the uncracked body, and then numerically integrating this solution over the entire body to determine the total stored strain energy, U_T. L_{eff} was determined from U_T using the following equation:

$$L_{eff} = \left.\frac{D_p \cdot E}{\sigma}\right|_{Uncracked} = \frac{2 \cdot E \cdot U_T}{P^2/A} \qquad (23)$$

where

P = Applied Load

Values of L_{eff} for various specimen height to maximum width ratios are presented in Table 1 for the modified SE(T) geometry tested.

Equation (22) may be solved for stress and substituted into eqn. (21) to give a constant displacement K_I calibration, as follows:

$$\frac{K_I \cdot \sqrt{W}}{D_p \cdot E} = \frac{\sqrt{\pi a W} \cdot F(a/W)}{H(a)} \qquad (24)$$

The calibration shown previously in Figure 4 for a SE(T)

specimen with L = 2·W was determined in this fashion using the F(a/W) function reported by Tada [9].

Table 1: Effective Length for the Modified SE(T) Specimen Having a Cutout of Radius 20.2% of the Maximum Specimen Width.

Actual L/W_{max}	Effective L/W_{max}
1.01	1.34
2.02	2.30
4.03	4.28

CHAPTER 3

EXPERIMENTAL TECHNIQUES

As mentioned earlier, photoelastic models were tested to obtain stresses from the specimen interior for use in the hybrid collocation analysis. Experiments were conducted in a dead weight loading fixture; weights being hung on a lever arm to reduce the required load. A multiple pin linkage was used to smoothly transfer the single point load into the models at four equally spaced points. This insured comparability with the boundary data by producing constant stress loading across the top of the model. Figure 11 shows this linkage, which was constructed to prevent any moment transfer to the specimen that could disturb this constant stress boundary condition. The effectiveness of this approach was confirmed upon initial loading of the models, when it was observed that the disturbance of the fringe pattern due to the four pin loading dissipated a very short distance from the loading points.

Both models were machined from 1/4-inch thick polycarbonate material having a nominal fringe constant (f_σ) of 7 kPa·m/fringe (40 psi·in/fringe). The exact fringe constant was determined for each model by incrementally loading a uniform section of the material

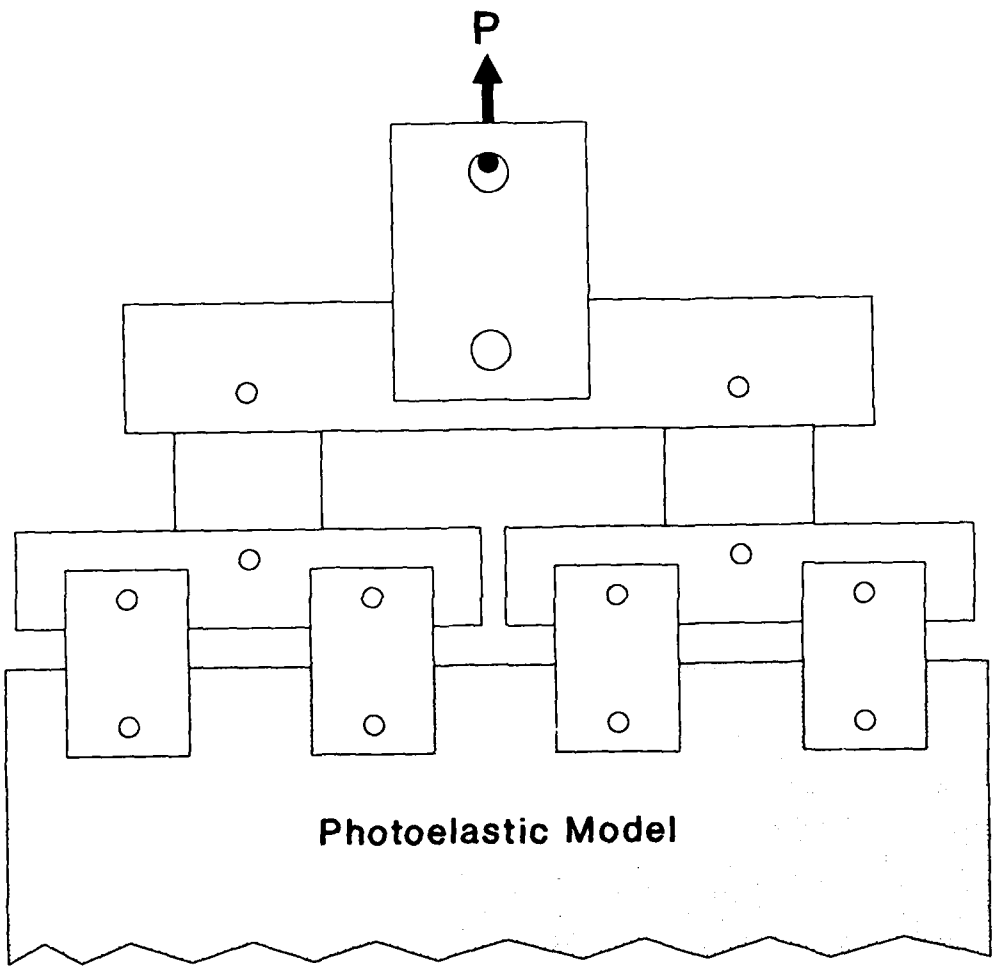

Figure 11: Multiple pin linkage used to impose a constant stress boundary condition on the photoelastic models.

and determining the fractional fringe order using Tardy compensation. The fringe constant was than calculated as the slope of the line relating the remote stress to the fringe order, divided by the model thickness.

Photographs were made on 4-inch x 5-inch positive/negative film through a full field circular polariscope illuminated with a monochromatic sodium vapor light source. At each crack length, both light and dark field photographs were taken. At short and long crack lengths, when the photographs at a single stress level did not provide an adequately detailed map of the stress contours, photographs were taken at multiple stress levels. For analysis purposes, fringes obtained at different loads were superimposed by scaling the fringe orders obtained at the auxiliary loads using the following equation:

$$N_{REF} = N_{AUX} \frac{P_{REF}}{P_{AUX}} \tag{25}$$

where

N_{REF} = fringe order scaled to the reference load
N_{AUX} = fringe order measured at the auxiliary load
P_{REF} = reference load
P_{AUX} = auxiliary load

To obtain digital data from these photographs, the negatives were placed in a photographic enlarger and projected onto a digitizing tablet attached to a personal computer. Enlargement ratios ranging from 2:1 to 5:1 were

used. Proper alignment of fringes from multiple photographs was insured by digitizing two stationary reference points in each photograph. The translation and rotation necessary to bring these points to identical locations on each photograph were then applied to all data obtained from a particular photograph.

Subsequent to scaling and rotating all of the digitized data at a given crack length, a candidate set of approximately 200 data was generated. These data were spaced so that the distance between two adjacent points on the same isochromatic decreased uniformly with the radial distance to the crack tip. To determine if any individual datum in this set had a large degree of error associated with it, the difference between the measured fringe order and that calculated from a two term local collocation solution fit to the data set was calculated. Figure 12 shows a typical plot of this difference (the fringe order error) as a function of radial distance from the crack tip. Graphs of this type were used to rapidly locate and eliminate data having fringe order errors considerably greater than the set as a whole; in this case all data having a fringe order error exceeding 0.7 were eliminated. Following this elimination, data sets ranging in size from 150 values to 220 values remained. Based on the number of photoelastic data points remaining, the number of boundary

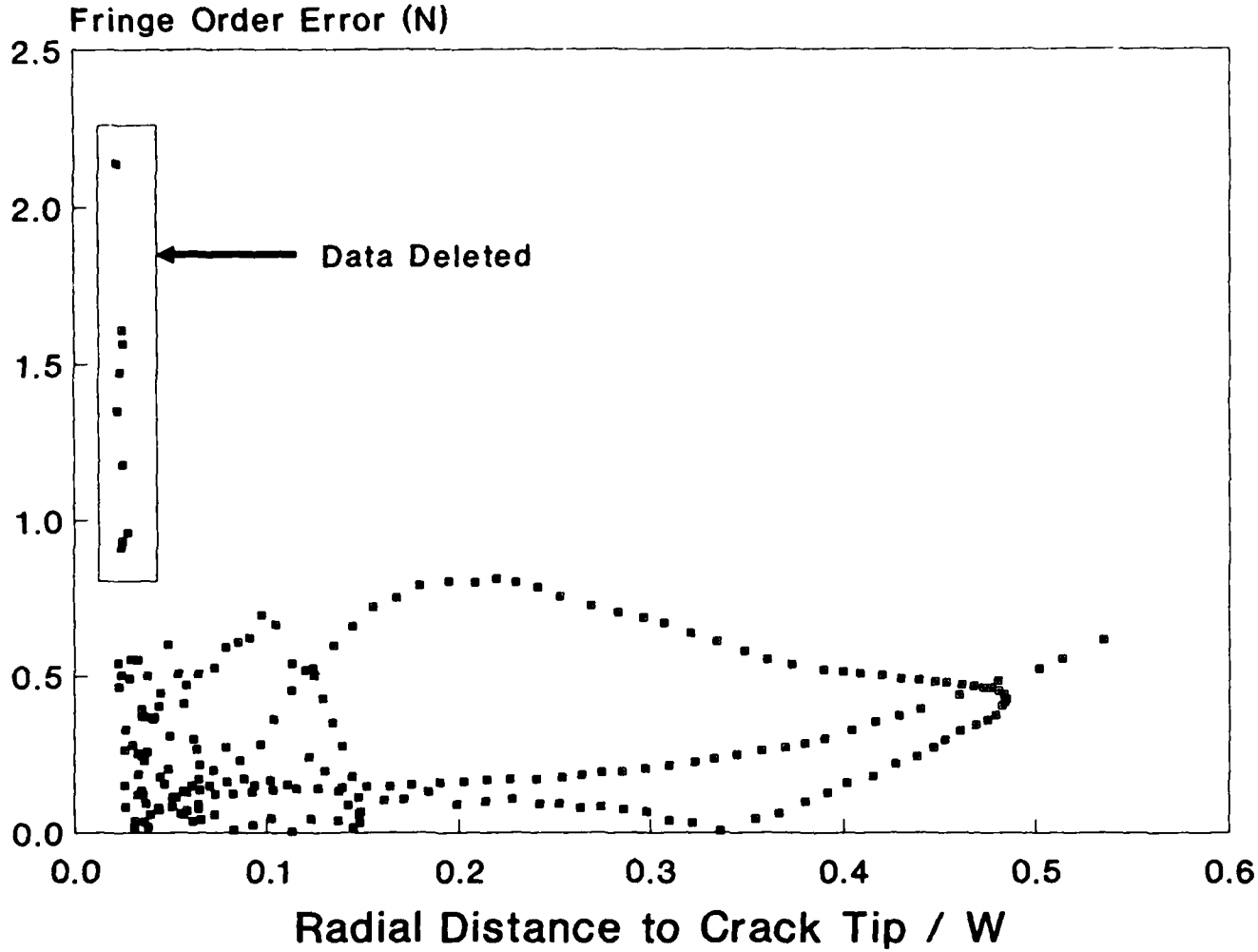

Figure 12: Fringe order error from a two term local collocation solution based on photoelastic data from a conventional SE(T) specimen having the crack tip at 0.40·W. Data points having high residuals relative to the data set were deleted prior to use in the hybrid collocation analysis.

points was scaled to give a ratio of one internal condition to every three boundary conditions.

CHAPTER 4

RESULTS AND DISCUSSION

4.1 Conventional SE(T) Specimen

To benchmark hybrid collocation results against an established solution, the variation of K_I^* and $CMOD^*$ with crack length were determined for a conventional SE(T) specimen. The variation of K_I^* with crack length for this specimen has been determined by various investigators using a wide variety of numerical [13, 18-20] and experimental [14] techniques. $CMOD^*$ calibrations have not received nearly such widespread attention, having been determined only by Gross, Roberts, and Srawley [30] using a boundary collocation technique. These previous results, along with empirical formulas due to Tada [9], are shown in Figure 13. The Tada formulas will be used to compare hybrid collocation results to these literature values.

Data obtained from a photoelastic model of a SE(T) specimen was used in this analysis. The specimen had a length to width (L/W) ratio of 2/1, which was selected based on the findings of Gross, Srawley, and Brown [13], who indicated that L/W ratios exceeding 1.6 have negligible influence on the calculated K_I^* values. The dimensions and material properties of the specimen used

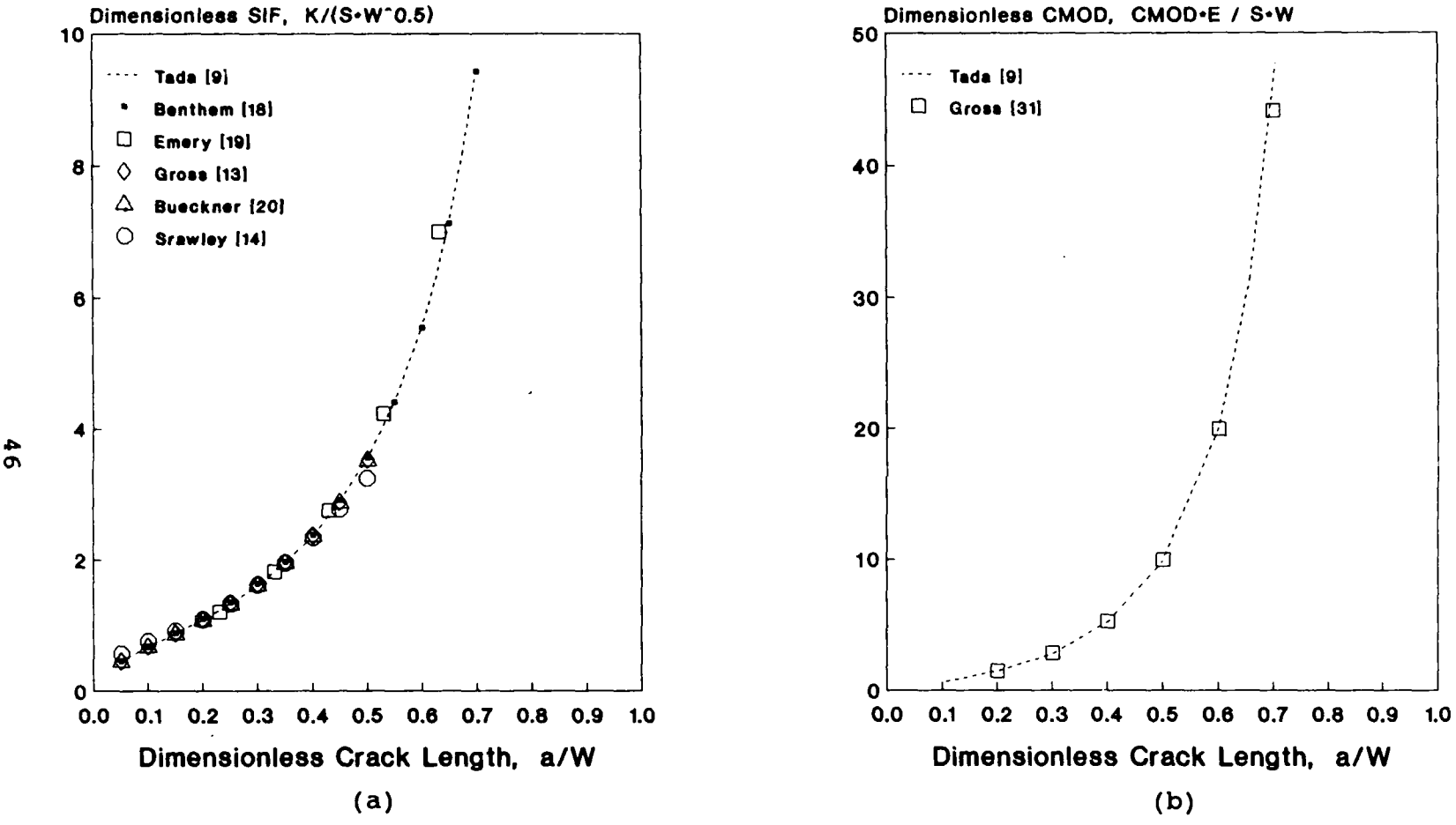

Figure 13: Literature (a) K and (b) CMOD calibrations for a conventional SE(T) specimen loaded with a constant remote stress.

are given in Figure 14.

In Figure 15, the convergence of K_I^* with increasing model order is shown for crack lengths ranging from 0.1 to 0.8 a/W; at crack lengths greater than 0.8·W, either convergence was not achieved or the RMS error indicated that the calculated values were not sufficiently accurate. The kink in the 0.4 a/W curve (Figure 15b) at 40 coefficients indicates the point at which this solution was allowed to auto-calibrate (see Section 2.2.1) by calculating Q ($f_\sigma/2 \cdot t$) as part of the least squares solution. Auto-calibration was employed when it reduced the RMS error, thus providing a solution that better matched the imposed conditions.

Figure 16 compares the K_I^* and $CMOD^*$ values determined from this analysis to the Tada formula, and to values determined from a boundary collocation analysis. As shown in Table 2, for crack lengths between 0.1·W and 0.8·W, the K_I^* and $CMOD^*$ values calculated using hybrid collocation differ from the Tada formula by at most -5.4% and -6.8%, respectively. The boundary collocation solution has equivalent accuracy only between 0.2 and 0.6 a/W. Clearly, inclusion of the data obtained from the photoelastic model was of considerable help in determining accurate K_I^* and $CMOD^*$ values for both very short and very

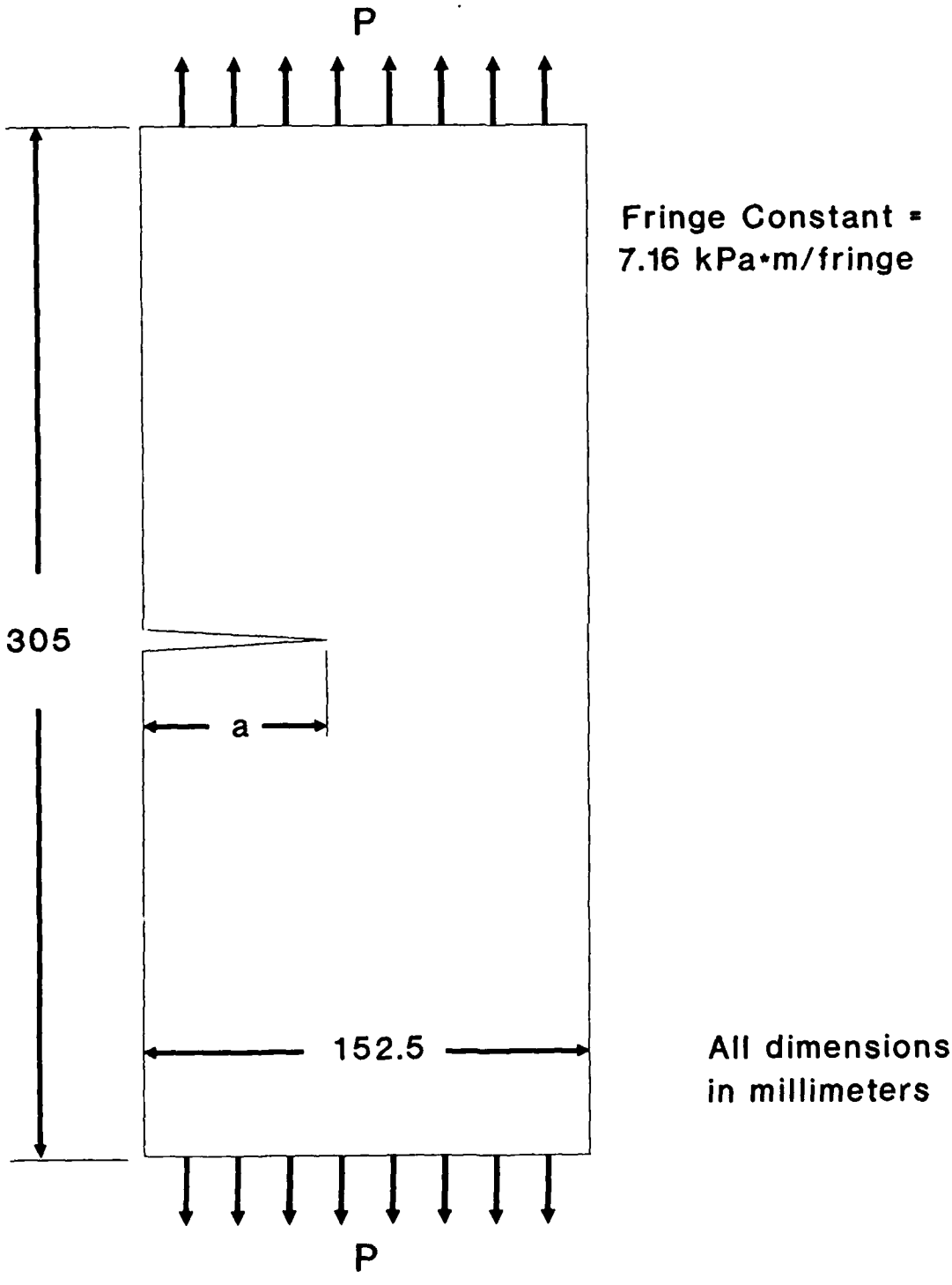

Figure 14: Dimensions and optical properties of the conventional SE(T) specimen tested.

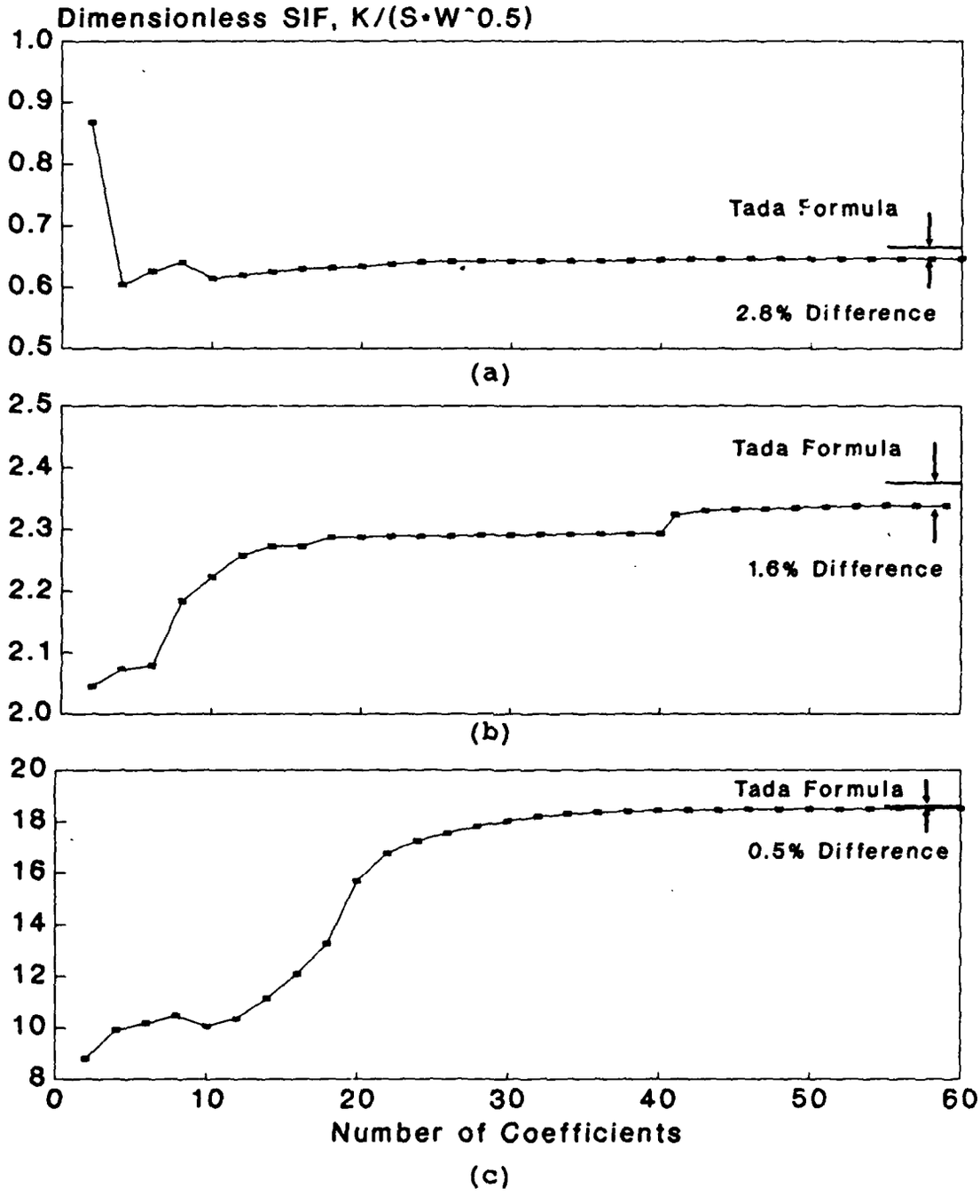

Figure 15: Convergence of dimensionless K calculated using hybrid collocation with increasing model order for a conventional SE(T) specimen having the crack tip at (a) 0.10·W, (b) 0.40·W, and (c) 0.80·W.

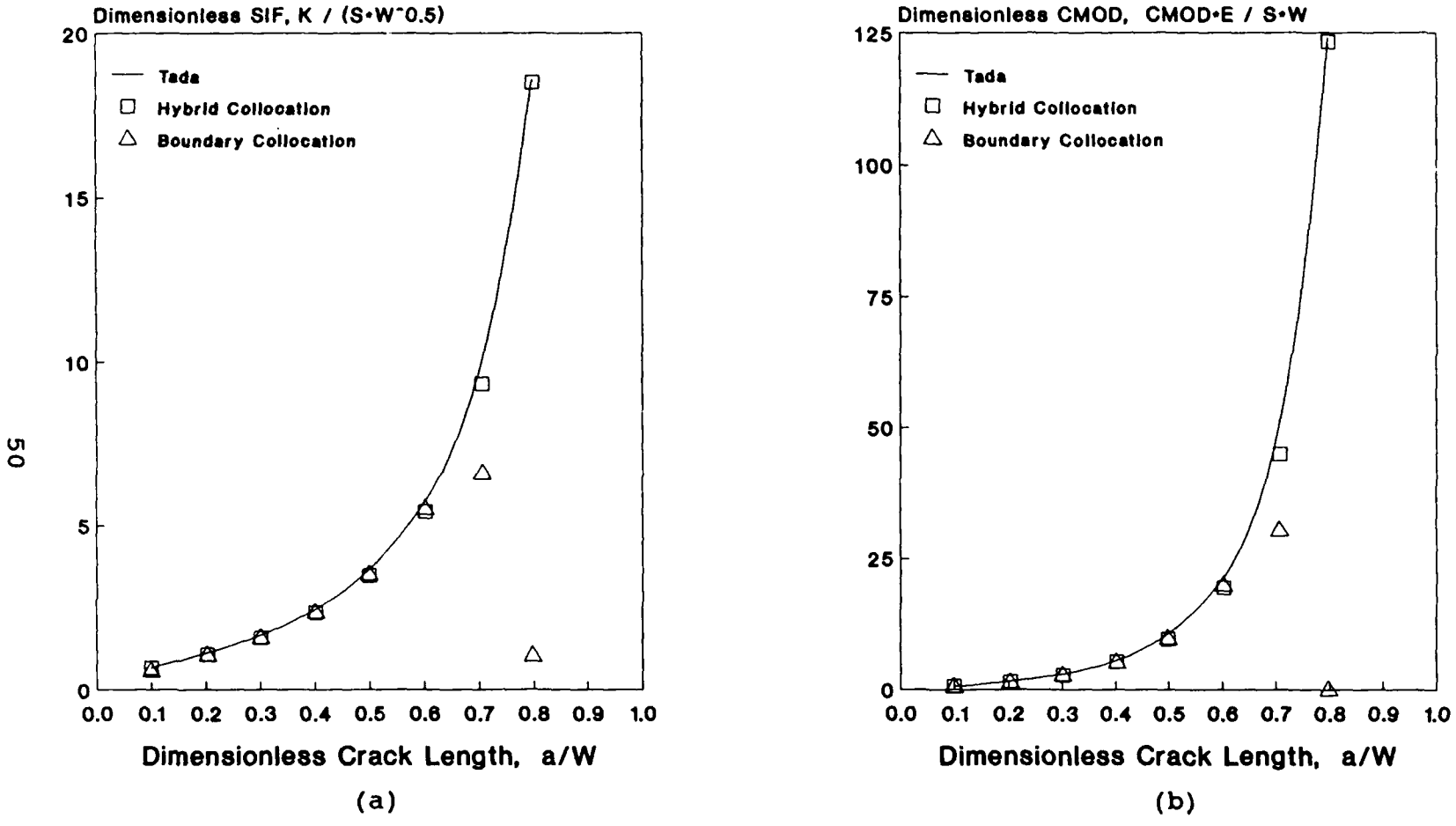

Figure 16: Comparison of hybrid collocation and boundary collocation estimates of dimensionless (a) K and (b) CMOD with the empirical formulas due to Tada [9].

Table 2: Comparison of Hybrid and Boundary Collocation K_I^* and CMOD* Results for a Conventional SE(T) Specimen with Literature Values.

Dimensionless Stress Intensity Factor, $[K_I/(\sigma \cdot \sqrt{W})]$

a/W	Hybrid Coll.	Boundary Coll.	Tada [9]	Hybrid % Diff.	Boundary % Diff.
0.0991	0.647	0.562	0.667	-2.9%	-15.7%
0.2023	1.041	1.044	1.094	-4.8%	-4.5%
0.2999	1.563	1.576	1.606	-2.7%	-1.9%
0.4013	2.338	2.360	2.375	-1.6%	-0.6%
0.4977	3.447	3.502	3.508	-1.8%	-0.2%
0.6007	5.413	5.524	5.570	-2.8%	-0.8%
0.7060	9.330	6.608	9.801	-4.8%	-32.6%
0.7974	18.505	1.026	18.606	-0.5%	-94.5%

Dimensionless CMOD, $[CMOD \cdot E/(\sigma \cdot W)]$

a/W	Hybrid Coll.	Boundary Coll.	Tada [9]	Hybrid % Diff.	Boundary % Diff.
0.0991	0.569	0.480	0.610	-6.7%	-21.3%
0.2023	1.364	1.366	1.463	-6.8%	-6.6%
0.2999	2.693	2.716	2.769	-2.7%	-1.9%
0.4013	5.149	5.202	5.208	-1.1%	-0.1%
0.4977	9.548	9.723	9.697	-1.5%	0.3%
0.6007	19.408	19.888	20.040	-3.2%	-0.8%
0.7060	44.906	30.402	47.738	-5.9%	-36.3%
0.7974	123.265	-1.743	124.120	-0.7%	-101.4%

long cracks. Additionally, Figure 17 illustrates that full field isochromatic fringe patterns calculated from a hybrid collocation series expansion matches the experimental data much better than do boundary collocation fringe patterns. For cracks deeper than 0.8·W, local collocation can be used to estimate K_I. Complete 60 coefficient solutions for the various crack lengths investigated are included in Appendix D.

As discussed in Section 2.3, the variation of K_I^* with crack length for fixed grip boundary conditions can be calculated from the data presented in Figure 16a. Because the hybrid collocation results agree with those previously reported, the Tada [9] F(a/W) function was used in eqn. (24). The results of this calculation is shown in Figure 18 for two different length to width ratios. The modified SE(T) specimen described in the following section was developed to increase the maximum K_I achievable in a tension loaded specimen subjected to fixed grip boundary conditions.

4.2 Modified SE(T) Specimen

A SE(T) specimen, modified by placing a semi-circular cutout in front of the crack, was tested and is shown in Figure 19. Figure 20 compares the convergence of K_I^* with

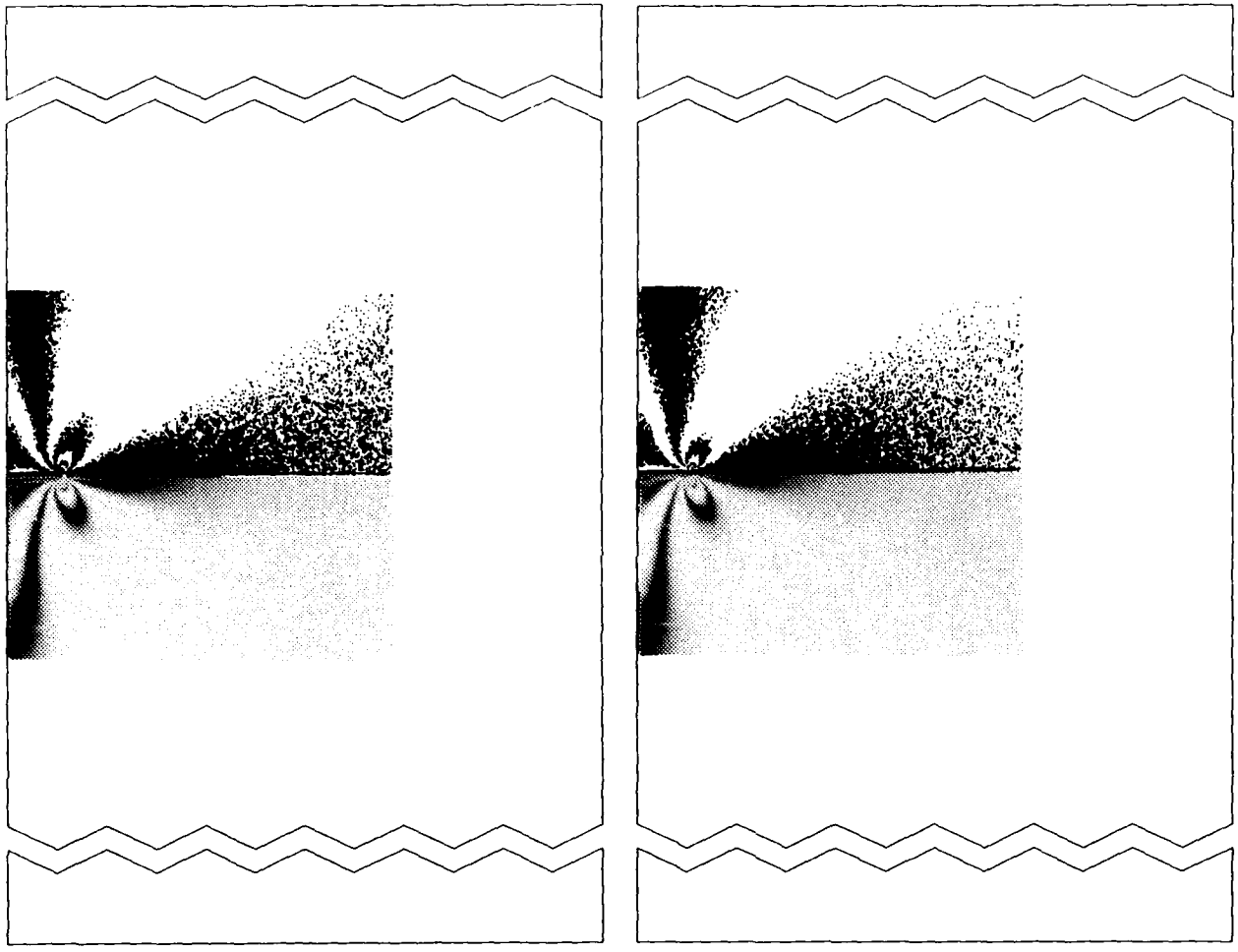

(a) (b)

Figure 17 (a,b): Comparison of experimental isochromatic fringe patterns (lower) at 0.10·W with those calculated (upper) using (a) hybrid collocation and (b) boundary collocation for a conventional SE(T) specimen. Note the fringe loop differences near the crack tip.

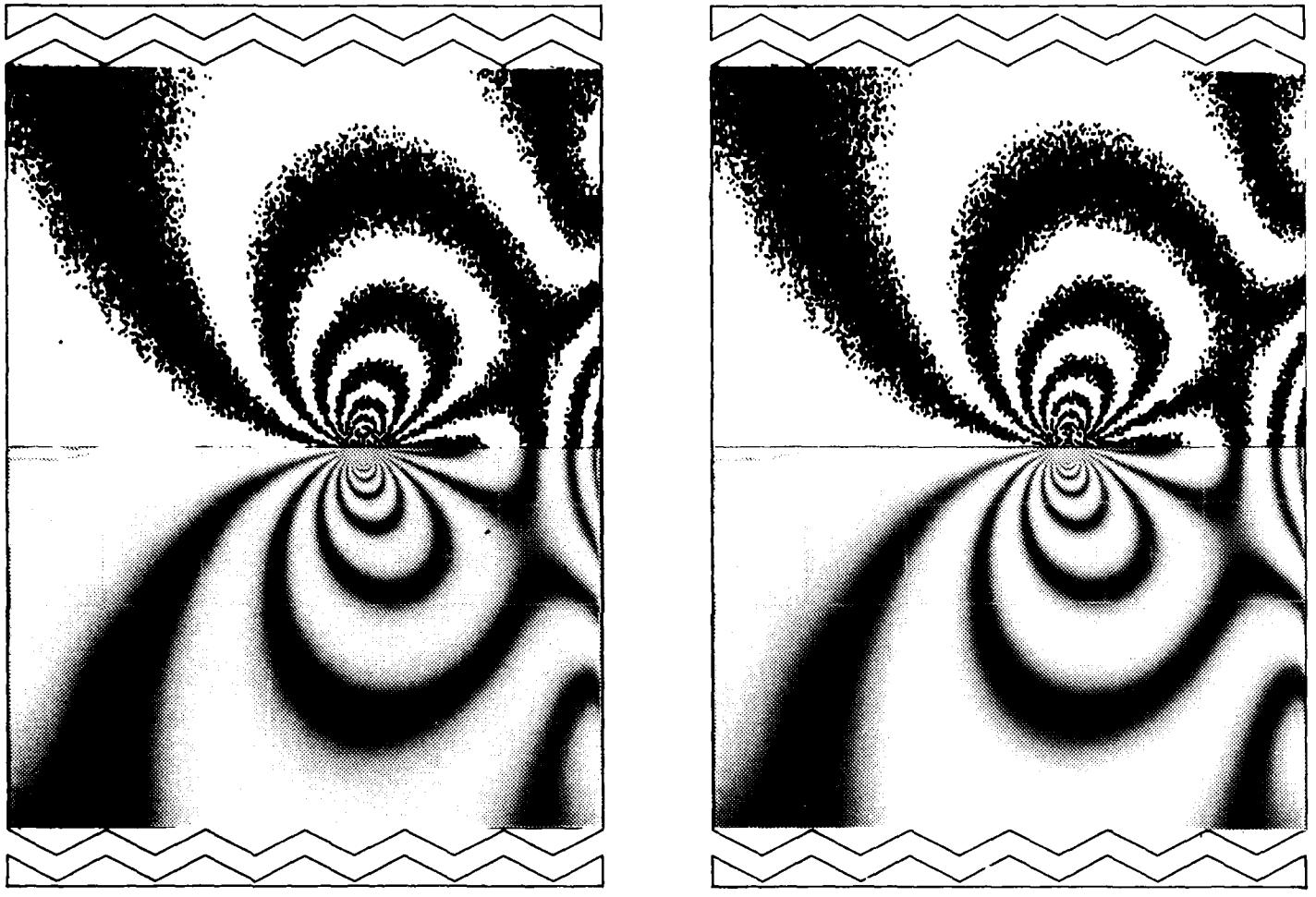

(c) (d)

Figure 17 (c,d): Comparison of experimental isochromatic fringe patterns (lower) at 0.60·W with those calculated (upper) using (c) hybrid collocation and (d) boundary collocation for a conventional SE(T) specimen. Both collocation techniques give comparable results at this crack depth.

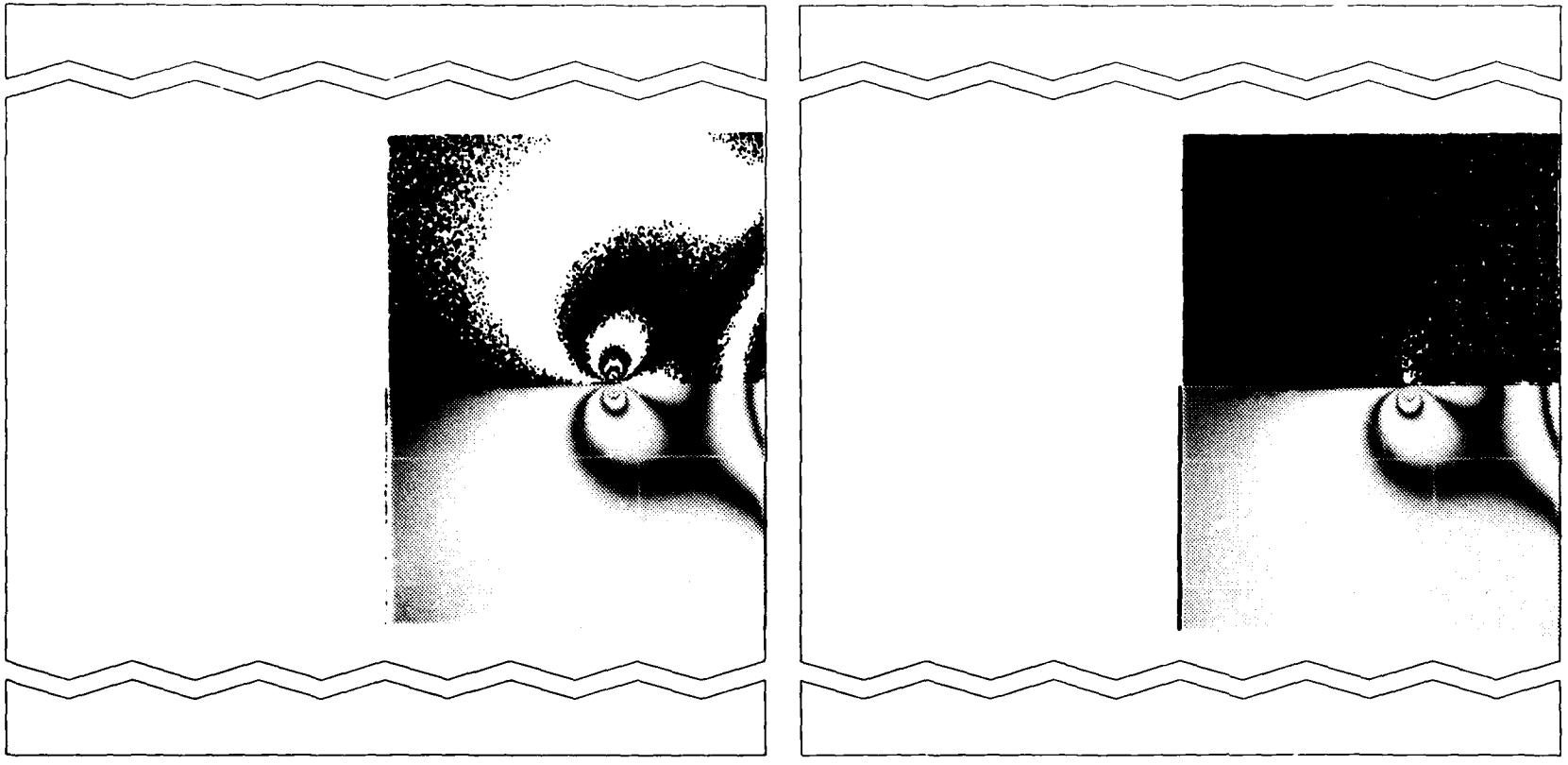

(e) (f)

Figure 17 (e,f): Comparison of experimental isochromatic fringe patterns (lower) at 0.80·W with those calculated (upper) using (e) hybrid collocation and (f) boundary collocation for a conventional SE(T) specimen. The superiority of the hybrid collocation technique is obvious.

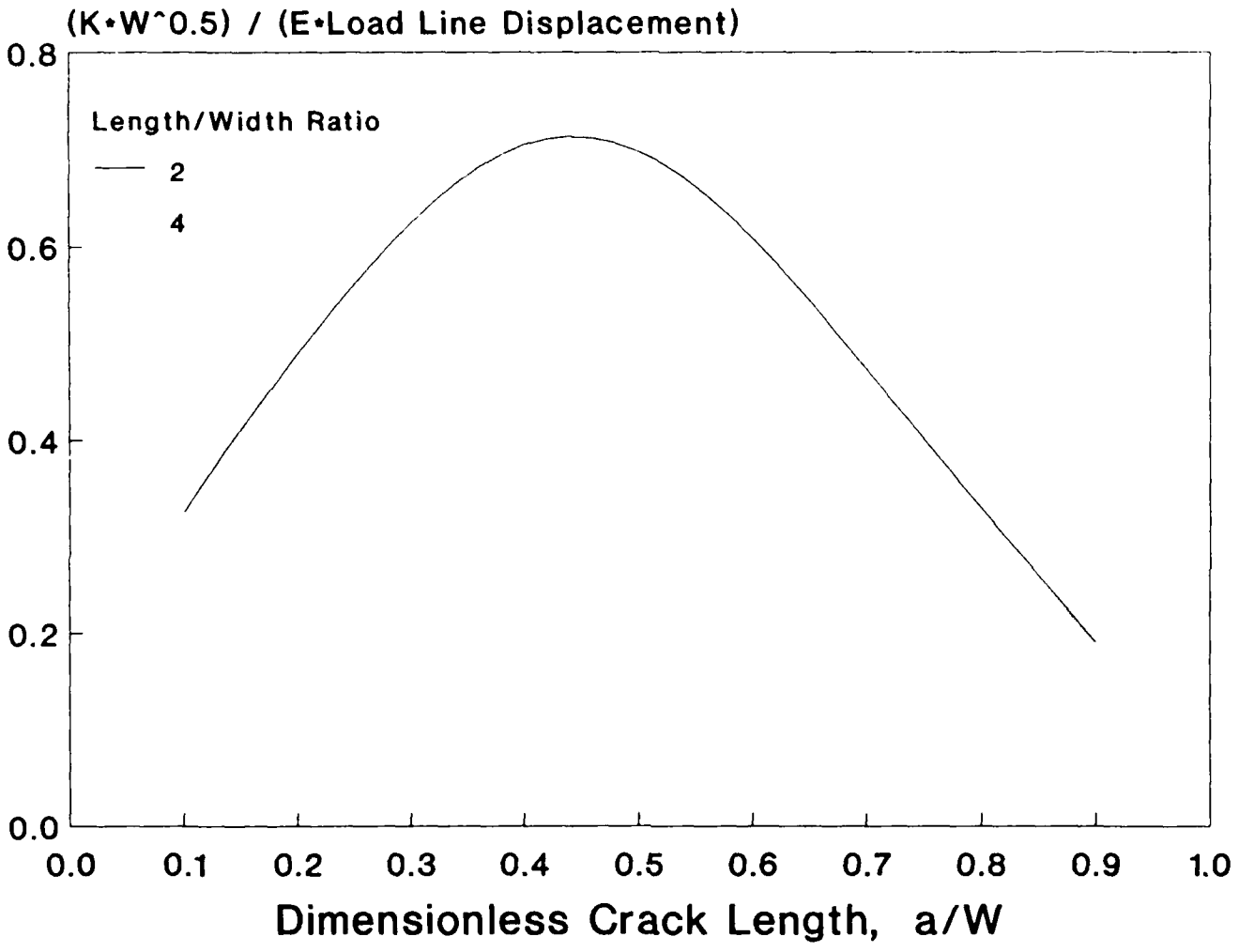

Figure 18: Fixed grip stress intensity factor calibration for conventional SE(T) specimens having various length to width ratios.

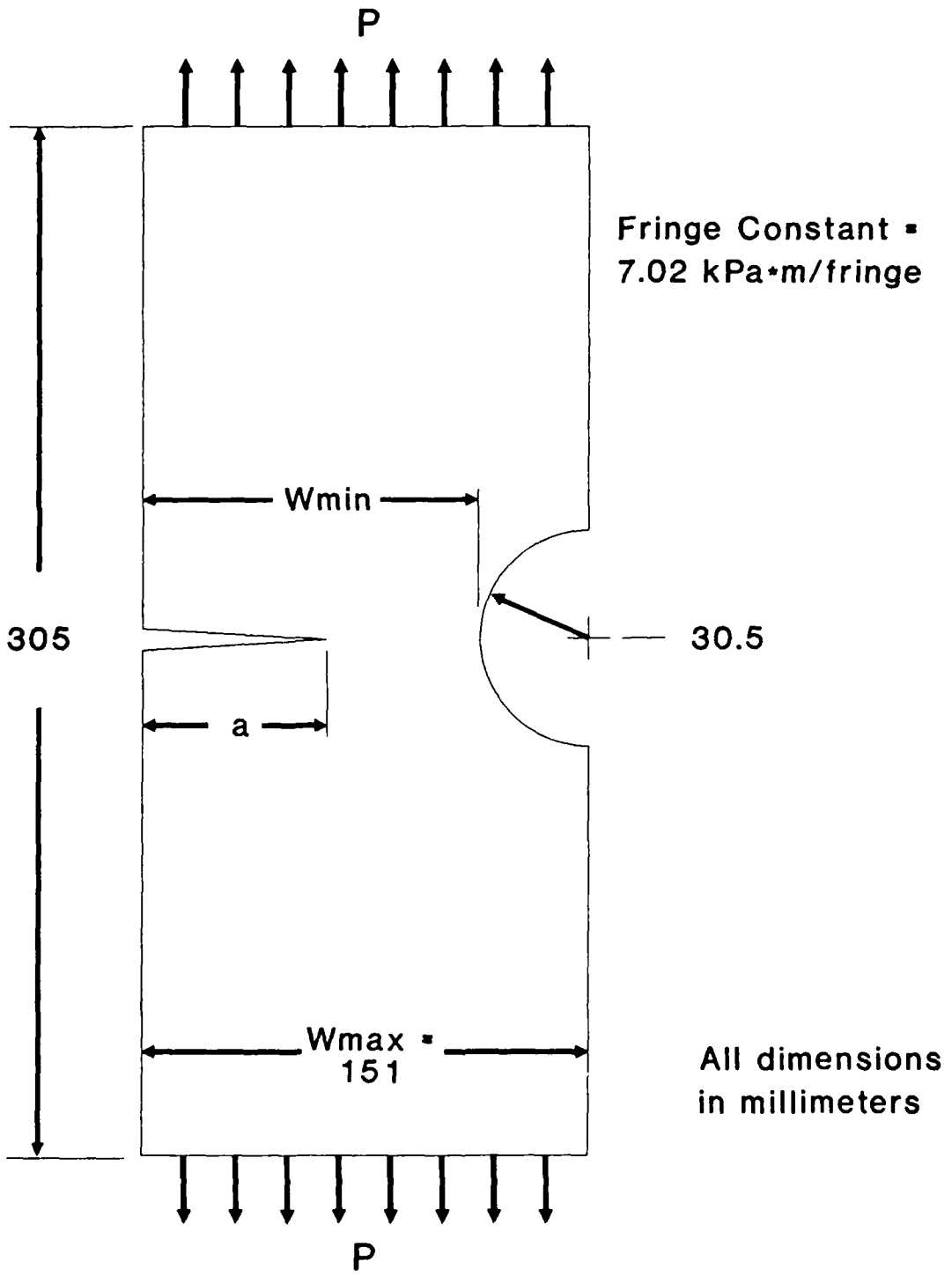

Figure 19: Dimensions and optical properties of the modified SE(T) specimen tested.

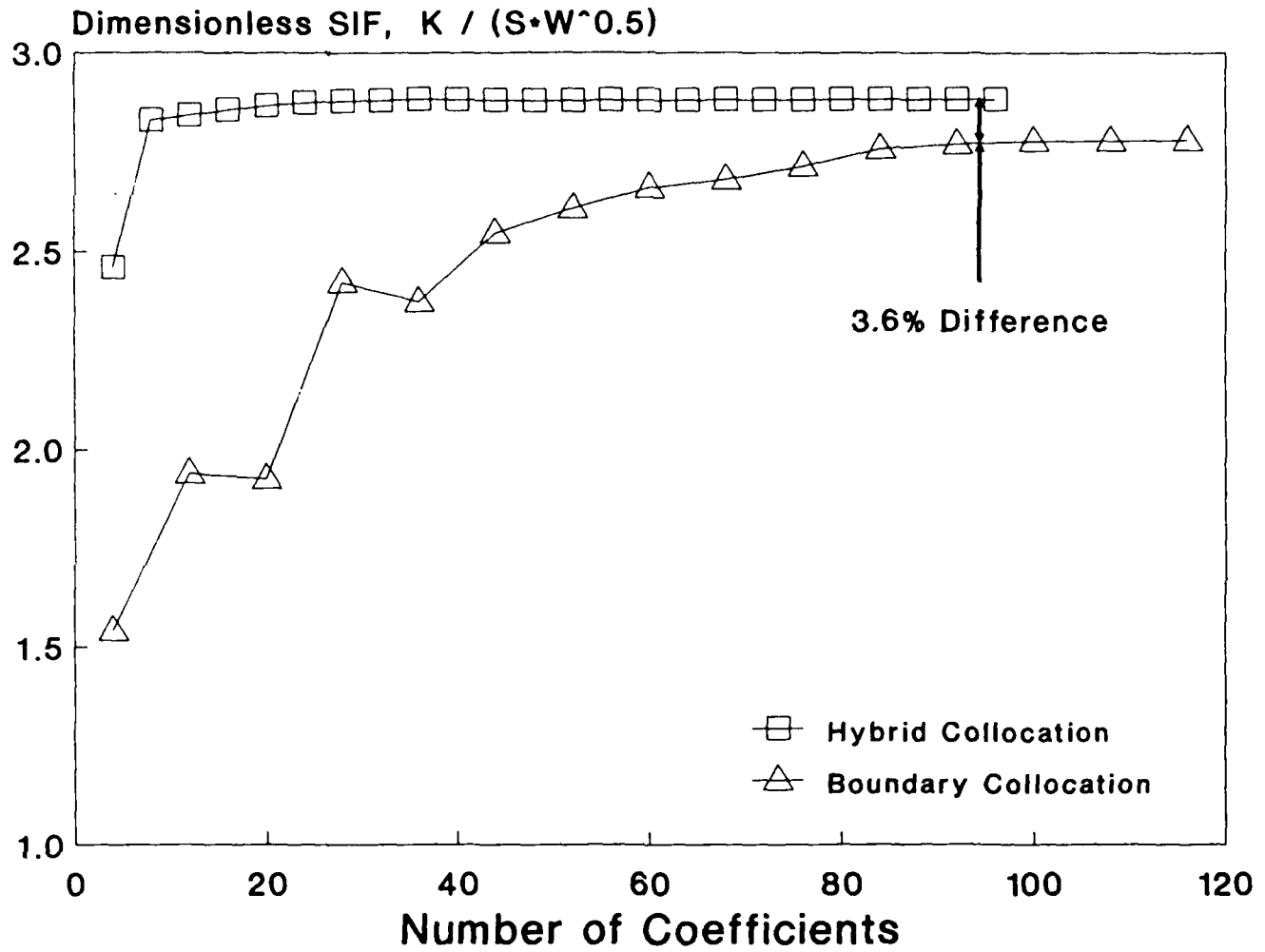

Figure 20: Convergence of dimensionless K, calculated using hybrid and boundary collocation, with increasing model order for a modified SE(T) specimen having the crack tip at 0.51·W.

increasing model order, K_I^* having been determined using both boundary and hybrid collocation techniques. These data again indicate that, for crack lengths at which both collocation techniques converge to the correct solution, inclusion of the photoelastic data leads to more rapid convergence of the hybrid collocation solution.

In Figure 21 and Table 3, the variation of K_I^* with crack length under fixed load conditions is compared for both collocation techniques. While it might appear that both boundary collocation and hybrid collocation give similar results for crack lengths of $0.4 \cdot W$ and less, a comparison of the reconstructed fringe patterns (Figure 22) demonstrates that the hybrid collocation approach produces results which more closely match the experimental data. For longer cracks ($0.5 \cdot W$ to $0.7 \cdot W$), either collocation technique works equally well, as illustrated in Figure 23.

In contrast with the conventional SE(T), boundary collocation solutions for this specimen were accurate even for very long cracks, as can be seen by comparing the boundary collocation fringe pattern to the actual photograph at $a = 0.90 \cdot W$ (Figure 24). This occurred because the stress gradient caused by the cutout was explicitly accounted for in the mathematical formulation of the problem. For the conventional SE(T) this was not

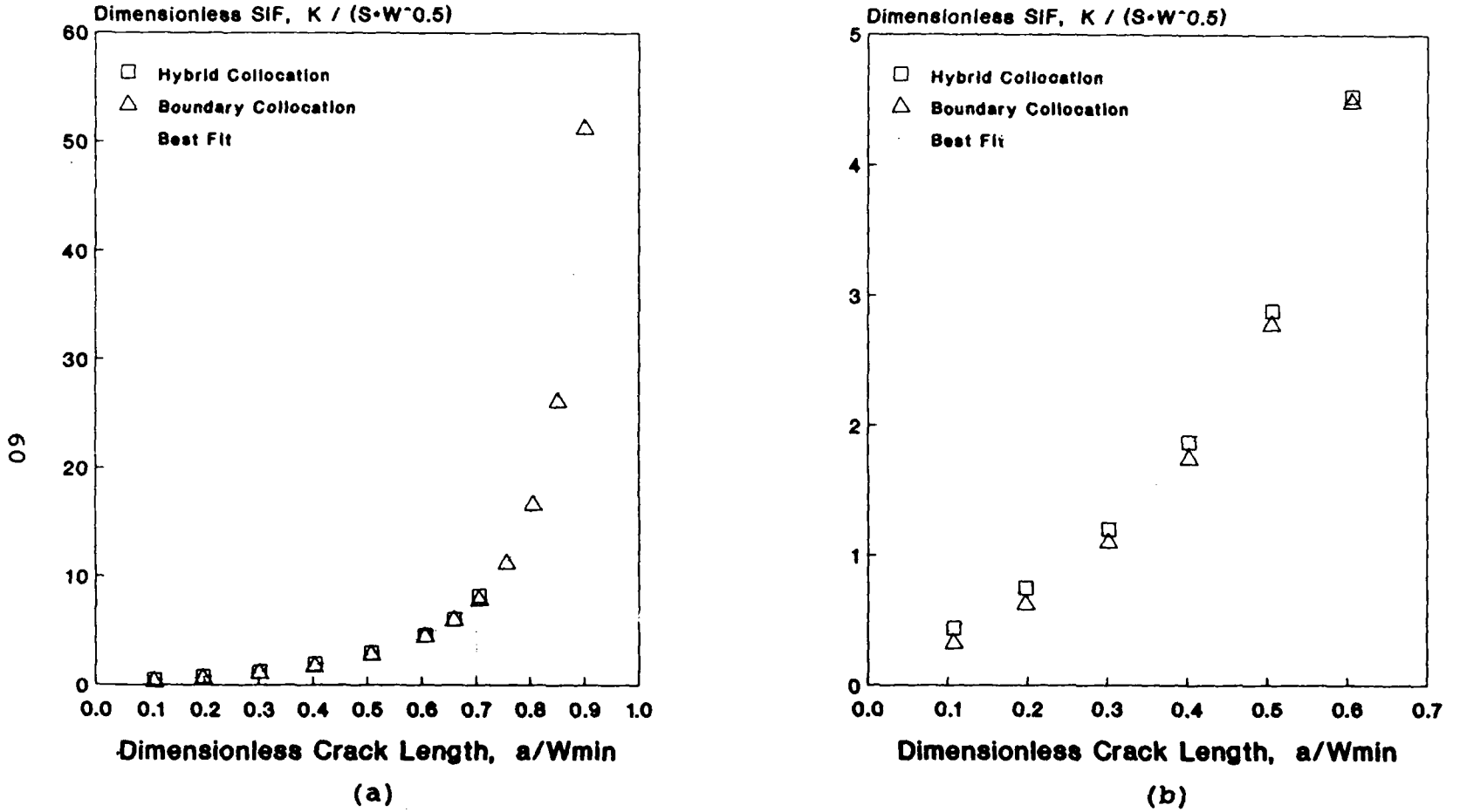

Figure 21 (a,b): Comparison of hybrid collocation and boundary collocation estimates of dimensionless K for the modified SE(T) specimen. (a) all a/W, (b) a/W < 0.6 only.

Table 3: Comparison of Hybrid and Boundary Collocation K_I* Results for a Modified SE(T) Specimen.

	Hybrid Collocation		Boundary Collocation		
a/W_{min}	$K_I/(\sigma\sqrt{\bar{W}})$	$\sigma_{err}/\sigma_{appl}$	$K_I/(\sigma\sqrt{\bar{W}})$	$\sigma_{err}/\sigma_{appl}$	% Diff
0.107	0.438*	1.7%	0.325	1.7%	34.8%
0.197	0.744*	1.5%	0.628	1.6%	18.5%
0.301	1.188*	2.2%	1.106	1.3%	7.4%
0.402	1.869*	1.8%	1.748	1.0%	7.0%
0.506	2.882*	2.0%	2.781*	0.7%	3.6%
0.605	4.525*	1.3%	4.488*	0.5%	0.8%
0.659	5.978*	3.0%	6.007*	0.5%	-0.5%
0.704	8.160	8.3%	7.884*	0.4%	3.5%
0.756			11.221*	0.4%	
0.805			16.651*	0.4%	
0.850			26.151*	0.4%	
0.900			51.242*	0.3%	

* Solutions that produce fringe plots which match the experimental data.

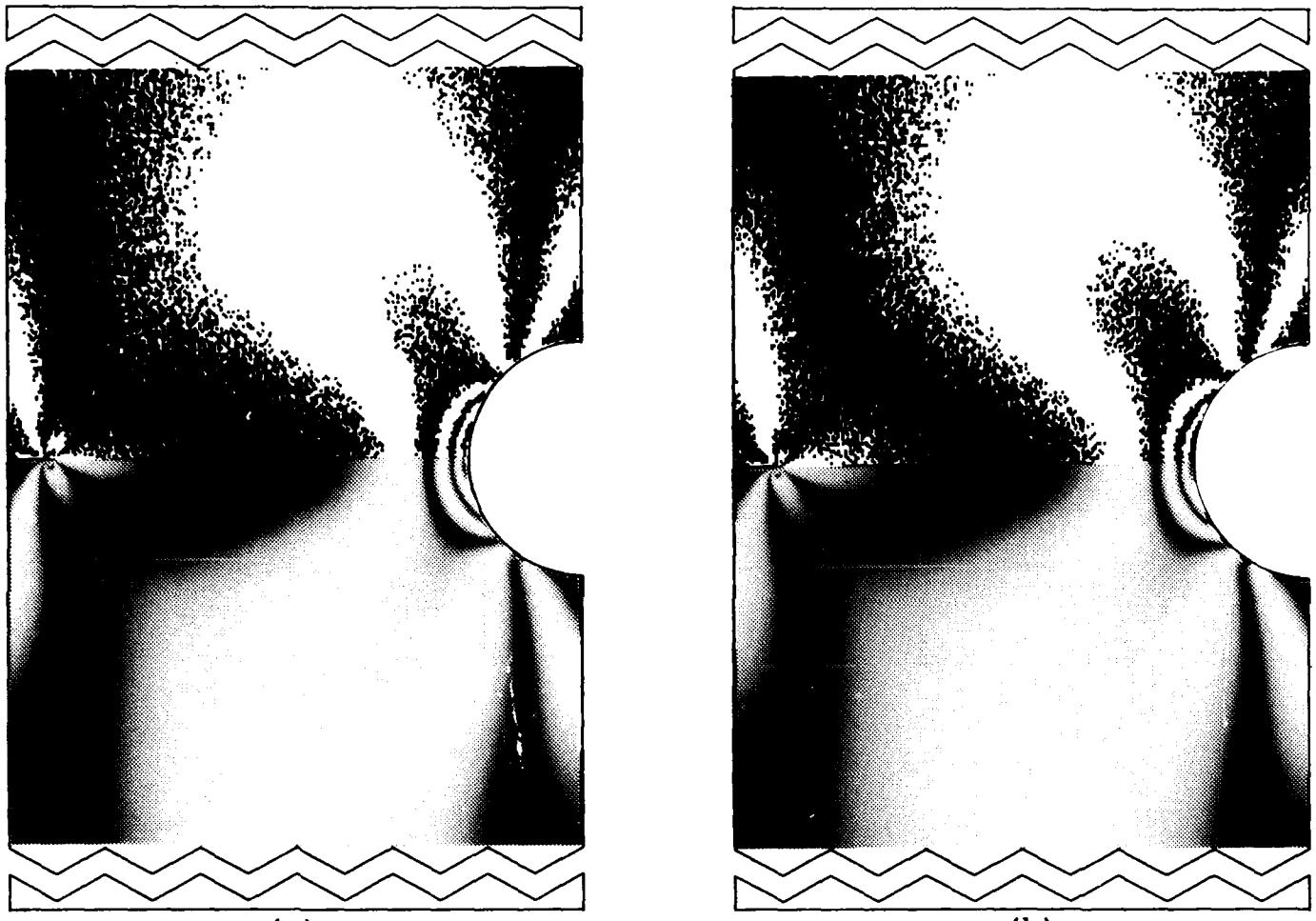

(a) (b)

Figure 22 (a,b): Comparison of experimental isochromatic fringe patterns (lower) at 0.1·W with those calculated (upper) using (a) hybrid collocation and (b) boundary collocation for a modified SE(T) specimen. Note the subtile differences between the calculated patterns at the crack tip.

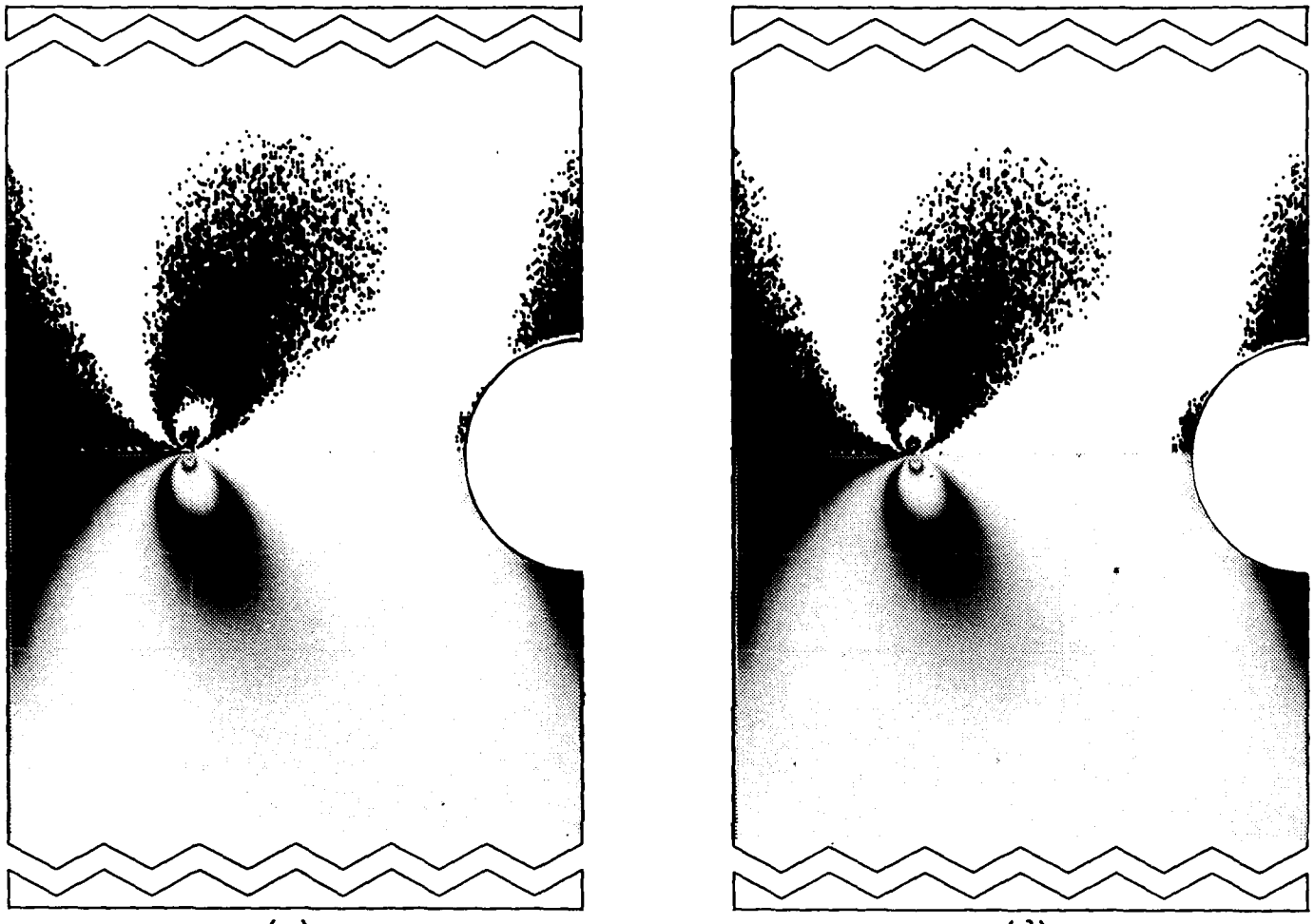

(c) (d)

Figure 22 (c,d): Comparison of experimental isochromatic fringe patterns (lower) at 0.4·W with those calculated (upper) using (c) hybrid collocation and (d) boundary collocation for a modified SE(T) specimen. Note the slight fringe loop differences near the crack tip.

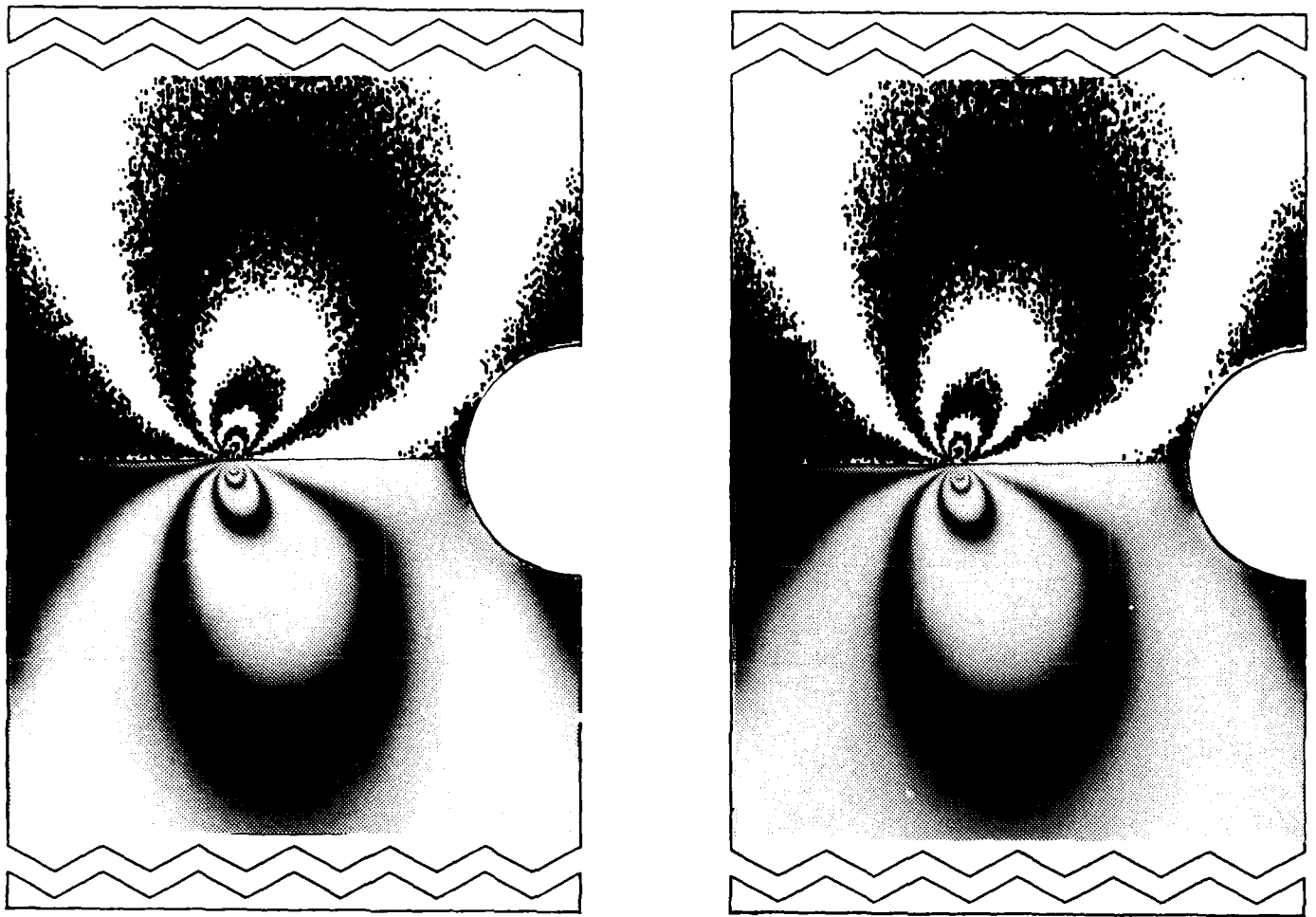

(a) (b)

Figure 23: Comparison of experimental isochromatic fringe patterns (lower) with those calculated (upper) using (a) hybrid collocation and (b) boundary collocation for a modified SE(T) specimen at 0.506·W. Both collocation techniques give comparable results at this crack depth.

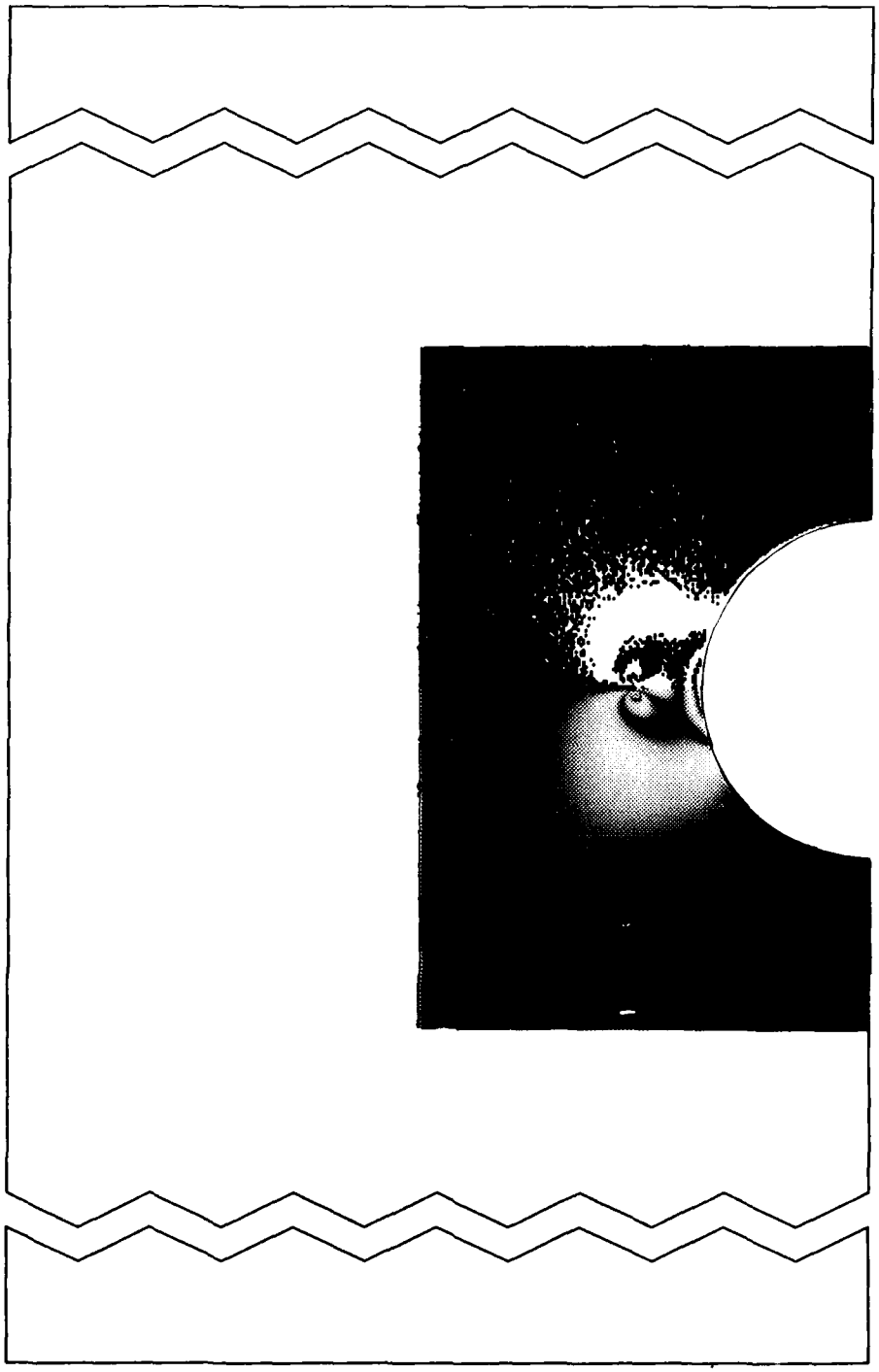

Figure 24: Comparison of experimental isochromatic fringe patterns with those calculated using boundary collocation for the modified SE(T) specimen at 0.90·W.

the case, the mathematical formulation requiring that stresses continuously decrease as the distance from the crack tip increases.

As was seen for the conventional SE(T), there is a maximum a/W beyond which the hybrid collocation solution does not agree well with the experimental results. For the conventional SE(T), this limit was $0.8 \cdot W$, while for the modified SE(T) it was $0.65 \cdot W_{min}$. This lack of agreement results from insufficient accuracy of the photoelastic data in these cases, rather than any theoretical limitations of the hybrid collocation technique. The small physical size of the deep crack fringe patterns caused the effects of random position errors on the hybrid collocation solution to be quite large. This, combined with the considerable influence that these data have on the solution due to their close proximity to the crack tip, caused the RMS error to stabilize at a high value, indicating that these solutions did not match the imposed conditions well. An experiment in which the photoelastic fringes were recorded at higher magnifications, and the small loads applied to the specimen measured more accurately than was possible with the loading fixture employed in this study, would most likely produce more accurate hybrid collocation results.

In Figure 25, the fixed grip variation of K_I^* with crack length is compared for conventional and modified SE(T) specimens. These data indicate that there are two advantages to the modified SE(T) specimen design. First, there is a slight increase in the region of the specimen over which K_I increases with increasing crack length. Second, and more significant, there is nearly a factor of two increase (assuming an initial crack depth of $0.1 \cdot W$) in maximum K_I from that achievable with a conventional SE(T) specimen of the same overall dimensions. This feature makes the modified SE(T) a useful specimen for characterization of crack arrest toughness in the upper transition region.

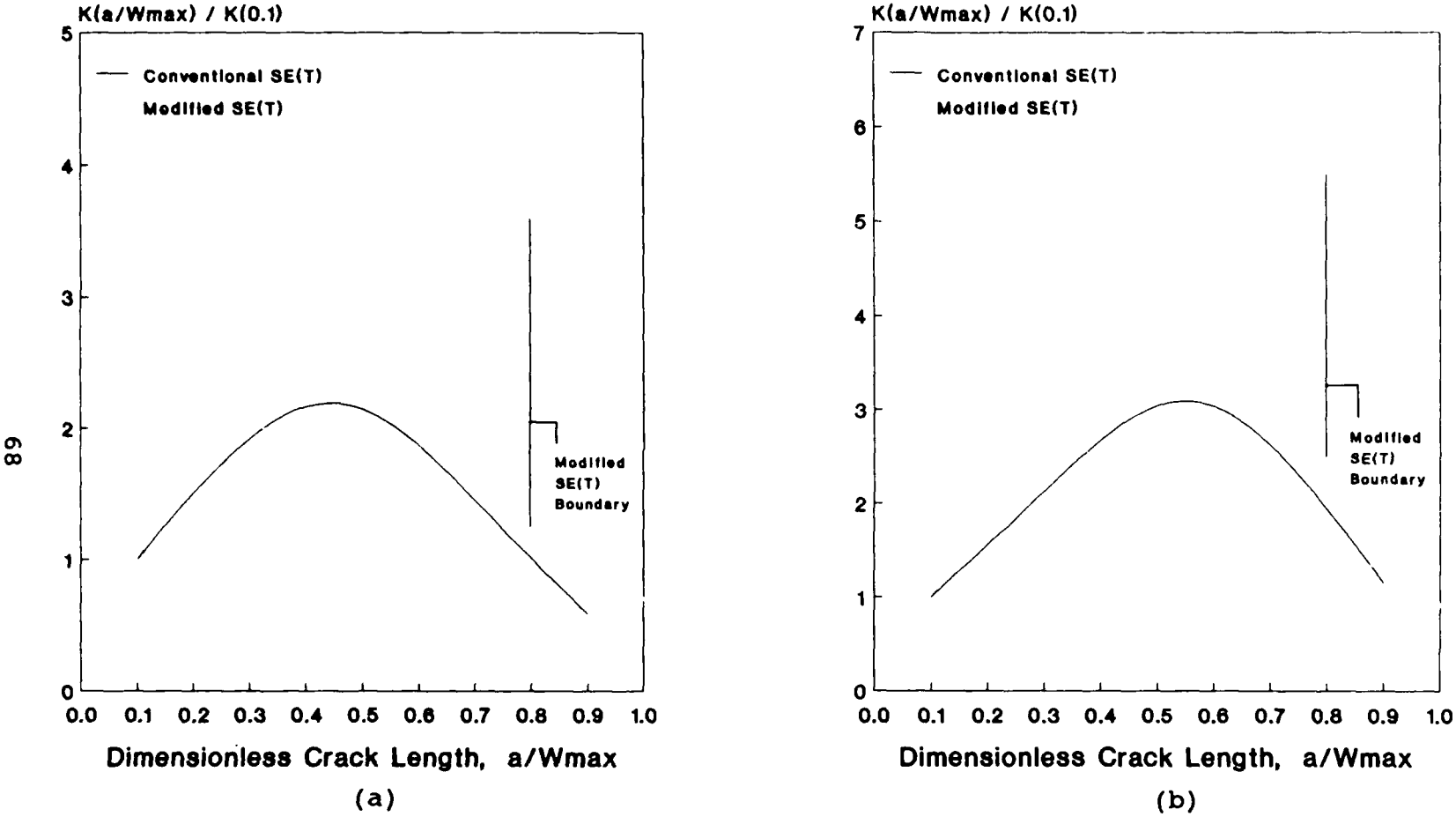

Figure 25: Comparison of fixed grip stress intensity factor calibrations for conventional and modified SE(T) specimens having length to width ratios of (a) 2:1, and (b) 4:1.

CHAPTER 5

SUMMARY AND CONCLUSIONS

A combined experimental/numerical collocation technique was developed for analysis of finite body, single-ended crack problems. This technique, referred to as hybrid collocation, uses stress conditions from the boundary (known a priori) and from the interior (determined experimentally) of a cracked specimen to specify the imposed loading. The variation of the mode one stress intensity factor, K_I, and the crack mouth opening displacement, CMOD, with crack length was determined for two specimen geometries using this technique. One specimen was a conventional single edge notch tension, SE(T), while the other was a SE(T) modified by placing a semi-circular cutout in front of the crack. Based on the results of these analyses, the following conclusions may be drawn:

1. K_I and CMOD were accurately determined between 0.1 and 0.65 or 0.80 a/W when both internal and boundary stress conditions were used to specify the loading imposed on the specimen. This is a much wider range of crack lengths than can be obtained using boundary collocation alone.

2. Inclusion of stress conditions from the interior of a cracked specimen causes the calculated K_I and CMOD values to converge much more rapidly than would be possible otherwise.

3. The modified SE(T) specimen can produce K_I values approximately two times greater than can a conventional SE(T) specimen of the same size, assuming an initial crack depth of $0.1 \cdot W$ and fixed grip boundary conditions. Thus, the modified SE(T) specimen could be used to investigate upper transition crack arrest phenomena with smaller specimens and testing machine capacities than were previously possible.

APPENDIX A

SERIES EXPANSIONS OF STRESS AND DISPLACEMENT EQUATIONS

The functions Z(z) and Y(z), given by eqs. (3) and (4) may be substituted into eqs. (2), and (6) to give expressions for stress and displacement in series expansion form as follows:

$$\sigma_{xx} =$$

$$\sum_{j=0}^{J} A_j'(r/W)^{j-1/2}\Big[\cos[(j-1/2)\theta] - (j-1/2)\cdot\sin\theta\cdot\sin[(j-3/2)\theta]\Big] +$$

$$\sum_{m=0}^{M} B_m'(r/W)^{m}\Big[2\cdot\cos(m\theta) - m\cdot\sin\theta\cdot\sin[(m-1)\theta]\Big] +$$

$$\sum_{u=1}^{U} C_u'\frac{W^{u+1/2}}{r^{*u}\sqrt{r}}\Big[\cos(\theta/2)\cdot\cos(u\theta^*) - \sin(\theta/2)\cdot\sin(u\theta^*) - u\cdot\sin\theta^*\Big[\cos[\theta/2]\cdot\sin[(u+1)\theta^*] + \sin(\theta/2)\cdot\cos[(u+1)\theta^*]\Big] - 1/2\cdot\sin\theta\Big[\cos(3\cdot\theta/2)\cdot\sin(u\theta^*) + \sin(3\cdot\theta/2)\cdot\cos(u\theta^*)\Big]\Big] +$$

$$\sum_{v=1}^{V} D_v'(W/r^*)^{v}\Big[2\cdot\cos(v\theta^*) - v\cdot\sin\theta^*\cdot\sin[(v+1)\theta^*]\Big] \qquad (A1)$$

$$\sigma_{yy} =$$

$$\sum_{j=0}^{J} A_j'(r/W)^{j-1/2}\Big[\cos[(j-1/2)\theta] + (j-1/2)\cdot\sin\theta\cdot\sin[(j-3/2)\theta]\Big] +$$

$$\sum_{m=0}^{M} B_m'(r/W)^m\Big[m\cdot\sin\theta\cdot\sin[(m-1)\theta]\Big] +$$

$$\sum_{u=1}^{U} C_u'\frac{W^{u+1/2}}{r^{*u}\sqrt{r}}\Bigg[\cos(\theta/2)\cdot\cos(u\theta^*) - \sin(\theta/2)\cdot\sin(u\theta^*) + u\cdot\sin\theta^*\Big[\cos(\theta/2)\cdot\sin[(u+1)\theta^*] + \sin(\theta/2)\cdot\cos[(u+1)\theta^*]\Big] + 1/2\cdot\sin\theta\Big[\cos(3\cdot\theta/2)\cdot\sin(u\theta^*) + \sin(3\cdot\theta/2)\cdot\cos(u\theta^*)\Big]\Bigg] +$$

$$\sum_{v=1}^{V} D_v'(W/r^*)^v\Big[v\cdot\sin\theta^*\cdot\sin[(v+1)\theta^*]\Big] \qquad (A2)$$

$$\tau_{xy} =$$

$$\sum_{j=0}^{J} -A_j'(r/W)^{j-1/2}\Big[(j-1/2)\cdot\sin\theta\cdot\cos[(j-3/2)\theta]\Big] -$$

$$\sum_{m=0}^{M} B_m'(r/W)^m\Big[m\cdot\sin\theta\cdot\cos[(m-1)\theta] + \sin(m\theta)\Big] +$$

$$\sum_{u=1}^{U} C_u'\frac{W^{u+1/2}}{r^{*u}\sqrt{r}}\Bigg[u\cdot\sin\theta^*\Big[\cos(\theta/2)\cdot\cos[(u+1)\theta^*] - \sin(\theta/2)\cdot\sin[(u+1)\theta^*]\Big] + 1/2\cdot\sin\theta\Big[\cos(3\cdot\theta/2)\cdot\cos(u\theta^*) - \sin(3\cdot\theta/2)\cdot\sin(u\theta^*)\Big]\Bigg] +$$

$$\sum_{v=1}^{V} D_v'(W/r^*)^v\Big[v\cdot\sin\theta^*\cdot\cos[(v+1)\theta^*] + \sin(v\theta^*)\Big] \qquad (A3)$$

$$
\begin{aligned}
\tau_{max}^2 = & \\
& \left[\sum_{j=0}^{J} -A_j'(r/W)^{j-1/2}\left[(j-1/2)\cdot\sin\theta\cdot\sin[(j-3/2)\theta]\right] + \right. \\
& \sum_{m=0}^{M} B_m'(r/W)^m\left[\cos(m\theta) - m\cdot\sin\theta\cdot\sin[(m-1)\theta]\right] - \\
& \sum_{u=1}^{U} C_u'\frac{W^{u+1/2}}{r^{*u}/r}\left[u\cdot\sin\theta^*\cdot\right. \\
& \quad \left[\cos(\theta/2)\cdot\sin[(u+1)\theta^*] + \sin(\theta/2)\cdot\cos[(u+1)\theta^*]\right] \\
& + \frac{1}{2\sin\theta}\left[\cos(3\cdot\theta/2)\cdot\sin(u\theta^*) + \sin(3\cdot\theta/2)\cdot\cos(u\theta^*)\right]\Big] + \\
& \left. \sum_{v=1}^{V} D_v'(W/r^*)^v\left[\cos(v\theta^*) - v\cdot\sin\theta^*\cdot\sin[(v+1)\theta^*]\right]\right]^2 \\
+ & \left[\sum_{j=0}^{J} -A_j'(r/W)^{j-1/2}\left[(j-1/2)\cdot\sin\theta\cdot\cos[(j-3/2)\theta]\right]\right. \\
& - \sum_{m=0}^{M} B_m'(r/W)^m\left[m\cdot\sin\theta\cdot\cos[(m-1)\theta] + \sin(m\theta)\right] \\
& + \sum_{u=1}^{U} C_u'\frac{W^{u+1/2}}{r^{*u}/r}\left[u\cdot\sin\theta^*\cdot\right. \\
& \quad \left[\cos(\theta/2)\cdot\cos[(u+1)\theta^*] - \sin(\theta/2)\cdot\sin[(u+1)\theta^*]\right] \\
& + \frac{1}{2\sin\theta}\left[\cos(3\cdot\theta/2)\cdot\cos(u\theta^*) - \sin(3\cdot\theta/2)\cdot\sin(u\theta^*)\right]\Big] \\
& \left. + \sum_{v=1}^{V} D_v'(W/r^*)^v\left[v\cdot\sin\theta^*\cdot\cos[(v+1)\theta^*] + \sin(v\theta^*)\right]\right]^2 \\
& = D^2 + T^2 = \left[\frac{N\cdot f_\sigma}{2t}\right]^2 \qquad \text{(A4)}
\end{aligned}
$$

In all of the above,

$A_j' = A_j \cdot W^{j-1/2}$
$B_m' = B_m \cdot W^m$
$C_u' = C_u / W^{u+1/2}$
$D_v' = D_v / W^v$
W = specimen width
N = photoelastic fringe order
f_σ = photoelastic fringe constant
t = specimen thickness
(r,θ) = right handed polar co-ordinates having an origin at the crack tip
(r^*,θ^*) = right handed polar co-ordinates having an origin on the crack line and outside of the collocated region

APPENDIX B

PARTIAL DERIVATIVES FOR THE [H] MATRIX

The [H] matrix is an array of partial derivatives of the homogeneous form of the stress equations, found in Appendix A, taken with respect to the normalized series coefficients, as well as the value of Q. The equations for matrix entries associated with locations on the specimen boundary are given below:

When $g = \sigma_{xx}$

$$\left.\frac{\partial g}{\partial A_j'}\right|_k = (r_k/W)^{j-1/2} \cdot \left[\cos[(j-1/2)\theta_k] - (j-1/2)\sin\theta_k \cdot \sin[(j-3/2)\theta_k]\right] \quad \text{(B1)}$$

$$\left.\frac{\partial g}{\partial B_m'}\right|_k = (r_k/W)^{m} \cdot \left[2\cos(m\theta_k) - m \cdot \sin\theta_k \cdot \sin[(m-1)\theta_k]\right] \quad \text{(B2)}$$

$$\left.\frac{\partial g}{\partial C_u'}\right|_k = \frac{W^{u+1/2}}{r^*{}_k{}^u / r_k}\Big[\cos(\theta_k/2) \cdot \cos(u\theta^*{}_k) - \sin(\theta_k/2) \cdot \sin(u\theta^*{}_k) - u \cdot \sin\theta^*{}_k \cdot \left[\cos(\theta_k/2) \cdot \sin[(u+1)\theta^*{}_k] + \sin(\theta_k/2) \cdot \cos[(u+1)\theta^*{}_k]\right] - 1/2 \cdot \sin\theta_k \cdot \left[\cos(3\theta_k/2) \cdot \sin(u\theta^*{}_k) + \sin(3\theta_k/2) \cdot \cos(u\theta^*{}_k)\right]\Big] \quad \text{(B3)}$$

$$\left.\frac{\partial g}{\partial D_v'}\right|_k = (W/r^*_k)^v\left[2\cos(v\theta^*_k) - v\cdot\sin\theta^*_k\cdot\sin[(v+1)\theta^*_k]\right] \quad \text{(B4)}$$

When $g = \sigma_{yy} - \sigma_{APPLIED}$

$$\left.\frac{\partial g}{\partial A_j'}\right|_k = (r_k/W)^{j-1/2}\cdot\left[\cos[(j-1/2)\theta_k] + (j-1/2)\sin\theta_k\cdot\sin[(j-3/2)\theta_k]\right] \quad \text{(B5)}$$

$$\left.\frac{\partial g}{\partial B_m'}\right|_k = (r_k/W)^m\cdot\left[m\cdot\sin\theta_k\cdot\sin[(m-1)\theta_k]\right] \quad \text{(B6)}$$

$$\left.\frac{\partial g}{\partial C_u'}\right|_k = \frac{W^{u+1/2}}{r^*_k{}^u/r_k}\Big[\cos(\theta_k/2)\cdot\cos(u\theta^*_k) - \sin(\theta_k/2)\cdot \sin(u\theta^*_k) + u\cdot\sin\theta^*_k\cdot \left[\cos(\theta_k/2)\cdot\sin[(u+1)\theta^*_k] + \sin(\theta_k/2)\cdot\cos[(u+1)\theta^*_k]\right] + 1/2\cdot\sin\theta_k\cdot \left[\cos(3\theta_k/2)\cdot\sin(u\theta^*_k) + \sin(3\theta_k/2)\cdot\cos(u\theta^*_k)\right]\Big] \quad \text{(B7)}$$

$$\left.\frac{\partial g}{\partial D_v'}\right|_k = (W/r^*_k)^v\cdot\left[v\cdot\sin\theta^*_k\cdot\sin[(v+1)\theta^*_k]\right] \quad \text{(B8)}$$

When $g = \tau_{xy}$

$$\left.\frac{\partial g}{\partial A_j'}\right|_k = -(r_k/W)^{j-1/2}\cdot\left[(j-1/2)\cdot\sin\theta_k\cdot\cos[(j-3/2)\theta_k]\right] \quad \text{(B9)}$$

$$\left.\frac{\partial g}{\partial B_m'}\right|_k = -(r_k/W)^m\cdot\left[m\cdot\sin\theta_k\cdot\cos[(m-1)\theta_k] + \sin(m\theta_k)\right] \quad \text{(B10)}$$

$$\left.\frac{\partial g}{\partial C_u'}\right|_k = \frac{W^{u+1/2}}{r^*_k{}^u \sqrt{r_k}}\Bigg[u\cdot\sin\theta^*_k\cdot \Big[\cos(\theta_k/2)\cdot\cos[(u+1)\theta^*_k] - \sin(\theta_k/2)\cdot\sin[(u+1)\theta^*_k]\Big] + 1/2\cdot\sin\theta_k\cdot \Big[\cos(3\theta_k/2)\cdot\cos(u\theta^*_k) - \sin(3\theta_k/2)\cdot\sin(u\theta^*_k)\Big]\Bigg] \quad \text{(B11)}$$

$$\left.\frac{\partial g}{\partial B_v'}\right|_k = (W/r^*_k)^v\Big[v\cdot\sin\theta^*_k\cdot\cos[(v+1)\theta^*_k] + \sin(v\theta^*_k)\Big] \quad \text{(B12)}$$

Also, when $g = \sigma_{xx}$, σ_{yy}, or τ_{xy},

$$\left.\frac{\partial g}{\partial Q}\right|_k = 0 \quad \text{(B13)}$$

In all of the above,

$A_j' = A_j\cdot W^{j-1/2}$
$B_m' = B_m\cdot W^m$
$C_u' = C_u/W^{u+1/2}$
$D_v' = D_v/W^v$
W = specimen width, as shown in Figure xx
(r,θ) = right handed polar co-ordinates having an origin at the crack tip
(r^*,θ^*) = right handed polar co-ordinates having an origin on the crack line and outside of the collocated region
k = point in model at which equation is defined

None of the preceding equations depend on the current estimates of the series coefficients, therefore these entries for [H] need only be calculated at the start of each iteration. Conversely, eqn. (6) for τ_{max}, used to describe the photoelastic data taken from the specimen

interior, is linearized by the differentiation. As a result, derivatives of this equation depend on the current estimates of the series coefficients as follows:

$$\left.\frac{\partial g}{\partial A_j'}\right|_k = \frac{-1}{\tau_{max_k}} \cdot (r_k/W)^{j-1/2} \cdot (j-1/2) \cdot \sin\theta_k \cdot \left[\sin[(j-3/2)\theta_k] \cdot D_k + \cos[(j-3/2)\theta_k] \cdot T_k\right] \quad \text{(B14)}$$

$$\left.\frac{\partial g}{\partial B_m'}\right|_k = \frac{(r_k/W)^m}{\tau_{max_k}} \left[\left[\cos(m\theta_k) - m \cdot \sin\theta_k \cdot \sin[(m-1)\theta_k]\right] \cdot D_k - \left[m \cdot \sin\theta_k \cdot \cos[(m-1)\theta_k] + \sin(m\theta_k)\right] \cdot T_k\right] \quad \text{(B15)}$$

$$\left.\frac{\partial g}{\partial C_u'}\right|_k = \frac{W^{u+1/2}}{\tau_{max_k} \cdot r^*{}_k{}^u / r_k} \left[-\left[u \cdot \sin\theta^*{}_k \cdot \left[\cos(\theta_k/2) \cdot \sin[(u+1)\theta^*{}_k] + \sin(\theta_k/2) \cdot \cos[(u+1)\theta^*{}_k]\right] + 1/2 \cdot \sin\theta_k \cdot \left[\cos(3 \cdot \theta_k/2) \cdot \sin(u\theta^*{}_k) + \sin(3 \cdot \theta_k/2) \cdot \cos(u\theta^*{}_k)\right]\right] \cdot D_k + \left[u \cdot \sin\theta^*{}_k \cdot \left[\cos(\theta_k/2) \cdot \cos[(u+1)\theta^*{}_k] - \sin(\theta_k/2) \cdot \sin[(u+1)\theta^*{}_k]\right] + 1/2 \cdot \sin\theta_k \cdot \left[\cos(3\theta_k/2) \cdot \cos(u\theta^*{}_k) - \sin(3\theta_k/2) \cdot \sin(u\theta^*{}_k)\right]\right] \cdot T_k\right] \quad \text{(B16)}$$

$$\left.\frac{\partial g}{\partial D_v'}\right|_k = \frac{1}{\tau_{max_k}} \cdot (W/r^*_k)^v \cdot \Bigg[\Big[\cos(v\theta^*_k) - v \cdot \sin\theta^*_k \cdot \sin[(v+1)\theta^*_k]\Big] \cdot D_k + \Big[v \cdot \sin\theta^*_k \cdot \cos[(v+1)\theta^*_k] + \sin(v\theta^*_k)\Big] \cdot T_k \Bigg] \qquad \text{(B17)}$$

$$\left.\frac{\partial g}{\partial Q}\right|_k = - N_k \qquad \text{(B18)}$$

where

$$g_k = (D_k^2 + T_k^2)^{1/2} - N_k \cdot f_\sigma/(2 \cdot t)$$

$$D_k = \sum_{j=0}^{J} -A_j'(r_k/W)^{j-1/2}\Big[(j-1/2) \cdot \sin\theta_k \cdot \sin[(j-3/2)\theta_k]\Big]$$

$$+ \sum_{m=0}^{M} B_m'(r_k/W)^m\Big[\cos(m\theta_k) - m \cdot \sin\theta_k \cdot \sin[(m-1)\theta_k]\Big]$$

$$- \sum_{u=1}^{U} C_u' \frac{W^{u+1/2}}{r^*_k{}^u \sqrt{r_k}} \Bigg[u \cdot \sin\theta^*_k \cdot \Big[\cos(\theta_k/2) \cdot \sin[(u+1)\theta^*_k] + \sin(\theta_k/2) \cdot \cos[(u+1)\theta^*_k]\Big]$$

$$+ 1/2 \cdot \sin\theta_k \cdot \Big[\cos(3\theta_k/2) \cdot \sin(u\theta^*_k) + \sin(3\theta_k/2) \cdot \cos(u\theta^*_k)\Big]\Bigg]$$

$$+ \sum_{v=1}^{V} D_v'(W/r^*_k)^v\Big[\cos(v\theta^*_k) - v \cdot \sin\theta^*_k \cdot \sin[(v+1)\theta^*_k]\Big]$$

$$T_k = \sum_{j=0}^{J} -A_j'(r_k/W)^{j-1/2}\left[(j-1/2)\cdot\sin\theta_k\cdot\cos[(j-3/2)\theta_k]\right]$$

$$- \sum_{m=0}^{M} B_m'(r_k/W)^m\left[m\cdot\sin\theta_k\cdot\cos[(m-1)\theta_k] + \sin(m\theta_k)\right]$$

$$+ \sum_{u=1}^{U} C_u'\frac{W^{u+1/2}}{r^*{}_k{}^u\sqrt{r_k}}\left[u\cdot\sin\theta^*{}_k\cdot\right.$$

$$\left[\cos(\theta_k/2)\cdot\cos[(u+1)\theta^*{}_k] - \sin(\theta_k/2)\cdot\sin[(u+1)\theta^*{}_k]\right]$$

$$+ 1/2\cdot\sin\theta_k\cdot$$

$$\left.\left[\cos(3\cdot\theta_k/2)\cdot\cos(u\theta^*{}_k) - \sin(3\cdot\theta_k/2)\cdot\sin(u\theta^*{}_k)\right]\right]$$

$$+ \sum_{v=1}^{V} D_v'(W/r^*{}_k)^v\left[v\cdot\sin\theta^*{}_k\cdot\cos[(v+1)\theta^*{}_k] + \sin(v\theta^*{}_k)\right]$$

APPENDIX C

EQUATIONS RELATING K_I AND CMOD TO SERIES COEFFICIENTS

Opening Mode Stress Intensity Factor, K_I

The opening mode stress intensity factor is defined as follows:

$$K_I = \lim_{r \to 0} \left(\sqrt{2\pi r} \cdot \sigma_{yy}|_{y=0} \right) \tag{D1}$$

Recalling that

$$\sigma_{yy} = \text{Re } Z + y\text{Im } Z' + y\text{Im } Y' \tag{D2}$$

eqn. (D1) reduces to

$$K_I = \lim_{r \to 0} \left(\sqrt{2\pi r} \cdot \text{Re } Z|_{y=0} \right) \tag{D3}$$

The real part of Z can be expressed as

$$\text{Re } Z = \sum_{j=0}^{J} A_j' (r/W)^{j-1/2} \left[\cos[(j-1/2)\theta] \right] + \tag{D4}$$

$$\sum_{u=1}^{U} C_u' \frac{W^{u+1/2}}{r^{*u}\sqrt{r}} \left[\cos(\theta/2) \cdot \cos(u\theta^*) - \sin(\theta/2) \cdot \sin(u\theta^*) \right]$$

On the crack line (y=0), $\theta=0°$ and $\theta^*=180°$, so eqn. (D4) becomes

$$\text{Re } Z = \sum_{j=0}^{J} A_j'(r/W)^{j-1/2} + \sum_{u=1}^{U} C_u' \frac{W^{u+1/2}}{r^{*u}\sqrt{r}} \cdot S(u) \qquad \text{(D5)}$$

where

$S(u) = +1$ if u is even
$\quad\quad -1$ if u is odd

By substituting (D5) into (D3), and taking the limit as r approaches zero, the relation between K_I and the series coefficients may be determined to be as follows:

$$K_I = \left[A_o' + S(u) \cdot \sum_{u=1}^{U} C_u'(W/b)^u \right] \cdot \sqrt{2\pi W} \qquad \text{(D6)}$$

where

$b = W_{max} - a$

For the conventional SE(T) specimen, all of the C_u' coefficients are zero.

Crack Mouth Opening Displacement, CMOD

For plane stress, displacements perpendicular to the crack line are given by

$$u_y \cdot E = 2 \cdot \text{Im } \overline{Z} - y \cdot (1+v) \cdot [\text{Re } Z + \text{Re } Y] + (1-v) \cdot \text{Im } \overline{Y} \qquad \text{(D7)}$$

where

E = Young's modulus
v = Poisson's ratio

On the crack line, eqn. (D7) reduces to

$$U_y \cdot E = 2 \cdot \mathrm{Im}\ \bar{Z} \tag{D8}$$

Recalling that, for the conventional SE(T),

$$Z = \sum_{j=0}^{J} A_j' (z/W)^{j-1/2} \tag{D9}$$

integration gives

$$\bar{Z} = \sum_{j=0}^{J} A_j' \frac{z^{j+1/2}}{(j+1/2) \cdot W^{j-1/2}} \tag{D10}$$

the imaginary part of which is

$$\mathrm{Im}\ \bar{Z} = \sum_{j=0}^{J} A_j' \frac{r^{j+1/2}}{(j+1/2) \cdot W^{j-1/2}} \sin[(j+1/2)\theta] \tag{D11}$$

CMOD is typically measured on the crack line at the front face of the specimen. At this location, r = a, and $\theta = 180°$. Thus, eqs. (D8) and (D11) give CMOD as follows:

$$\mathrm{CMOD} = \frac{4}{E} \cdot \sum_{j=0}^{J} A_j' \frac{a^{j+1/2}}{(j+1/2) \cdot W^{j-1/2}} S(j) \tag{D12}$$

where

$S(j) = +1$ if j is 0 or even
$\quad\quad -1$ if j is odd
a = Crack length

An expression for CMOD for the modified SE(T) geometry could be derived similarly by integrating eqn. (4a).

APPENDIX D
SERIES SOLUTIONS FOR THE CONVENTIONAL SE(T) SPECIMEN

	a/W = 0.099		a/W = 0.202	
j or m	A_j^*	B_m^*	A_j^*	B_m^*
0	1.0000E+00	-1.0936E+00	1.0000E+00	-7.2098E-01
1	4.1613E+00	-5.0967E+00	1.7239E+00	-2.0736E+00
2	3.2563E+00	1.5788E+01	1.0217E+00	5.2934E+00
3	-3.2422E+01	-2.7492E+01	-1.0239E+01	-7.3163E+00
4	1.1156E+02	1.0226E+01	2.9569E+01	4.0747E-01
5	-2.6078E+02	9.9535E+01	-6.2317E+01	3.2306E+01
6	4.5325E+02	-3.7133E+02	9.6680E+01	-1.0836E+02
7	-5.9199E+02	8.1517E+02	-1.0676E+02	2.3601E+02
8	5.4392E+02	-1.3229E+03	5.1227E+01	-3.9325E+02
9	-2.3867E+02	1.6892E+03	9.8284E+01	5.2773E+02
10	-2.4225E+02	-1.7284E+03	-3.3305E+02	-5.7346E+02
11	6.7980E+02	1.4106E+03	5.8964E+02	4.9158E+02
12	-8.5600E+02	-8.9311E+02	-7.7309E+02	-2.9982E+02
13	7.1030E+02	4.1163E+02	8.0435E+02	7.2259E+01
14	-3.7715E+02	-1.1958E+02	-6.7022E+02	1.0184E+02
15	6.9823E+01	1.5825E+01	4.3299E+02	-1.6948E+02
16	7.8695E+01	-3.5837E+00	-1.9366E+02	1.4071E+02
17	-7.9138E+01	-7.2312E-01	3.1655E+01	-7.0201E+01
18	2.3753E+01	1.5467E+01	3.2351E+01	1.3828E+01
19	1.3579E+01	-2.1654E+01	-3.0488E+01	5.6863E+00
20	-1.9207E+01	1.0584E+01	9.6650E+00	4.5461E-01
21	1.3092E+01	4.6526E+00	1.3375E+00	-9.2807E+00
22	-9.5893E+00	-9.7059E+00	-3.4364E-01	8.6651E+00
23	7.5776E+00	4.8889E+00	-2.8151E+00	-1.4307E+00
24	-3.3889E+00	8.9142E-01	1.9294E+00	-4.3551E+00
25	-1.3461E+00	-2.4062E+00	1.4513E+00	5.0664E+00
26	3.2496E+00	1.2043E+00	-3.3793E+00	-2.8530E+00
27	-2.4089E+00	-7.6059E-02	2.9174E+00	7.0404E-01
28	9.3212E-01	-1.4897E-01	-1.3665E+00	6.2647E-02
29	-1.7712E-01	5.8127E-02	3.5266E-01	-1.0886E-01

Note: The table entries are defined as follows:

$A_j^* = A_j' / A_0'$
$B_m^* = B_m' / A_0'$

All values are dimensionless.

	a/W = 0.300		a/W = 0.401	
j or m	A_j^*	B_m^*	A_j^*	B_m^*
0	1.0000E+00	-4.8650E-01	1.0000E+00	-3.0610E-01
1	3.6715E-01	-8.5130E-01	-6.7718E-01	-2.2917E-01
2	-3.2993E-01	2.4607E+00	-1.0986E+00	1.4291E+00
3	-3.9097E+00	-2.7582E+00	-2.3448E+00	-5.8024E-01
4	8.3913E+00	1.8745E+00	1.2781E+00	2.0534E+00
5	-1.8151E+01	6.8837E+00	-6.8017E+00	1.9941E+00
6	2.5377E+01	-2.4792E+01	5.3555E+00	-3.4655E+00
7	-2.7956E+01	5.7520E+01	-9.4283E+00	1.2728E+01
8	1.1319E+01	-9.9340E+01	3.0767E+00	-1.9117E+01
9	3.1548E+01	1.4157E+02	2.0771E+00	3.1723E+01
10	-1.0732E+02	-1.6482E+02	-2.1728E+01	-3.6226E+01
11	2.0431E+02	1.5463E+02	4.2058E+01	3.9397E+01
12	-3.0211E+02	-1.0330E+02	-7.3042E+01	-2.7545E+01
13	3.6979E+02	2.2207E+01	9.7013E+01	9.7443E+00
14	-3.8601E+02	6.5908E+01	-1.1880E+02	2.0816E+01
15	3.4315E+02	-1.3116E+02	1.2218E+02	-4.9401E+01
16	-2.5889E+02	1.5695E+02	-1.1494E+02	7.6893E+01
17	1.5971E+02	-1.4041E+02	9.0401E+01	-8.9606E+01
18	-7.6088E+01	9.8570E+01	-6.3335E+01	9.2682E+01
19	2.1628E+01	-5.0853E+01	3.2364E+01	-8.0231E+01
20	2.3138E+00	1.4384E+01	-1.1799E+01	6.4566E+01
21	-6.8541E+00	5.6100E+00	-4.3995E+00	-4.3304E+01
22	3.7373E+00	-1.2303E+01	8.2733E+00	2.8325E+01
23	1.8820E-01	1.1150E+01	-1.0587E+01	-1.4328E+01
24	-1.5036E+00	-8.4198E+00	6.6896E+00	7.9731E+00
25	2.2810E+00	4.9868E+00	-5.2479E+00	-2.6808E+00
26	-1.7978E+00	-2.8297E+00	2.1247E+00	1.4407E+00
27	1.6828E+00	8.6645E-01	-1.4199E+00	-1.3646E-01
28	-8.0591E-01	-1.9133E-01	3.3340E-01	1.2421E-01
29	3.5153E-01	-9.6080E-02	-2.0014E-01	5.7419E-02

Note: The table entries are defined as follows:

$$A_j^* = A_j' / A_0'$$
$$B_m^* = B_m' / A_0'$$

All values are dimensionless.

	a/W = 0.498		a/W = 0.601	
j or m	A_j^*	B_m^*	A_j^*	B_m^*
0	1.0000E+00	-1.5347E-01	1.0000E+00	3.6001E-03
1	-1.7025E+00	2.1525E-01	-3.0286E+00	7.0416E-01
2	-2.0641E+00	1.3805E+00	-3.8155E+00	2.2385E+00
3	-2.9472E+00	1.1079E+00	-6.0772E+00	4.1101E+00
4	-2.6720E+00	3.1370E+00	-9.5579E+00	8.1795E+00
5	-6.0890E+00	3.3176E+00	-1.5767E+01	1.3164E+01
6	-3.3575E+00	3.6967E+00	-2.2707E+01	2.1168E+01
7	-8.9045E+00	7.4711E+00	-3.4923E+01	3.2394E+01
8	-5.7514E+00	2.9766E+00	-4.7985E+01	4.5558E+01
9	-9.8162E+00	1.3396E+01	-6.5789E+01	6.2873E+01
10	-1.1628E+01	1.6443E+00	-8.2745E+01	7.6984E+01
11	-6.1526E+00	1.8148E+01	-9.8011E+01	9.2060E+01
12	-2.1575E+01	3.0661E+00	-1.0835E+02	9.5518E+01
13	1.7121E+00	1.6632E+01	-1.0636E+02	9.4558E+01
14	-3.0529E+01	8.7765E+00	-9.8875E+01	7.9684E+01
15	9.5937E+00	6.8648E+00	-7.5205E+01	6.0553E+01
16	-3.1053E+01	1.5832E+01	-5.4528E+01	3.7195E+01
17	1.1870E+01	-5.5622E+00	-2.5182E+01	1.5468E+01
18	-2.1129E+01	1.8170E+01	-9.5147E+00	2.3049E+00
19	7.9943E+00	-1.2155E+01	5.5599E+00	-6.9066E+00
20	-7.9858E+00	1.4061E+01	6.7931E+00	-5.1372E+00
21	2.4157E+00	-1.0436E+01	6.4068E+00	-4.0012E+00
22	-2.4115E-02	7.6479E+00	1.2737E+00	1.7789E+00
23	-8.9901E-01	-5.1049E+00	-2.1906E+00	3.1491E+00
24	1.5925E+00	3.0443E+00	-4.1229E+00	4.7947E+00
25	-1.4546E+00	-1.2747E+00	-4.1762E+00	3.4608E+00
26	7.3523E-01	8.9608E-01	-2.9327E+00	2.4558E+00
27	-7.7747E-01	-1.1399E-02	-1.6918E+00	1.0576E+00
28	1.2097E-01	1.5938E-01	-6.4600E-01	4.2396E-01
29	-1.8466E-01	6.2586E-02	-1.9861E-01	6.0948E-02

Note: The table entries are defined as follows:

$A_j^* = A_j' / A_0'$
$B_m^* = B_m' / A_0'$

All values are dimensionless.

	a/W = 0.706		a/W = 0.797	
j or m	A_j^*	B_m^*	A_j^*	B_m^*
0	1.0000E+00	2.3044E-01	1.0000E+00	4.1085E-01
1	-5.3237E+00	1.6747E+00	-8.5695E+00	3.4905E+00
2	-8.1816E+00	5.4969E+00	-1.8683E+01	1.6163E+01
3	-1.6810E+01	1.4334E+01	-5.3336E+01	5.6018E+01
4	-3.5127E+01	3.3818E+01	-1.4032E+02	1.5517E+02
5	-7.0210E+01	7.0840E+01	-3.2061E+02	3.5303E+02
6	-1.2993E+02	1.3372E+02	-6.2899E+02	6.7195E+02
7	-2.2067E+02	2.2509E+02	-1.0585E+03	1.0806E+03
8	-3.3804E+02	3.3777E+02	-1.5283E+03	1.4751E+03
9	-4.6625E+02	4.5074E+02	-1.8899E+03	1.7056E+03
10	-5.7359E+02	5.3184E+02	-1.9875E+03	1.6515E+03
11	-6.2591E+02	5.5134E+02	-1.7505E+03	1.3042E+03
12	-5.9813E+02	4.9401E+02	-1.2528E+03	7.8925E+02
13	-4.9151E+02	3.7378E+02	-6.8485E+02	3.0390E+02
14	-3.3501E+02	2.2429E+02	-2.4778E+02	3.1577E+00
15	-1.7315E+02	9.0212E+01	-4.1449E+01	-8.0080E+01
16	-4.8662E+01	7.6462E-01	-2.8632E+01	-2.6322E+01
17	2.0299E+01	-3.5386E+01	-9.2285E+01	4.9573E+01
18	3.6710E+01	-3.2923E+01	-1.3015E+02	7.8488E+01
19	2.5109E+01	-1.4769E+01	-1.1103E+02	5.9647E+01
20	6.1400E+00	1.4619E+00	-6.2726E+01	2.8515E+01
21	-4.6882E+00	7.6598E+00	-2.4355E+01	1.2183E+01
22	-7.1099E+00	7.2798E+00	-1.0491E+01	1.2297E+01
23	-4.7013E+00	4.1457E+00	-1.1875E+01	1.6320E+01
24	-2.4060E+00	2.5197E+00	-1.3714E+01	1.5196E+01
25	-1.6534E+00	1.8460E+00	-1.0690E+01	9.6633E+00
26	-1.5226E+00	1.5842E+00	-5.5124E+00	4.1701E+00
27	-1.2164E+00	9.4842E-01	-1.8363E+00	1.1925E+00
28	-5.8634E-01	3.5592E-01	-3.5020E-01	1.9420E-01
29	-1.4347E-01	4.6979E-02	-2.2129E-02	1.5283E-02

Note: The table entries are defined as follows:

$$A_j^* = A_j' / A_0'$$
$$B_m^* = B_m' / A_0'$$

All values are dimensionless.

APPENDIX E
SERIES SOLUTIONS FOR THE MODIFIED SE(T) SPECIMEN

$a/W_{min} = 0.107$

j,m,u or v	A_j^*	B_m^*	C_u^*	D_v^*
0	1.0000E+00	-6.2828E-01		
1	6.3578E-01	-3.9547E-01	1.4598E+00	-9.1162E-01
2	4.2118E-01	-4.0555E-01	4.2056E-01	-2.3722E-01
3	5.2095E-01	-9.3636E-02	9.1156E-02	-3.5413E-02
4	-3.1333E-01	-1.0874E-01	8.9042E-03	5.5516E-03
5	1.0037E+00	-4.9011E-01	-2.7380E-03	5.8998E-03
6	-1.0151E+00	9.0472E-01	-1.6977E-03	2.2456E-03
7	1.0814E+00	-1.5588E+00	-4.2341E-04	4.8437E-04
8	-5.8534E-01	1.8020E+00	-2.5360E-05	2.2580E-05
9	6.2487E-02	-1.7512E+00	2.4662E-05	-2.8842E-05
10	4.5448E-01	1.3161E+00	1.2034E-05	-1.3648E-05
11	-6.4185E-01	-8.0554E-01	3.0456E-06	-3.5194E-06
12	5.8197E-01	3.6542E-01	3.9710E-07	-5.1438E-07
13	-3.5900E-01	-1.1989E-01	-3.0159E-08	6.1642E-09
14	1.5322E-01	2.0711E-02	-3.1172E-08	2.7559E-08
15	-2.5372E-02	-4.2029E-03	-8.9474E-09	8.7353E-09
16	-1.8189E-02	5.7801E-03	-1.5078E-09	1.5961E-09
17	2.0737E-02	-6.4157E-03	-1.0903E-10	1.4921E-10
18	-1.1558E-02	3.4819E-03	2.2299E-11	-1.2118E-11
19	5.1096E-03	-1.2925E-03	1.0024E-11	-8.1198E-12
20	-1.9454E-03	3.1811E-04	2.1321E-12	-1.8543E-12
21	7.1044E-04	-1.1023E-04	3.1072E-13	-2.7917E-13
22	-1.9116E-04	3.7923E-05	3.2340E-14	-2.9663E-14
23	3.2788E-05	-1.0678E-05	2.2519E-15	-2.0992E-15
24			8.0605E-17	-7.6199E-17

Note: The table entries are defined as follows:

$A_j^* = A_j' / A_0'$
$B_m^* = B_m' / A_0'$
$C_u^* = C_u' / A_0'$
$D_v^* = D_v' / A_0'$

All values are dimensionless.

$a/W_{min} = 0.197$

j,m,u or v	A_j^*	B_m^*	C_u^*	D_v^*
0	1.0000E+00	-9.0350E-01		
1	6.6463E-01	-5.9658E-01	1.4123E+00	-1.2984E+00
2	4.6861E-01	-5.5038E-01	4.4823E-01	-4.4279E-01
3	5.5449E-01	-2.1868E-01	1.1466E-01	-1.2530E-01
4	-2.0622E-01	-1.4754E-01	1.7467E-02	-2.5948E-02
5	8.6071E-01	-5.7429E-01	-1.6558E-03	-2.5685E-03
6	-6.5649E-01	8.5101E-01	-2.4495E-03	7.8445E-04
7	6.2063E-01	-1.4942E+00	-1.0350E-03	4.8414E-04
8	1.5409E-02	1.6255E+00	-2.8210E-04	1.2594E-04
9	-5.5421E-01	-1.5651E+00	-4.7514E-05	9.5547E-06
10	1.0738E+00	1.1045E+00	-3.8628E-07	-7.4352E-06
11	-1.1852E+00	-6.2257E-01	2.9978E-06	-4.3126E-06
12	1.0340E+00	2.0227E-01	1.2200E-06	-1.3783E-06
13	-6.8367E-01	6.8508E-04	2.9766E-07	-3.0168E-07
14	3.6244E-01	-6.0959E-02	4.6708E-08	-4.1708E-08
15	-1.3797E-01	3.6558E-02	2.9171E-09	-8.7868E-10
16	3.6626E-02	-9.5363E-03	-7.5636E-10	1.3212E-09
17	-3.0295E-03	-4.4657E-03	-2.7069E-10	4.0023E-10
18	-3.9906E-04	4.1005E-03	-3.7331E-11	6.2744E-11
19	2.9015E-04	-1.7128E-03	4.3038E-13	3.7864E-12
20	-7.9142E-05	1.1307E-04	1.3511E-12	-7.7727E-13
21	3.9290E-04	-7.5290E-07	3.1998E-13	-2.5896E-13
22	-2.1392E-04	8.4880E-06	4.2369E-14	-3.7681E-14
23	7.5883E-05	-2.4544E-05	3.2716E-15	-3.0447E-15
24			1.1426E-16	-1.0916E-16

Note: The table entries are defined as follows:

$A_j^* = A_j' / A_0'$
$B_m^* = B_m' / A_0'$
$C_u^* = C_u' / A_0'$
$D_v^* = D_v' / A_0'$

All values are dimensionless.

$a/W_{min} = 0.301$

j,m,u or v	A_j^*	B_m^*	C_u^*	D_v^*
0	1.0000E+00	-5.7690E-01		
1	5.2146E-01	-2.4061E-01	1.7146E+00	-1.0532E+00
2	3.0269E-01	-3.7091E-01	9.7594E-01	-6.5748E-01
3	5.1092E-01	1.4796E-01	4.3564E-01	-2.9715E-01
4	-6.7313E-01	4.1961E-02	1.5406E-01	-1.0261E-01
5	1.0976E+00	-5.5809E-01	4.4393E-02	-2.7798E-02
6	-1.2426E+00	1.5078E+00	1.0183E-02	-5.5537E-03
7	7.5939E-01	-2.2783E+00	1.8664E-03	-7.7563E-04
8	6.5831E-02	2.9778E+00	3.1038E-04	-1.0647E-04
9	-1.4385E+00	-2.8849E+00	7.7506E-05	-5.3729E-05
10	2.5388E+00	2.3684E+00	3.1231E-05	-3.2832E-05
11	-3.3176E+00	-1.3335E+00	1.1536E-05	-1.3436E-05
12	3.2909E+00	4.0039E-01	3.1036E-06	-3.7293E-06
13	-2.7807E+00	3.2815E-01	5.2582E-07	-6.5080E-07
14	1.9111E+00	-6.0369E-01	1.7264E-08	-2.7249E-08
15	-1.1150E+00	5.9956E-01	-2.1082E-08	2.4783E-08
16	5.0594E-01	-4.1305E-01	-7.5518E-09	9.5730E-09
17	-1.7739E-01	2.2978E-01	-1.4058E-09	1.9818E-09
18	3.0537E-02	-9.4557E-02	-1.2436E-10	2.4206E-10
19	4.3291E-03	3.0538E-02	1.0662E-11	7.6055E-12
20	-6.7976E-03	-5.5252E-03	5.7027E-12	-3.5535E-12
21	1.4948E-03	6.7076E-04	1.0069E-12	-8.2173E-13
22	-8.4896E-05	9.2114E-05	1.0251E-13	-9.1603E-14
23	-2.1234E-04	7.3781E-05	5.8146E-15	-5.4175E-15
24			1.3011E-16	-1.2221E-16

Note: The table entries are defined as follows:

$A_j^* = A_j' / A_0'$
$B_{m*} = B_m' / A_0'$
$C_{u*} = C_u' / A_0'$
$D_v^* = D_v' / A_0'$

All values are dimensionless.

$a/W_{min} = 0.402$

j,m,u or v	A_j^*	B_m^*	C_u^*	D_v^*
0	1.0000E+00	-7.5374E-01		
1	8.1083E-01	-6.2341E-01	1.1891E+00	-8.9283E-01
2	6.4661E-01	-4.8211E-01	4.0209E-01	-2.8954E-01
3	4.9112E-01	-4.1112E-01	1.1389E-01	-7.5330E-02
4	4.3734E-01	-3.0078E-01	2.5993E-02	-1.3977E-02
5	2.4073E-01	-2.1380E-01	4.2456E-03	-8.4608E-04
6	2.9375E-01	-2.3578E-01	2.7957E-04	5.8539E-04
7	1.1301E-01	-2.2376E-02	-9.5535E-05	2.9056E-04
8	1.2697E-01	-2.2985E-01	-3.8846E-05	7.6623E-05
9	1.3477E-01	8.6770E-02	-6.0497E-06	1.1957E-05
10	-6.5599E-02	-1.6988E-01	3.0703E-07	3.3115E-07
11	2.0585E-01	5.7307E-02	4.3332E-07	-4.1711E-07
12	-1.6863E-01	-4.6163E-02	1.3349E-07	-1.4409E-07
13	1.8991E-01	-2.5603E-02	2.9014E-08	-3.1747E-08
14	-1.3234E-01	3.8987E-02	6.2141E-09	-6.7833E-09
15	9.6252E-02	-5.3840E-02	1.5488E-09	-1.7517E-09
16	-4.8978E-02	4.2769E-02	3.6974E-10	-4.5215E-10
17	2.1820E-02	-3.0376E-02	6.2007E-11	-8.7844E-11
18	-4.9936E-03	1.6696E-02	2.8925E-12	-8.8380E-12
19	-1.0746E-03	-7.5017E-03	-1.9451E-12	9.4828E-13
20	1.9777E-03	2.6477E-03	-7.1386E-13	5.9779E-13
21	-1.3420E-03	-5.4903E-04	-1.3836E-13	1.3057E-13
22	4.6382E-04	6.5385E-05	-1.7221E-14	1.7222E-14
23	-1.2848E-04	2.9935E-05	-1.3242E-15	1.3750E-15
24			-4.8941E-17	5.2250E-17

Note: The table entries are defined as follows:

$A_j^* = A_j' / A_0'$
$B_m^* = B_m' / A_0'$
$C_u^* = C_u' / A_0'$
$D_v^* = D_v' / A_0'$

All values are dimensionless.

$a/W_{min} = 0.506$

j,m,u or v	A_j^*	B_m^*	C_u^*	D_v^*
0	1.0000E+00	-8.6877E-01		
1	6.3768E-01	-6.9751E-01	1.0604E+00	-1.0004E+00
2	4.6606E-01	-4.4611E-01	4.3636E-01	-4.0842E-01
3	2.6592E-01	-4.0964E-01	1.4478E-01	-1.3332E-01
4	2.9510E-01	-1.7789E-01	3.9340E-02	-3.5786E-02
5	-9.1027E-02	-8.5437E-02	9.2281E-03	-8.3964E-03
6	1.5984E-01	-1.2278E-01	2.1508E-03	-2.0736E-03
7	-2.3107E-01	2.3346E-01	6.2519E-04	-6.7483E-04
8	-5.2236E-02	-1.6883E-01	2.1973E-04	-2.5606E-04
9	-1.1849E-01	4.0391E-01	7.3931E-05	-8.8697E-05
10	-3.1337E-01	-1.4543E-01	2.0314E-05	-2.4588E-05
11	1.0140E-01	3.2512E-01	4.2005E-06	-5.0725E-06
12	-4.4678E-01	-8.9718E-03	5.8041E-07	-6.7626E-07
13	1.9716E-01	1.1953E-01	3.4724E-08	-2.5023E-08
14	-3.5946E-01	1.0565E-01	-1.7881E-09	9.0289E-09
15	1.3142E-01	-1.7380E-02	1.4307E-09	2.1945E-10
16	-1.7307E-01	1.0893E-01	1.1648E-09	-1.0206E-09
17	3.4559E-02	-3.7005E-02	3.6799E-10	-3.9935E-10
18	-4.4978E-02	5.2943E-02	6.7195E-11	-8.2110E-11
19	-5.3524E-03	-1.3999E-02	5.9918E-12	-9.0386E-12
20	-3.5232E-03	1.3024E-02	-4.2950E-13	6.6191E-14
21	-5.5800E-03	-1.3777E-03	-2.3722E-13	2.1868E-13
22	6.8910E-04	1.1789E-03	-3.9328E-14	4.0909E-14
23	-1.0013E-03	2.3991E-04	-3.5154E-15	3.8633E-15
24			-1.4435E-16	1.6452E-16

Note: The table entries are defined as follows:

$A_j^* = A_j' / A_0'$
$B_m^* = B_m' / A_0'$
$C_u^* = C_u' / A_0'$
$D_v^* = D_v' / A_0'$

All values are dimensionless.

$a/W_{min} = 0.605$

j,m,u or v	A_j^*	B_m^*	C_u^*	D_v^*
0	1.0000E+00	-7.3674E-01		
1	7.2458E-01	-6.9146E-01	9.1972E-01	-7.3749E-01
2	7.0325E-01	-6.0521E-01	3.2170E-01	-2.5842E-01
3	6.3304E-01	-5.8121E-01	9.9751E-02	-7.6362E-02
4	5.9852E-01	-4.6911E-01	2.6104E-02	-1.8347E-02
5	4.4068E-01	-4.1333E-01	5.9165E-03	-3.5706E-03
6	4.4532E-01	-3.4803E-01	1.1115E-03	-4.7477E-04
7	2.6995E-01	-2.2277E-01	1.6497E-04	-1.2814E-05
8	2.5393E-01	-2.2828E-01	9.6148E-06	2.3123E-05
9	1.4502E-01	-6.5818E-02	-5.9760E-06	1.2608E-05
10	7.4782E-02	-1.1488E-01	-3.6947E-06	5.1363E-06
11	7.1037E-02	1.6411E-02	-1.3827E-06	1.7479E-06
12	-3.8841E-02	-2.3106E-02	-3.8955E-07	4.8694E-07
13	2.7629E-02	3.1876E-02	-8.2671E-08	1.0549E-07
14	-6.8125E-02	2.3908E-02	-1.2017E-08	1.6006E-08
15	3.0397E-03	1.8949E-02	-7.3759E-10	1.0932E-09
16	-4.6716E-02	2.8844E-02	1.2539E-10	-1.7548E-10
17	-6.5211E-03	6.7807E-03	2.5184E-11	-5.2436E-11
18	-1.8883E-02	1.5565E-02	-6.6911E-12	1.2384E-12
19	-5.7228E-03	1.8188E-03	-4.3496E-12	3.8648E-12
20	-4.4234E-03	4.6379E-03	-1.1754E-12	1.2206E-12
21	-2.2368E-03	4.5616E-04	-2.0461E-13	2.2763E-13
22	-4.6445E-04	6.4400E-04	-2.4271E-14	2.8214E-14
23	-3.9633E-04	9.6397E-05	-1.8495E-15	2.2257E-15
24			-7.0902E-17	8.8060E-17

Note: The table entries are defined as follows:

$$A_j^* = A_j' / A_0'$$
$$B_m^* = B_m' / A_0'$$
$$C_u^* = C_u' / A_0'$$
$$D_v^* = D_v' / A_0'$$

All values are dimensionless.

a/W_{min} = 0.704

j,m,u or v	A_j^*	B_m^*	C_u^*	D_v^*
0	1.0000E+00	-7.3324E-01		
1	7.7585E-02	-6.8181E-01	6.4450E-01	-7.0220E-01
2	2.7303E-01	-5.8148E-01	2.1378E-01	-2.8129E-01
3	2.6665E-01	-5.4397E-01	6.8736E-02	-9.4045E-02
4	2.5653E-01	-4.0898E-01	1.5098E-02	-2.3773E-02
5	1.4381E-01	-3.5145E-01	2.2355E-03	-4.7905E-03
6	1.7134E-01	-2.5957E-01	-1.3483E-04	-4.9193E-04
7	4.3875E-02	-1.5763E-01	-1.6902E-04	2.9001E-05
8	6.4493E-02	-1.3145E-01	-5.4889E-05	2.8140E-05
9	-1.1449E-02	-1.7266E-02	-9.0640E-06	4.3289E-06
10	-1.3519E-02	-4.8358E-02	-2.8994E-07	-3.9094E-07
11	-1.3824E-02	4.4196E-02	2.6750E-07	-3.0647E-07
12	-4.6809E-02	-7.5062E-03	5.3788E-08	-2.7115E-08
13	1.2590E-02	3.8415E-02	-6.1400E-09	1.9870E-08
14	-3.8692E-02	4.5636E-03	-5.3240E-09	8.9813E-09
15	3.3063E-02	9.9427E-03	-1.1333E-09	1.6206E-09
16	-1.7142E-02	6.7354E-03	-4.1817E-11	3.3844E-12
17	3.0996E-02	-7.1103E-03	3.1020E-11	-6.4749E-11
18	-2.5944E-03	6.7721E-03	4.1177E-12	-1.0362E-11
19	1.6183E-02	-7.6616E-03	-1.7742E-12	2.1441E-12
20	1.2163E-03	5.6169E-03	-8.2860E-13	1.3279E-12
21	4.0379E-03	-2.8111E-03	-1.5021E-13	2.8796E-13
22	5.3728E-04	3.3534E-03	-8.3678E-15	2.8072E-14
23	-4.1192E-04	-1.5948E-04	1.3319E-15	-4.8202E-16
24	-4.8805E-05	1.2849E-03	-1.1572E-16	-1.0203E-16
25	-6.2339E-04	2.1884E-04	-2.1374E-16	1.8095E-16
26	-6.2133E-05	2.7795E-04	-6.3337E-17	6.6673E-17
27	-1.7415E-04	6.8785E-05	-9.8815E-18	1.1432E-17
28	-6.5614E-06	2.3261E-05	-8.1821E-19	1.0028E-18
29	-1.6153E-05	6.7729E-06	-1.6812E-20	2.0424E-20
30			1.8790E-21	-2.6675E-21

Note: The table entries are defined as follows:

$A_j^* = A_j' / A_0'$
$B_{m*} = B_m' / A_0'$
$C_{u*} = C_u' / A_0'$
$D_v^* = D_v' / A_0'$

All values are dimensionless.

a/W_{min} = 0.805

j,m,u or v	A_j^*	B_m^*	C_u^*	D_v^*
0	1.0000E+00	-9.0172E-02		
1	-1.2048E+00	-4.6337E-02	2.5717E-01	-7.1912E-02
2	-5.7400E-01	9.1331E-03	2.1174E-02	-2.8955E-02
3	-4.6259E-01	1.6402E-02	9.8757E-03	-1.0938E-02
4	-4.0710E-01	5.4009E-02	-8.6682E-05	-4.1130E-04
5	-3.8164E-01	2.5373E-02	-3.7255E-05	-1.0719E-04
6	-2.8846E-01	1.0398E-02	-1.3813E-04	1.6942E-04
7	-2.5110E-01	-1.9601E-02	-8.6392E-06	1.1650E-05
8	-1.5405E-01	-5.9004E-02	5.2968E-07	1.9935E-06
9	-1.1058E-01	-6.5854E-02	1.8350E-06	-1.7097E-06
10	-5.1324E-02	-8.8639E-02	3.5020E-07	-2.8304E-07
11	-2.7597E-02	-6.2674E-02	3.1297E-08	-3.2017E-08
12	-1.6440E-02	-6.1272E-02	-1.9372E-08	1.8074E-08
13	-6.7228E-03	-2.7381E-02	-9.3264E-09	7.8295E-09
14	-1.8171E-02	-1.8197E-02	-2.9172E-09	2.5225E-09
15	-8.6618E-03	2.1619E-05	-6.2082E-10	5.3952E-10
16	-1.7786E-02	3.6191E-03	-8.6611E-11	7.4745E-11
17	-5.5368E-03	5.1201E-03	-1.4201E-12	-2.1380E-12
18	-8.1898E-03	5.2002E-03	2.3743E-12	-3.6159E-12
19	-2.2299E-04	1.8361E-03	5.1444E-13	-8.3484E-13
20	-1.1820E-03	2.3334E-03	2.2967E-14	-7.4033E-14
21	1.0665E-03	2.3233E-04	-2.1588E-15	-5.8602E-15
22	3.5043E-04	9.1936E-04	4.0183E-15	-7.1293E-15
23	3.3989E-04	1.2616E-04	2.2350E-15	-3.5604E-15
24	1.2354E-04	3.6003E-04	5.0404E-16	-8.6489E-16
25	-3.2520E-05	8.8618E-05	3.4953E-17	-9.2728E-17
26	3.6539E-06	8.9165E-05	-1.2338E-17	9.2538E-18
27	-3.0797E-05	2.2462E-05	-4.5016E-18	5.3867E-18
28	-1.1757E-06	1.0129E-05	-7.4268E-19	9.9172E-19
29	-5.2821E-06	2.6264E-06	-6.7883E-20	9.6621E-20
30			-2.8057E-21	4.1984E-21

Note: The table entries are defined as follows:

$A_j^* = A_j' / A_0'$
$B_{m*} = B_m' / A_0'$
$C_{u*} = C_u' / A_0'$
$D_v^* = D_v' / A_0'$

All values are dimensionless.

a/W_{min} = 0.900

j,m,u or v	A_j^*	B_m^*	C_u^*	D_v^*
0	1.0000E+00	-3.8229E-02		
1	-1.0509E+00	-4.1777E-02	2.9119E-01	-2.2031E-02
2	-3.6156E-01	-4.3898E-02	4.4199E-02	-2.6375E-03
3	-2.1080E-01	-4.9209E-02	1.4375E-02	1.2554E-03
4	-1.3950E-01	-4.7121E-02	2.0749E-03	2.4941E-03
5	-9.5366E-02	-4.9572E-02	3.7846E-04	9.7513E-04
6	-5.9658E-02	-4.4774E-02	-3.0418E-05	4.2240E-04
7	-3.9523E-02	-3.9842E-02	-5.8906E-06	9.1591E-05
8	-2.0892E-02	-3.2008E-02	-2.1287E-06	1.9794E-05
9	-1.3461E-02	-2.2479E-02	8.2486E-07	1.1522E-06
10	-6.6722E-03	-1.4728E-02	2.0860E-07	-5.8790E-08
11	-5.3149E-03	-6.8668E-03	5.0144E-08	-8.7842E-08
12	-3.2773E-03	-3.5342E-03	-4.9349E-09	3.3796E-09
13	-2.5012E-03	-1.1362E-04	-2.0107E-09	3.1690E-09
14	-1.8525E-03	-1.2974E-04	-4.3702E-10	1.3735E-09
15	-8.8103E-04	6.8094E-04	6.5306E-11	1.0752E-10
16	-9.2493E-04	-5.1719E-05	1.7877E-11	1.3767E-11
17	-1.3312E-04	1.1189E-04	1.4480E-14	2.1134E-12
18	-5.1082E-04	-1.6002E-04	-2.0340E-12	2.6555E-12
19	3.6525E-05	-1.1835E-04	-4.2922E-13	4.6519E-13
20	-2.4457E-04	-6.6989E-05	-1.6633E-14	1.1524E-14
21	7.7075E-05	-9.2092E-05	1.7827E-14	-2.7177E-14
22	-7.3696E-05	3.6312E-05	2.5194E-15	-2.8561E-15
23	3.1081E-05	-1.1712E-05	-4.2063E-16	1.0306E-15
24	-3.1628E-05	5.8487E-05	-2.0495E-16	4.7873E-16
25	-1.0077E-05	4.2784E-06	2.0698E-18	3.3324E-17
26	-9.7485E-06	1.8565E-05	1.1887E-17	-1.4639E-17
27	-5.1051E-06	-8.0009E-06	2.1251E-18	-4.0414E-18
28	3.3415E-06	-2.3622E-06	-3.3479E-19	3.0721E-19
29	-6.4579E-07	-4.6821E-06	-1.6092E-19	2.7775E-19
30	9.5624E-07	-8.5507E-07	-2.9947E-21	3.5244E-20
31	-1.5845E-06	1.0432E-07	1.3559E-20	-1.2279E-20
32	-6.6401E-07	2.9040E-07	4.8418E-21	-6.0563E-21
33	-5.1762E-07	1.5834E-07	9.3433E-22	-1.3230E-21
34	-6.6561E-08	-1.2036E-08	1.0677E-22	-1.6329E-22
35			6.4054E-24	-1.0743E-23

Note: The table entries are defined as follows:

$A_j^* = A_j' / A_0'$
$B_m^* = B_m' / A_0'$
$C_u^* = C_u' / A_0'$
$D_v^* = D_v' / A_0'$

All values are dimensionless.

REFERENCES

[1] Irwin, G.R., and Kies, J.A., "Critical Energy Release Rate Analysis of Fracture Strength," Welding Journal Research Supplement, Vol. 33, pp. 193s-198s, 1954.

[2] Ostervig, C.B., "Stress Intensity Factor Determination from Isochromatic Fringe Patterns - A Review," Engineering Fracture Mechanics, Vol. 26, No. 6, pp. 937-944, 1987.

[3] Sanford, R.J., and Dally, J.W., "A General Method for Determining Mixed-Mode Stress Intensity Factors from Isochromatic Fringe Patterns," Engineering Fracture Mechanics, Vol. 11, pp. 621-633, 1979.

[4] Sanford, R.J., and Chona, R., "Analysis of Photoelastic Fracture Patterns with a Sampled Least-Squares Method," Proceedings of the SESA Annual Spring Meeting, Dearborn, MI, pp. 273-276, May 1980.

[5] Barker, D.B., Sanford, R.J., and Chona, R., "Determining K and Related Stress Field Parameters from Displacement Fields," 1983 SESA Proceedings, Presented at the spring meeting in Cleveland, OH, May 1983.

[6] Newman, J.C., Stress Analysis of Simply and Multiply Connected Regions Containing Cracks by the Method of Boundary Collocation, MS Thesis, Virginia Polytechnic Institute and State University, 1969.

[7] Muskhelishvili, N.I., Some Basic Problems of the Mathematical Theory of Elasticity, P. Noordhoff, 1953.

[8] Sanford, R.J., and Berger, J.R., "An Improved Method of Boundary Collocation for the Analysis of Finite Body Opening Mode Fracture Problems," to appear in Engineering Fracture Mechanics.

[9] Tada, H., Paris, P.C., and Irwin, G.R., The Stress Analysis of Cracks Handbook, Del Research Corp., 1973.

[10] Williams, M.L., "On the Stress Distribution at the Base of a Stationary Crack," Journal of Applied Mechanics, Vol. 24, pp. 109-114, 1957.

[11] Sanford, R.J., "A Critical Re-examination of the Westergaard Method for Solving Opening Mode Crack Problems," Mechanics Research Communications, Vol. 6, 1979.

[12] Kobayashi, A.S., Cherepy, R.D., and Kinsel, W.C., "A Numerical Procedure for Estimating the Stress Intensity Factor of a Crack in a Finite Plate," Journal of Basic Engineering, pp.681-684, December 1964.

[13] Gross, B., Srawley, J.E., and Brown, W.F., "Stress-Intensity Factors for a Single Edge-Edge Notch Tension Specimen by Boundary Collocation of a Stress Function," NASA TN D-2395, August 1964.

[14] Srawley, J.E., Jones, M.H., and Gross, B., "Experimental Determination of the Dependence of Crack Extension Force on Crack Length for a Single-Edge-Notch Tension Specimen," NASA TN D-2396, August 1964.

[15] Hulbert, L.E., The Numerical Solution of Two Dimensional Problems of the Theory of Elasticity, Bulletin 198, Engineering Experiment Station, Ohio State University, 1963.

[16] Newman, J.C., "Crack Opening Displacements in Center-Crack, Compact, and Crack-Line Wedge-Loaded Specimens," NASA TN D-8268, July 1976.

[17] Berger, J.R., An Improved Method of Boundary Collocation for the Analysis of Finite Body Opening Mode Fracture Problems, MS Thesis, University of Maryland, 1986.

[18] Benthem, J.P., and Koiter, W.T., "Asymptotic Approximations to Crack Problems," Methods of Analysis of Crack Problems, G.C. Shih, ed., January 1972.

[19] Emery, A.F., Walker, G.E., and Williams, J.A., "A Green's Function for the Stress-Intensity Factors of Edge Cracks and its Application to Thermal Stresses," Journal of Basic Engineering, Vol. 88, p. 47, 1966.

[20] Bueckner, H.F., "A Novel Principle for the Computation of Stress Intensity Factors," ZAMM (Zeitschrift fur Angewandte Mathemetik und Mechanik) Band 56, pp. 529-545, 1970.

[21] Barker, D.B., Chona, R., Fourney, W.L., and Irwin, G.R., "A Report on the Round Robin Program Conducted to Evaluate the Proposed ASTM Standard Test Method for Determining the Plane Strain Crack Arrest Fracture Toughness, K_{Ia}, of Ferritic Materials," NUREG/CR-4996, ORNL/Sub/79-7778/4, January 1988.

[22] Kalthoff, J.F. et al., "Experimental Analysis of Dynamic Effects in Different Crack Arrest Test Specimens," Crack Arrest Methodology and Applications, ASTM STP 711, G.T. Hahn and M.F. Kannenin, Eds., American Society for Testing and Materials, 1980, pp.109-127.

[23] Naus, D.J. et al., "Crack-Arrest Behavior in SEN Wide Plates of Quenched and Tempered A 533 Grade B Steel Tested Under Nonisothermal Conditions," NUREG/CR-4930, ORNL-6388, August 1987.

[24] ASTM Standard E-1221, "Standard Testing Procedure for Determination of Crack Arrest Toughness," Annual Book of ASTM Standards, Vol 03.01, 1988.

[25] Westergaard, H.M., "Bearing Pressures and Cracks," Journal of Applied Mechanics, Vol. 6, pp. 49-53, 1939.

[26] Sanford, R.J., "Application of the Least-squares Method to Photoelastic Analysis," Experimental Mechanics, Vol. 20, No. 6, June 1980.

[27] Longley, J.W., Least Squares Computations Using Orthogonalization Methods, Marcel Dekker, Inc., 1984.

[28] Dungarra, J.J., Moler, C.B., Bunch, J.R., and Stewart, G.W., LINPACK Users Guide, Society for Industrial and Applied Mathematics, 1979.

[29] Paris, P.C., "The Mechanics of Fracture Propagation and Solutions to Fracture Arrester Problems," Boeing Co. Document No. D2-2195, 1957.

[30] Gross, B., Roberts, E., and Srawley, J.E., "Elastic Displacements for Various Edge-Cracked Plate Specimens," NASA TN D-4232, 1967.

INITIAL DISTRIBUTION

OUTSIDE CENTER

Copies

4 NRL

1 Code 6000
1 Code 6380
1 Code 6320
1 Code 6396

8 NAVSEA

1 SEA 05R
1 SEA 05M
1 SEA 05M2
1 SEA 08
1 SEA 55Y
1 SEA 55Y1
1 SEA 55Y3
1 SEA 092

1 NISC Code 369

12 DTIC

CENTER DISTRIBUTION

1	011	
1	011.5	Caplan
1	17	Krenske
1	173	Beach
1	1720.4	Wiggs
1	28	Wacker
1	2801	Crisci
1	2803	Hardy
1	281	Gudas
1	2814	Montemarano
10	2814	Kirk
1	522.1	TIC
1	5231	Office Services